CHARACTERIZATIONS AND MECHANISMS OF METHANE AND NITROUS OXIDE EMISSIONS IN SHALLOW LAKES

Ph.D. advisors:
Professor Terada Akihiko

ZHOU YIWEN
(Student ID: 18832702)

Graduate School of Engineering
Tokyo University of Agriculture and Technology

2021

CONTENTS

Chapter 1: Introduction for greenhouse gases emission in shallow lakes

1.1 Introduction

Carbon dioxide (CO_2), methane (CH_4), and nitrous oxide (N_2O) are well-known greenhouse gasses (GHGs) (Lashof and Ahuja, 1990). The rapid increase in GHGs in the atmosphere is one of the primary reasons for global warming. Recently, World Meteorological Organization (WMO) reported that CO_2, CH_4, and N_2O concentrations in the atmosphere have reached 408 ppm, 1869 ppb, and 331 ppb, steadily increasing by 147%, 259%, and 147% since the mid-18th century, respectively (WMO, 2019). The global warming potential of CH_4 is approximately 34-times greater than that of CO_2 (Beaulieu et al., 2019). N_2O is an ozone-depleting and highly potent GHG with a too-long lifetime, causing serious global warming after CO_2 and CH_4 in the stratosphere (Ravishankara et al., 2009). Given that the increasing GHGs concentrations in the atmosphere, GHGs emissions from natural ecosystems and engineering systems are paying more attention.

It has been well documented that the CH_4 emission from aquatic ecosystems significantly contributes to the global GHGs balance (Bastviken, 2011). Although the total area of freshwater lakes worldwide does not exceed 2% of the Earth's surface area, lakes have been considered as hotspots for CO_2 and CH_4 emissions. Recent studies indicate that CH_4 emissions from lakes account for 6–16% of the non-anthropogenic emissions, particularly the small size water bodies are significantly contribute to CH_4 emissions (Bastviken et al., 2008; Holgerson and Raymond, 2016). There are understood to be great uncertainties regarding the production and emission of CH_4 from shallow lakes (Li et al., 2018; Palma-Silva et al., 2013). The global average CH_4 flux from freshwaters is estimated to be 225.7 mmol m^{-2} yr^{-1} (Bastviken, 2011); however, this potentially includes an underestimation of the emissions from eutrophic lakes. The average CH_4 flux from Chinese lakes is estimated to be 531.5 mmol m^{-2} yr^{-1}, and emissions of up to 2106.3

mmol m^{-2} yr^{-1} have been reported for Lake Taihu, which is a hyper-eutrophic shallow lake (Yang et al., 2011). The underestimation of CH_4 emissions from hypereutrophic systems has also been mentioned in other studies (DelSontro et al., 2019; Schilder et al., 2018).

On the other hand, the atmospheric N_2O has increased by 20%, from 1750 to 2018, and a steadily increasing trend at a rate of 0.2% per year (Tian et al., 2020). The IPCC reported that approximately 10% of anthropogenic N_2O sources were derived from freshwater and coastal marine systems (IPCC, 2013). Given that inland freshwater lakes are recipients of nutrients transported from terrestrial ecosystems to trigger uncertainty of GHGs emissions (Wang et al., 2009; Zhou et al., 2020), they function as N_2O hot spots where the turnovers of nitrogen (N) compounds are high. Hence, the N_2O emissions from aquatic ecosystems have received considerable attention (Beaulieu et al., 2011; Kortelainen et al., 2020). Although multiple factors, *e.g.*, nutrients compositions, eutrophication, temperature, and so on, likely regulate N_2O emissions from freshwater lakes at regional and global scales, a dominant factor for N_2O emissions in freshwater lakes remains poorly understood (Kortelainen et al., 2020; Li et al., 2018; Yan et al., 2017). Moreover, there is a growing need to better evaluate and quantify freshwater lake ecosystems as a globally crucial N_2O source (Lauerwald et al., 2019).

Given that the dramatically uncertain of GHGs emissions in aquatic ecosystems, understanding the mechanisms that drive the differences and order of magnitude changes in CH_4 and N_2O emissions from freshwater lakes is crucial when effective policies and measures to tackle global warming are designed.

1.2 Lake eutrophication

In the 1920s, the concept of lake eutrophication is first proposed by Nauman (1919). Lake eutrophication refers to the natural phenomenon that occurs during the development or aging of the lake, that is, the large accumulation of nutrients such as nitrogen and phosphorus in the lake exceeds the lake environmental threshold. Subsequently, Carlson

(1977) first proposed the numerical trophic state index (TSI) to describe the difference of the trophic state in different water bodies. Of that the model incorporates most lakes in a scale of 0 to 100. Correspondingly, the different trophic state lakes are clearly classified into five states: oligotrophic, mesotrophic, eutrophic, middle-eutrophic, and hyper-eutrophic. With the development of industrialization, a large number of nutrients and organic matters were transported to the lake, the trophic state was shifted from oligotrophic to eutrophic. Previously study reported that more than 30% of lakes in the world display a state of eutrophication, and they are showing a rapid upward trend (Ortiz-Llorente and Alvarez-Cobelas, 2012). To date, eutrophication, which has become a major problem affecting the lake manager, brings many environmental problems of such as water crisis, biodiversity destruction, alga booms, etc. Importantly, the uncertainty of GHG emission in the different trophic state lakes has brough considerable attentions (Chen et al., 2016; Beaulieu et al., 2019; Xiao et al., 2019).

1.3 CH_4 emissions in the lake ecosystems

As we know, organic matter degradation is one of the most important processes for dominated CH_4 production and emission in aquatic ecosystems. In lacustrine ecosystems, methanogenic archaea and methanotrophic bacteria function as a CH_4 source and sink, respectively (Bastviken et al., 2008; Borrel et al., 2011). It has been well documented that CH_4 production rates are positively correlated with the diversities of methanogenic archaea and methanotrophic bacteria (He et al., 2019), and that their abundances and compositions are sensitive to environmental factors such as temperature, dissolved oxygen (DO), and organic matter concentrations (He et al., 2019; Henckel et al., 2000; Yang et al., 2019). Studies have documented that methanogenesis in lakes mainly occurs in anaerobic zones, whereas methanotrophic bacteria are present in oxic zones (Sepulveda-Jauregui et al., 2018). Therefore, the level of oxygen is a key parameter for determining the production and consumption of CH_4 in various situations (Bastviken et al., 2008; Borrel et al., 2011; Holgerson and Raymond, 2016). Temperature is also a

crucial controlling factor for these microbial processes (Marotta et al., 2014; Yvon-Durocher et al., 2014). A study reported a linear response of methanotrophy with increasing temperature under substrate-saturated conditions (Lofton et al., 2007), while substrate availability has been found to positively affect the methanotrophy rate more strongly than temperature (Dunfield et al., 1993; Nguyen et al., 2010). The growth of methanogenic archaea, however, is significantly facilitated by increasing concentrations of organic matter (Musenze et al., 2016). Moreover, the composition of organic matter has a close relationship with the microbial community structure. A previous study observed that different sources of organic matter had a significant influence on CH_4 emissions (Zhou et al., 2018). In particular, an elevated terrestrial organic matter input may potentially enhance the level of dissolved CH_4 in eutrophic shallow lakes. Collectively, these environmental factors determine the microbial processes that occur in lakes, and yet the various combinations of environmental factors induce a greater uncertainty regarding the actual CH_4 emissions from shallow lakes (Yvon-Durocher et al., 2014).

Shallow lakes are considered to be one of the important sources of CH_4 released into the atmosphere. The eutrophication of lakes is exacerbating CH_4 emissions from shallow lakes. It has been reported that eutrophic lakes have a larger emission of CH_4 to the atmosphere than oligotrophic lakes (Chen et al., 2016; Juutinen et al., 2009; Ortiz-Llorente and Alvarez-Cobelas, 2012). For example, the excessive growth of aquatic plants and algae is a source of organic matter, and the decomposition of this material by microorganisms can lead to the development of strong anaerobic conditions. This redox transition provides a positive feedback for CH_4 emissions from eutrophic shallow lakes (Schilder et al., 2018; Yan et al., 2017). To date, the production and flux of CH_4 from lakes have been extensively investigated (Bastviken et al., 2004; Beaulieu et al., 2019; DelSontro et al., 2019; Li et al., 2018). It is estimated that global GHG emissions are strongly biased by traditional approaches that extrapolate average emissions (DelSontro

et al., 2019). On the other hand, the estimation of CH_4 emissions from the world's lakes without taking account of nutrients and organic matter also results in great uncertainty (Beaulieu et al., 2019). Many previous studies were largely based on individual lakes, and the biogeographic-scale patterns of different types of trophic lakes have not been systematically investigated. The driving factors that induce extensive CH_4 emissions are also yet to be clarified. It is important to establish the relationship between the driving factors and CH_4 emissions by studying lake emissions with this biogeographic scale in mind (Beaulieu et al., 2019; DelSontro et al., 2019).

1.4 N_2O production and consumption in nitrogen cycles

As the Fig. 1 shown that N_2O is mainly produced by a by-product from nitrification and an intermediate from denitrification (Wenk et al., 2016). Of these multiple sources, denitrification is deemed a main N_2O source in aquatic ecosystems (Beaulieu et al., 2011; Li et al., 2019; Salk and Ostrom, 2019). Importantly, N_2O reduction, as the final step of denitrification ($NO_3^- \rightarrow NO_2^- \rightarrow NO \rightarrow N_2O \rightarrow N_2$), is catalyzed by N_2O reductase encoded by *nosZ* gene (Yoon et al., 2016). Namely, denitrification exerts either an N_2O source or sink to determine N_2O emission fluxes. Reportedly, N_2O production is regulated by microbial community structures in an aquatic ecosystem (Zhao et al., 2018; Zhao et al., 2019). Therefore, understanding the impacts of N_2O production and consumption by the variations of environmental factors and its contribution to the changes of microbial community structure is crucial.

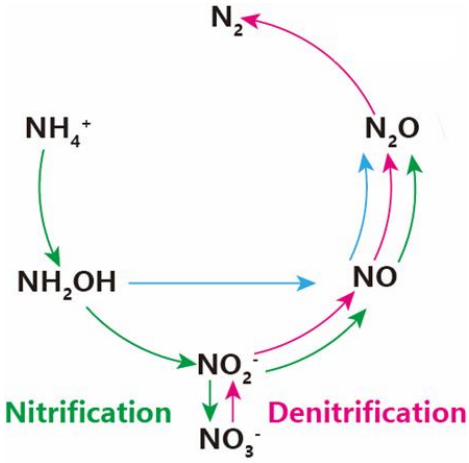

Fig. 1 N_2O production and consumption pathway in nitrification and denitrification.

N_2O-reducing bacteria (N_2ORB), carried *nosZ* gene, is considered the N_2O sink in N cycle (Conthe et al., 2019). Owing to differences in the N_2O reeducates (N_2OR) amino acid sequences (similarity < 50%) and the protein-translocation pathways, N_2O-reducing bacteria (N_2ORB) harboring a functional *nosZ* gene can be classified into either clade I or clade II (Conthe et al., 2018; Jones et al., 2013; Sanford et al., 2012). Recently, Zhao et al. (2018) reported that the *nosZ* clade II-type N_2ORB showed a higher diversity in the riparian zone than in other environments. Whereas some clade II type N_2ORB display a higher affinity for N_2O than clade I type N_2ORB (Suenaga et al., 2018; Yoon et al., 2016), research on N_2ORB biokinetics of N_2O consumption toward an effective strategy to reduce N_2O emissions is limited (Hallin et al., 2018; Yoon et al., 2016; Yoon et al., 2019). Therefore, more knowledge regarding the N_2O sinks of N_2ORB to understand the N_2O sink activities in natural and engineering systems are urged.

The microbial community compositions are important for the amount of N_2O emissions as some bacteria lack *nosZ* and nitrite reductase genes, significantly contributing to N_2O consumption and production in natural ecosystems, respectively (Domeignoz-Horta et al., 2016). Among myriad environmental factors, nutrients, redox conditions, and temperature determine microbial guilds for N_2O production and consumption (Hinshaw and Dahlgren, 2013; Xiao et al., 2019). Seasonal changes cover

multiple environmental fluctuations, probably affecting lacustrine microbial community structures and causing the uncertainty of N_2O emissions (Song et al., 2012). Especially, the microbial N_2O production and consumption processes carried different temperature dependencies. N conversion rates and eutrophication progress are crucial to regulate final N forms (N_2 or N_2O) in aquatic ecosystems (Jiang et al., 2020; Salk and Ostrom, 2019; Zhu et al., 2020). Such N conversions are dynamic and dependent on eutrophication progress (Li et al., 2018; Liikanen et al., 2003).

1.5 N_2O emission in the lake ecosystems

N_2O emissions from eutrophic shallow lakes have been also surveyed, providing the way how different N_2O emission fluxes are among shallow lakes with different trophic states. For the survey, the commonly used default emission factor (EF_{5r}) by the IPCC has been applied (Maavara et al., 2019), resulting in the underestimation or overestimation of the N_2O budgets in freshwater ecosystems with different trophic states (Zhang et al., 2020). For instance, Xiao et al. (2019) indicated that the mean N_2O emission fluxes in the East and West zones of Lake Taihu (eutrophic and oligotrophic, respectively) were substantially different, partially caused by the N-loadings flowing to the lake. Besides, N-loadings regulate the distributions of denitrifying bacteria, often indicated by functional genes for N_2O production (*nirS* and *nirK*) and reduction (*nosZ*) (Huang et al., 2011; Zhao et al., 2018). Importantly, a high N-loading to a eutrophic lake accumulates algal growth, potentially enhancing N_2O emissions and N turnover rates (Yan et al., 2017; Zhu et al., 2020). As the algal accumulation regarding decomposition for altering the redox condition favors denitrification (Yan et al., 2017), while further the anoxic condition limited nitrification for supplying nitrogen oxides to denitrification (Zhu et al., 2020), hence, these observations limit our understanding in the role of algae in N_2O emission. Such correlation in eutrophic and hypereutrophic lakes have been intensively investigated (Lauerwald et al., 2019; Xiao et al., 2019); however, shallow lakes have not been subject to the systematic investigation, particularly comparing N_2O emission fluxes among the

different trophic states (Salk and Ostrom, 2019). The trophic states of lakes brought the uncertainty of N_2O emission estimates (Kortelainen et al., 2020), yet the relationship between N_2O emission fluxes and trophic states of lakes is not holistically disentangled. Therefore, the investigation of N_2O emissions associated with lacustrine trophic states on a biogeographic scale could help understand the potentials as N_2O emission sources.

1.6 Objectives of this study

Currently, numerous studies have well documented that the aquatic ecosystems are significantly contribute to CH_4 and N_2O emission (Beaulieu et al., 2019; Beaulieu et al., 2010; DelSontro et al., 2019). However, the eutrophication of water bodies (*e.g.*, shallow lake, river, and reservoir) results to a large uncertainty in the CH_4 and N_2O emission fluxes (Li et al., 2018). It is worth noted that the complex nitrogen cycles contained multiple pathways to produce N_2O, while only one pathway can be the N_2O sink. Therefore, understanding the denitrifier carried out the *nosZ* gene, encoding N_2O reductase, to act the N_2O sink is very important. Given that the shallow lakes carried different nutrients loadings, the carbon and nitrogen cycles associated the CH_4 and N_2O emissions needs to be clarified. In this study, we investigated the CH_4 and N_2O emission fluxes and environmental variables for different lakes along a trophic state gradient at the biogeographic scale of the Yangtze River basin, China, which includes a large number of shallow lakes. Based on the pure culture denitrifier, the key driving factors affecting N_2O consumption were further analyzed. The key contents of research are listed in Fig. 2. The aims of this study were to (1) identify CH_4 and N_2O emission patterns in the different trophic state shallow lakes; (2) analyze the relationship between the CH_4 and N_2O emission flux and environmental variables as a means of exploring the driving factors that can be used to predict the CH_4 and N_2O fluxes; (3) investigate the discrepancy of main microorganisms and functional genes for N_2O emissions in the sediments of different trophic state shallow lakes; (4) understanding the N_2O consumption process of N_2ORB. This study is expected to expand our knowledge to accurately predict CH_4 and

N_2O emission patterns from shallow lakes.

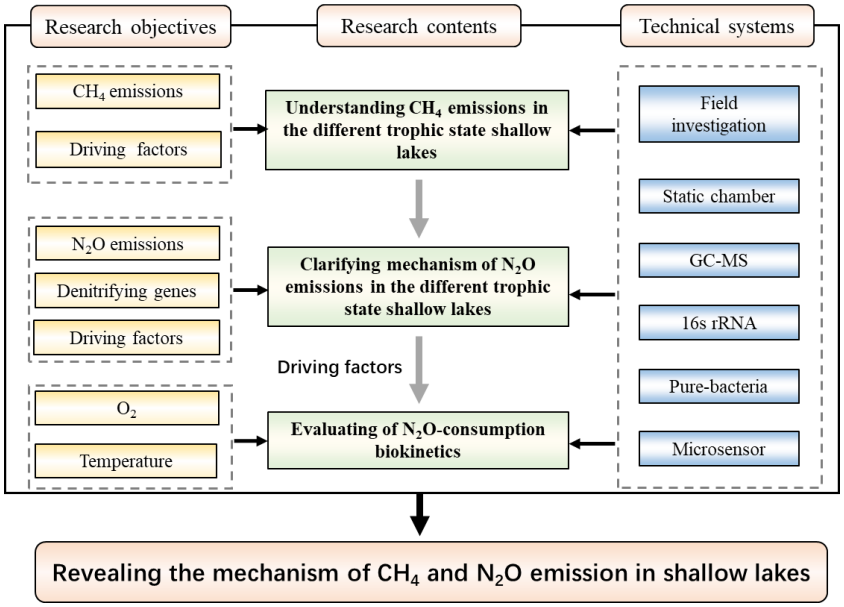

Fig. 2 Flow diagram of the research.

1.7 References

Bastviken, D., Cole, J., Pace, M., Tranvik, L., 2004. Methane emissions from lakes: Dependence of lake characteristics, two regional assessments, and a global estimate. Global Biogeochemical Cycles 18.

Bastviken, D., Cole, J.J., Pace, M.L., Van de Bogert, M.C., 2008. Fates of methane from different lake habitats: Connecting whole-lake budgets and CH_4 emissions. Journal of Geophysical Research-Biogeosciences 113.

Bastviken, D.T., L. J.; Downing, J. A.; Crill, P. M., 2011. Freshwater methane emissions offset the continental carbon sink. Science 311, 50.

Beaulieu, J.J., DelSontro, T., Downing, J.A., 2019. Eutrophication will increase methane emissions from lakes and impoundments during the 21st century. Natture Communication 10, 1375.

Beaulieu, J.J., Shuster, W.D., Rebholz, J.A., 2010. Nitrous oxide emissions from a large, impounded river: the Ohio River. Environmental Science & Technology 44, 7527-

7533.

Beaulieu, J.J., Tank, J.L., Hamilton, S.K., Wollheim, W.M., Hall, R.O., Jr., Mulholland, P.J., Peterson, B.J., Ashkenas, L.R., Cooper, L.W., Dahm, C.N., Dodds, W.K., Grimm, N.B., Johnson, S.L., McDowell, W.H., Poole, G.C., Valett, H.M., Arango, C.P., Bernot, M.J., Burgin, A.J., Crenshaw, C.L., Helton, A.M., Johnson, L.T., O'Brien, J.M., Potter, J.D., Sheibley, R.W., Sobota, D.J., Thomas, S.M., 2011. Nitrous oxide emission from denitrification in stream and river networks. Proceedings of the National Academy of Sciences of the United States of America 108, 214-219.

Borrel, G., Jezequel, D., Biderre-Petit, C., Morel-Desrosiers, N., Morel, J.P., Peyret, P., Fonty, G., Lehours, A.C., 2011. Production and consumption of methane in freshwater lake ecosystems. Reseasrch Microbiology 162, 832-847.

Chen, Y., Dong, S., Wang, F., Gao, Q., Tian, X., 2016. Carbon dioxide and methane fluxes from feeding and no-feeding mariculture ponds. Environmental Pollution 212, 489-497.

Conthe, M., Lycus, P., Arntzen, M.O., Ramos da Silva, A., Frostegard, A., Bakken, L.R., Kleerebezem, R., van Loosdrecht, M.C.M., 2019. Denitrification as an N_2O sink. Water Research 151, 381-387.

Conthe, M., Wittorf, L., Kuenen, J.G., Kleerebezem, R., van Loosdrecht, M.C.M., Hallin, S., 2018. Life on N_2O: deciphering the ecophysiology of N_2O respiring bacterial communities in a continuous culture. ISME J 12, 1142-1153.

DelSontro, T., Beaulieu, J.J., Downing, J.A., 2019. Greenhouse gas emissions from lakes and impoundments: upscaling in the face of global change. Limnology and Oceanography Letters 3, 64-75.

Domeignoz-Horta, L.A., Putz, M., Spor, A., Bru, D., Breuil, M.C., Hallin, S., Philippot, L., 2016. Non-denitrifying nitrous oxide-reducing bacteria - An effective N_2O sink in soil. Soil Biology and Biochemistry 103, 376-379.

Dunfield, P., Knowles, R., Dumont, R., Moore, T.R., 1993. Methane production and

consumption in temperate and subarctic peat soils: Response to temperature and pH. Soil Biology & Biochemistry 25, 321-326.

Hallin, S., Philippot, L., Löffler, F.E., Sanford, R.A., Jones, C.M., 2018. Genomics and ecology of novel N_2O-reducing microorganisms. Trends in Microbiology 26, 43-55.

He, Z., Wang, J., Hu, J., Yu, H., Jetten, M.S.M., Liu, H., Cai, C., Liu, Y., Ren, H., Zhang, X., Hua, M., Xu, X., Zheng, P., Hu, B., 2019. Regulation of coastal methane sinks by a structured gradient of microbial methane oxidizers. Environmental Pollution 244, 228-237.

Henckel, T., Roslev, P., Conrad, R., 2000. Effects of O_2 and CH_4 on presence and activity of the indigenous methanotrophic community in rice field soil. Environmental Microbiology 2, 666-679.

Hinshaw, S.E., Dahlgren, R.A., 2013. Dissolved nitrous oxide concentrations and fluxes from the eutrophic San Joaquin River, California. Environmental Science & Technology 47, 1313-1322.

Holgerson, M., Raymond, P., 2016. Large contribution to inland water CO_2 and CH_4 emissions from very small ponds. Nature Geoscience.

Huang, S., Chen, C., Yang, X., Wu, Q., Zhang, R., 2011. Distribution of typical denitrifying functional genes and diversity of the *nir*S-encoding bacterial community related to environmental characteristics of river sediments. Biogeosciences 8, 3041-3051.

IPCC, (eds)., I.S.T.e.a., 2013. Climate change 2013: the physical science Basis. Contribution of working group I to the fifth assessment report of the Intergovernmental Panel on Climate Change. Cambridge University Press, New York. Cambridge University Press, New York.

Jiang, X., Gao, G., Zhang, L., Tang, X., Shao, K., Hu, Y., Cai, J., 2020. Role of algal accumulations on the partitioning between N_2 production and dissimilatory nitrate reduction to ammonium in eutrophic lakes. Water Research 183, 116075.

Jones, C.M., Graf, D.R., Bru, D., Philippot, L., Hallin, S., 2013. The unaccounted yet

abundant nitrous oxide-reducing microbial community: a potential nitrous oxide sink. ISME J 7, 417-426.

Juutinen, S., Rantakari, M., Kortelainen, P., Huttunen, J.T., Larmola, T., Alm, J., Silvola, J., Martikainen, P.J., 2009. Methane dynamics in different boreal lake types. Biogeosciences, 6, 209-223.

Kortelainen, P., Larmola, T., Rantakari, M., Juutinen, S., Alm, J., Martikainen, P.J., 2020. Lakes as nitrous oxide sources in the boreal landscape. Global Change Biology 26, 1432-1445.

Lashof, D.A., Ahuja, D.R., 1990. Relative contributions of greenhouse gas emissions to global warming. Nature 344, 529-531.

Lauerwald, R., Regnier, P., Figueiredo, V., Enrich-Prast, A., Bastviken, D., Lehner, B., Maavara, T., Raymond, P., 2019. Natural Lakes are a minor global source of N_2O to the atmosphere. Global Biogeochemical Cycles 33, 1564-1581.

Li, Q., Wang, F., Yu, Q., Yan, W., Li, X., Lv, S., 2019. Dominance of nitrous oxide production by nitrification and denitrification in the shallow Chaohu Lake, Eastern China: Insight from isotopic characteristics of dissolved nitrous oxide. Environmental Pollution 255, 113212.

Li, S., Bush, R.T., Santos, I.R., Zhang, Q., Song, K., Mao, R., Wen, Z., Lu, X.X., 2018. Large greenhouse gases emissions from China's lakes and reservoirs. Water Research 147, 13-24.

Liikanen, A., Huttunen, J.T., Murtoniemi, T., Tanskanen, H., Vaisanen, T., Silvola, J., Alm, J., Martikainen, P.J., 2003. Spatial and seasonal variation in greenhouse gas and nutrient dynamics and their interactions in the sediments of a boreal eutrophic lake. Biogeochemistry 65, 83-103.

Lofton, D.D., Hershey, A.E., Whalen, S.C., 2007. Evaluation of denitrification in an urban stream receiving wastewater effluent. Biogeochemistry 86, 77-90.

Maavara, T., Lauerwald, R., Laruelle, G.G., Akbarzadeh, Z., Bouskill, N.J., Van Cappellen, P., Regnier, P., 2019. Nitrous oxide emissions from inland waters: Are

IPCC estimates too high? Global Change Biology 25, 473-488.

Marotta, H., Pinho, L., Gudasz, C., Bastviken, D., Tranvik, L.J., Enrich-Prast, A., 2014. Greenhouse gas production in low-latitude lake sediments responds strongly to warming. Nature Climate Change 4, 467-470.

Musenze, R.S., Fan, L., Grinham, A., Werner, U., Gale, D., Udy, J., Yuan, Z., 2016. Methane dynamics in subtropical freshwater reservoirs and the mediating microbial communities. Biogeochemistry 128, 233-255.

Naumann, E., 1919. Aspects on the ecology of limnoplankton with special focus on phytoplankton. Svensk Bot. Tidskr 13:51–58.

Nguyen, T.D., Crill, P., Bastviken, D., 2010. Implications of temperature and sediment characteristics on methane formation and oxidation in lake sediments. Biogeochemistry 100, 185-196.

Ortiz-Llorente, M.J., Alvarez-Cobelas, M., 2012. Comparison of biogenic methane emissions from unmanaged estuaries, lakes, oceans, rivers and wetlands. Atmospheric Environment 59, 328-337.

Palma-Silva, C., Marinho, C.C., Albertoni, E.F., Giacomini, I.B., Barros, M.P.F., Furlanetto, L.M., Trindade, C.R.T., Esteves, F.D., 2013. Methane emissions in two small shallow neotropical lakes: The role of temperature and trophic level. Atmospheric Environment 81, 373-379.

Ravishankara, A.R., Daniel, J.S., Portmann, R.W., 2009. Nitrous oxide (N_2O): the dominant ozone-depleting substance emitted in the 21st century. Science 326, 123-125.

Salk, K.R., Ostrom, N.E., 2019. Nitrous oxide in the Great Lakes: insights from two trophic extremes. Biogeochemistry 144, 233-243.

Sanford, R.A., Wagner, D.D., Wu, Q., Chee-Sanford, J.C., Thomas, S.H., Cruz-Garcia, C., Rodriguez, G., Massol-Deya, A., Krishnani, K.K., Ritalahti, K.M., Nissen, S., Konstantinidis, K.T., Loffler, F.E., 2012. Unexpected nondenitrifier nitrous oxide reductase gene diversity and abundance in soils. Proc Natl Acad Sci U S A 109,

19709-19714.

Schilder, J., Hardenbroek, M.V., Bodelier, P., Kirilova, E.P., Leuenberger, M., Lotter, A., Heiri, O., 2018. Trophic state changes can affect the importance of methane-derived carbon in aquatic food webs. Proceedings. Biological sciences 284.

Sepulveda-Jauregui, A., Hoyos-Santillan, J., Martinez-Cruz, K., Walter Anthony, K.M., Casper, P., Belmonte-Izquierdo, Y., Thalasso, F., 2018. Eutrophication exacerbates the impact of climate warming on lake methane emission. Scince of the Total Environment 636, 411-419.

Song, K., Kang, H., Zhang, L., Mitsch, W.J., 2012. Seasonal and spatial variations of denitrification and denitrifying bacterial community structure in created riverine wetlands. Ecological Engineering 38, 130-134.

Suenaga, T., Riya, S., Hosomi, M., Terada, A., 2018. Biokinetic characterization and activities of N_2O-reducing bacteria in response to various oxygen levels. Frontiers in Microbiology 9, 697.

Tian, H., Xu, R., Canadell, J.G., Thompson, R.L., Winiwarter, W., Suntharalingam, P., Davidson, E.A., Ciais, P., Jackson, R.B., Janssens-Maenhout, G., Prather, M.J., Regnier, P., Pan, N., Pan, S., Peters, G.P., Shi, H., Tubiello, F.N., Zaehle, S., Zhou, F., Arneth, A., Battaglia, G., Berthet, S., Bopp, L., Bouwman, A.F., Buitenhuis, E.T., Chang, J., Chipperfield, M.P., Dangal, S.R.S., Dlugokencky, E., Elkins, J.W., Eyre, B.D., Fu, B., Hall, B., Ito, A., Joos, F., Krummel, P.B., Landolfi, A., Laruelle, G.G., Lauerwald, R., Li, W., Lienert, S., Maavara, T., MacLeod, M., Millet, D.B., Olin, S., Patra, P.K., Prinn, R.G., Raymond, P.A., Ruiz, D.J., van der Werf, G.R., Vuichard, N., Wang, J., Weiss, R.F., Wells, K.C., Wilson, C., Yang, J., Yao, Y., 2020. A comprehensive quantification of global nitrous oxide sources and sinks. Nature 586, 248-256.

Wang, S., Liu, C., Yeager, K.M., Wan, G., Li, J., Tao, F., Lu, Y., Liu, F., Fan, C., 2009. The spatial distribution and emission of nitrous oxide (N_2O) in a large eutrophic lake in eastern China: anthropogenic effects. Science of the Total Environment 407,

3330-3337.

Wenk, C.B., Frame, C.H., Koba, K., Casciotti, K.L., Veronesi, M., Niemann, H., Schubert, C.J., Yoshida, N., Toyoda, S., Makabe, A., Zopfi, J., Lehmann, M.F., 2016. Differential N_2O dynamics in two oxygen-deficient lake basins revealed by stable isotope and isotopomer distributions. Limnology and Oceanography 61, 1735-1749.

WMO, 2019. WMO greenhouse gas bulletin: the state of greenhouse gases in the atmosphere based on global observations through 2018. Global Atmosphere Watch, World Meteorological Organization.

Xiao, Q., Xu, X., Zhang, M., Duan, H., Hu, Z., Wang, W., Xiao, W., Lee, X., 2019. Coregulation of nitrous oxide emissions by nitrogen and temperature in China's third largest freshwater lake (Lake Taihu). Limnology and Oceanography 64, 1070-1086.

Yan, X., Xu, X., Wang, M., Wang, G., Wu, S., Li, Z., Sun, H., Shi, A., Yang, Y., 2017. Climate warming and cyanobacteria blooms: Looks at their relationships from a new perspective. Water Res 125, 449-457.

Yang, H., Xie, P., Ni, L., Flower, R.J., 2011. Underestimation of CH_4 emission from freshwater lakes in China. Environmental Science & Technology 45, 4203-4204.

Yang, Y., Chen, J., Tong, T., Li, B., He, T., Liu, Y., Xie, S., 2019. Eutrophication influences methanotrophic activity, abundance and community structure in freshwater lakes. Science of the Total Environment 662, 863-872.

Yoon, S., Nissen, S., Park, D., Sanford, R.A., Loffler, F.E., 2016. Nitrous oxide reduction kinetics distinguish bacteria harboring clade I *nosZ* from those harboring clade II *nosZ*. Applied and Environmental Microbiology 82, 3793-3800.

Yoon, S., Song, B., Phillips, R.L., Chang, J., Song, M.J., 2019. Ecological and physiological implications of nitrogen oxide reduction pathways on greenhouse gas emissions in agroecosystems. FEMS Microbiology Ecology 95.

Yvon-Durocher, G., Allen, A.P., Bastviken, D., Conrad, R., Gudasz, C., St-Pierre, A., Thanh-Duc, N., del Giorgio, P.A., 2014. Methane fluxes show consistent temperature dependence across microbial to ecosystem scales. Nature 507, 488-491.

Zhang, W., Li, H., Xiao, Q., Jiang, S., Li, X., 2020. Surface nitrous oxide (N_2O) concentrations and fluxes from different rivers draining contrasting landscapes: Spatio-temporal variability, controls, and implications based on IPCC emission factor. Environmental Polluttion 263, 114457.

Zhao, S., Wang, Q., Zhou, J., Yuan, D., Zhu, G., 2018. Linking abundance and community of microbial N_2O-producers and N_2O-reducers with enzymatic N_2O production potential in a riparian zone. Science of the Total Environment 642, 1090-1099.

Zhao, S., Zhou, J., Yuan, D., Wang, W., Zhou, L., Pi, Y., Zhu, G., 2019. *Nir*S-type N_2O-producers and *nos*Z II-type N_2O-reducers determine the N_2O emission potential in farmland rhizosphere soils. Journal of Soils and Sediments.

Zhou, Y., Xiao, Q., Yao, X., Zhang, Y., Zhang, M., Shi, K., Lee, X., Podgorski, D.C., Qin, B., Spencer, R.G.M., Jeppesen, E., 2018. Accumulation of Terrestrial Dissolved Organic Matter Potentially Enhances Dissolved Methane Levels in Eutrophic Lake Taihu, China. Environmental Science & Technology 52, 10297-10306.

Zhou, Y., Xiao, Q., Zhou, L., Jang, K.S., Zhang, Y., Zhang, M., Lee, X., Qin, B., Brookes, J.D., Davidson, T.A., Jeppesen, E., 2020. Are nitrous oxide emissions indirectly fueled by input of terrestrial dissolved organic nitrogen in a large eutrophic Lake Taihu, China? Science of the Total Environment 722, 138005.

Zhu, L., Shi, W., Van Dam, B., Kong, L., Yu, J., Qin, B., 2020. Algal accumulation decreases sediment nitrogen removal by uncoupling nitrification-denitrification in shallow eutrophic lakes. Environmental Science & Technology 54, 6194-6201.

Chapter 2: Characterization of CH_4 emission and its microbial driven mechanisms in different trophic shallow lakes

2.1 Introduction

The rapid increase in greenhouse gases (GHGs) in the atmosphere is one of the primary reasons for global warming. The global warming potential of methane (CH_4) is approximately 34-times greater than that of carbon dioxide (CO_2) (IPCC, 2014). Bastviken et al. (2011) reported that the CH_4 fluxes from fresh waterbodies significantly contribute to the global GHG balance. Despite the fact that the total area of freshwater lakes worldwide does not exceed 2% of the Earth's surface area, lakes have been considered as hotspots for CO_2 and CH_4 emissions. Recent studies indicate that CH_4 emissions from lakes account for 6–16% of the non-anthropogenic missions, particularly the small size water bodies are significantly contribute to CH_4 emissions (Bastviken et al., 2008; Holgerson and Raymond, 2016). There are understood to be great uncertainties regarding the production and emission of CH_4 from shallow freshwater lakes (Zhuang et al., 2009; Palma-Silva et al., 2013; Li et al., 2018). The global average CH_4 flux from freshwaters is estimated to be 225.7 mmol m^{-2} yr^{-1} (Bastviken et al., 2011); however, this potentially includes an underestimation of the emissions from eutrophic lakes. The average CH_4 flux from Chinese lakes is estimated to be 531.5 mmol m^{-2} yr^{-1}, and emissions of up to 2106.3 mmol m^{-2} yr^{-1} have been reported for Lake Taihu, which is a hypereutrophic shallow lake (Yang et al., 2011). The underestimation of GHG emissions from hypereutrophic systems has also been mentioned in other studies (Schilder et al., 2017; DelSontro et al., 2018). Understanding the mechanisms that drive the order of magnitude differences in CH_4 emissions from lakes is crucial when designing effective measures to tackle global climate change.

Widespread evidence has revealed that the production and emission of CH_4 are

associated with microbial processes and are controlled by multiple environmental factors. In lacustrine ecosystems, methanogenic archaea and methanotrophic bacteria function as a CH_4 source and CH_4 sink, respectively (Borrel et al., 2011; Bastviken et al., 2015). It has been observed that CH_4 production rates are positively correlated with the diversities of methanogenic archaea and methanotrophic bacteria (He et al., 2019a), and that their abundances and compositions are sensitive to environmental factors such as temperature, dissolved oxygen (DO), and organic matter concentrations (Henckel et al., 2000; Yang et al., 2019; He et al., 2019a). Studies have documented that methanogenesis in lakes mainly occurs in anaerobic zones, whereas methanotrophic bacteria are present in oxic zones (Sepulveda-Jauregui et al., 2018). The level of oxygen is a key parameter for determining the production and consumption of CH_4 in various situations (Borrel et al., 2011; Bastviken et al., 2015; Holgerson and Raymond, 2016). Temperature is also a crucial controlling factor for these microbial processes (Yvon-Durocher et al., 2014; Marotta et al., 2014). Lofton et al. (2014) reported a linear response of methanotrophy with increasing temperature under substrate-saturated conditions, while substrate availability has been found to positively affect the methanotrophy rate more strongly than temperature (Dunfield et al., 1993; Duc et al., 2010). The growth of methanogenic archaea, however, is significantly facilitated by increasing concentrations of organic matter (Musenze et al., 2016). Moreover, the composition of organic matter has a close relationship with the microbial community structure. Zhou et al. (2018) observed that different sources of organic matter had a significant influence on CH_4 emissions. In particular, an elevated terrestrial organic matter input may potentially enhance the level of dissolved CH_4 in eutrophic shallow lakes. Collectively, these environmental factors determine the microbial processes that occur in lakes, and yet the various combinations of environmental factors induce a greater uncertainty regarding the actual CH_4 emissions from shallow lakes (Yvon-Durocher et al., 2014).

Shallow lakes receive and deposit nutrients and organic matter transported from the upstream regions of their catchments, which can lead to the transition from oligotrophic

to eutrophic states. It has been reported that eutrophic lakes have a larger emission of CH_4 to the atmosphere than oligotrophic lakes (Juutinen et al., 2009; Ortiz-Llorente and Alvarez-Cobelas, 2012; Chen et al., 2016). For example, the excessive growth of aquatic plants and algae is a source of organic matter, and the decomposition of this material by microorganisms can lead to the development of strong anaerobic conditions. This redox transition provides a positive feedback for CH_4 emissions from eutrophic shallow lakes (Schilder et al., 2017; Yan et al., 2017). To date, the production and flux of CH_4 from lakes have been extensively investigated (Bastviken et al., 2004; Rinta et al., 2015; DelSontro et al., 2018; Li et al., 2018; Beaulieu et al., 2019). It is estimated that global GHG emissions are strongly biased by traditional approaches that extrapolate average emissions (DelSontro et al. 2018). On the other hand, the estimation of CH_4 emissions from the world's lakes without taking account of nutrients and organic matter also results in great uncertainty (Beaulieu et al., 2019). Many previous studies were largely based on individual lakes, and the biogeographic-scale patterns of different types of trophic lakes have not been systematically investigated. The driving factors that induce extensive CH_4 emissions are also yet to be clarified. It is important to establish the relationship between the driving factors and CH_4 emissions by studying lake emissions with this biogeographic scale in mind (Rinta et al., 2015; DelSontro et al., 2018; Beaulieu et al., 2019).

In this study, we investigated the CH_4 emission fluxes and environmental variables for different lakes along a trophic state gradient at the biogeographic scale of the Yangtze River basin, China, which includes a large number of shallow lakes. We hypothesise that eutrophication, especially hyper-eutrophication, triggers a nonlinear increase in CH_4 emissions in shallow lakes. The aims of this study are to (1) elucidate the relationship between CH_4 emissions and the level of eutrophication in shallow lakes, and (2) analyse the relationship between the CH_4 emission flux and environmental variables as a means of exploring the driving factors that can be used to predict the CH_4 flux. The results of this study are intended to help guide the management of lakes and support the assessment of regional CH_4 budgets.

2.2 Material and methods

2.2.1 Sampling sites and sample collection

Overlying water and sediment samples from 17 shallow lakes along the middle and lower reaches of the Yangtze River (Fig. 1) were collected during August and September 2018. The lakes are located in Shanghai, Jiangsu, Anhui, Jiangxi, Hubei, and Hunan provinces, with a maximal distance between the lakes of > 1000 km. The selected shallow lakes had a mean depth of < 7 m and were selected based on their different trophic states, as determined from a literature review and government report. The physicochemical properties of the 17 sampling sites are listed in Table S1. Temperature, DO, and pH were measured *in-situ* at a water depth of ~20 cm using a HQ3d meter (Hach, USA). Triplicate water samples (20 cm below the water surface) and surface sediments samples (0–10 cm depth) were collected in the littoral zone of each lake. Gas samples were collected simultaneously using plastic, floating static chambers, which have been previously shown to provide unbiased measurements of water–gas exchange (Cole et al., 2010; Gålfalk et al., 2013). Measurements of GHG fluxes were made between 11:00 and 14:00 using a floating static chamber (38.5 cm × 30.5 cm × 18.5 cm), which was designed to collect gas samples every 10 minutes for 1 hour. Details of the sampling method can be found in Zhou et al. (2019).

2.2.2 Sample analysis

The water samples were analysed for total nitrogen (TN), total phosphorus (TP), NO_3^--N, NH_4^+-N, chlorophyll-*a* (chl-*a*), and dissolved organic carbon (DOC) contents. Triplicate water samples were collected using a tube sampler and mixed thoroughly. The ratio of C:N was determined by the DOC and TN concentrations in the overlying water. The analytical methods are described elsewhere (Liu et al., 2017; Xu et al., 2019a). The sediment samples were analysed for the sediment total nitrogen (STN), sediment total phosphorus (STP), and sediment total organic carbon (STOC) contents. The analytical

methods are given in Zhou et al. (2019). In addition, a conversion factor of 1.724 was used to estimate the organic matter (OM) content from TOC:OM = TOC × 1.724 (Zeng et al., 2018).

The CO_2 and CH_4 concentrations were analysed using a 7890B Agilent gas chromatography equipped with a flame ionisation detector (FID). The gas chromatography configurations described by Wu et al. (2018) were adopted for the gas concentration analysis.

2.2.3 DNA extraction and Illumina high-throughput sequencing

The biomass for the analysis of the sediment microbial community was collected from four lakes with a different trophic state: Lake Taihu (TH), Lake Honghu (HH), Lake Poyanghu (PYH), and Lake Baidanghu (BDH). A MOBIO PowerSoil® DNA Isolation Kit (MOBIO, USA) was used to extract DNA from the sediment according to the manufacturer's instructions. The concentration and purity of DNA were measured using the NanoDrop One (Thermo Fisher Scientific, Ma, USA), and the extracted DNA was then stored at −20℃ awaiting further analysis. The 16S rRNA gene sequencing was analysed using an Illumina Miseq platform at Magigene Biotechnology Institute (Guangzhou, China). The primers used for the high-throughput sequencing were modified 515F (5′- GTGYCAGCMGCCGCGGTAA - 3′) and 806R (5′ - GGACTACHVGGGTWTCTAAT - 3′), thus targeting the V3 + V4 regions of both bacterial and archaeal 16S rRNA genes (Chen et al., 2017; Gong et al., 2019). Polymerase chain reaction (PCR) samples containing 25 μl of 2 × Premix Taq (Takara Biotechnology, Dalian Co. Ltd., China), 1 μl of each primer (10 mM), and 3 μl of the DNA (20 ng μl^{-1}) template in a volume of 50 μl were amplified by thermocycling. The amplification program was as follows: 5 min at 94℃ for initialisation; 30 cycles of 30 s denaturation at 94℃, 30 s annealing at 52℃, and 30 s extension at 72℃; 10 min final elongation at 72℃. The PCRs were conducted on a BioRad S1000 (Bio-Rad Laboratory, CA, USA).

2.2.4 Calculated trophic state index and greenhouse gas concentrations

The trophic state of the 17 lake samples were evaluated using the trophic lake index (*TLI*) developed by Carlson (1977) and modified by Jin (1995) (Eq. 1), which is more suitable for Asian freshwater lakes. The lake trophic state was described by the *TLI* value, and the chl-*a* and TN concentration were used as criterion to calculate the lake trophic state (Zhang et al., 2011).

$$TLI(\sum) = \sum_{j=1}^{m} W_j \times TLI(j) \quad , \tag{1}$$

$$W_j = \frac{r_{ij}^2}{\sum_{j=1}^{m} r_{ij}^2}, \tag{2}$$

$$TLI\ (\text{chl-}a) = 10 \times [2.46 + \ln(\text{chl-}a)/\ln(2.5)], \tag{3}$$

$$TLI\ (\text{TN}) = 10 \times [5.453 + 1.694 \times \ln(\text{TN})], \tag{4}$$

where $TLI\ (\sum)$ is the integrated trophic level index; $TLI(j)$ is the trophic level index of j; W_j is the correlative constant for the *TLI* of j; r_{ij} is the relative coefficient, which was described by Zhang et al. (2011); j and m represent the parameters (*i.e.* chl-*a* and TN) and the number of parameters, respectively. Subsequently, the calculated $W_{\text{chl-a}}$ and W_{TN} were 0.5979 and 0.4021, respectively. The lake trophic state was further classified based on the $TLI\ (\sum)$ value as either oligotrophic ($TLI(\sum) \leq 30$), mesotrophic ($30 < TLI(\sum) \leq 50$), eutrophic ($50 < TLI(\sum) \leq 60$), middle eutrophic ($60 < TLI(\sum) \leq 70$), or hyper-eutrophic ($TLI\ (\sum) > 70$).

The CH_4 and CO_2 emission fluxes estimated by the floating static chamber method were calculated using Eq. (5) (Zhou et al., 2019):

$$F = K \times \frac{V}{A} \times \frac{dc}{dt}, \tag{5}$$

where F is the emission flux (mg m^{-2} h^{-1}), V (m^3) and A (m^2) are the static chamber volume and surface area, respectively, dc/dt is the variation rate of the gas concentration (mg L^{-1} min^{-1}), and K is a scaling factor ($K = 6 \times 10^4$).

2.2.5 Statistical analysis

Statistical analysis was conducted using the SPSS 19.0 software (SPSS Inc., Chicago, USA). Any significant differences between the lakes were tested by conducting a one-

way analysis of variance (ANOVA). The criteria of $p < 0.05$ and $p < 0.01$ were used to determine the statistical significance at the 0.05 and 0.01 levels (two-tailed), respectively. The K-S test was carried out to check if the data was of a normal distribution. Multiple stepwise linear regression analysis was conducted to estimate the best predictors of the CH_4 and CO_2 emission fluxes.

2.3 Results

2.3.1 Physicochemical parameters of the overlying water

The environmental variables of the overlying water and sediments from the sampled lakes included field monitoring indicators and nutrient parameters. The characteristics of these indicators are shown in Table 1 and S1. During the study period, the temperature of the overlying water ranged from 27.2℃ to 31.3℃; thus, all lakes had a temperature of > 25℃ (Table S1). The physicochemical parameters exhibited large spatial variations and followed a trend corresponding to the trophic state (Table 1, S1). As shown in Table 1, the TN concentration displayed an increasing trend (from 0.6 to 3.4 mg L^{-1}), whereby the eutrophic state shifted from mesotrophic to hypereutrophic. The concentrations of NO_3^-, NH_4^+, TP, and chl-*a* also showed the same tendency. The TN and TP concentrations of the hyper-eutrophic lakes were approximately 5- and 3-times higher than those of the mesotrophic lakes, respectively. In particular, the chl-*a* concentration in the hyper-eutrophic lakes was approximately 13-times higher than that in the mesotrophic lakes (Table 1). Compared to overlying water parameters, the STN, STOC, and OM contents of the sampled sediments of eutrophic lakes were not significantly different from mesotrophic or hyper-eutrophic lakes ($p > 0.05$) (Table 1). However, the STN, STOC, and OM concentrations of sediments in the mesotrophic lakes were significantly lower than those of the hyper-eutrophic lakes ($p < 0.01$). In addition, the DO concentrations (8.2–5.6 mg L^{-1}) were negatively correlated with the TN concentration ($p < 0.05$) (Tables 1 and S2). There were no significant changes in the pH and DOC of the overlying water among the different trophic states. However, pH was significantly positively correlated with the

DO concentrations ($p < 0.05$). The *TLI* and the C:N ratio displayed a negative correlation in the overlying water ($R^2 = 0.75$, $p < 0.01$) (Fig. 2). The C:N ratio decreased with the shift from a mesotrophic to hyper-eutrophic state.

2.3.2 CH_4 and CO_2 emissions fluxes in different trophic lakes

During the study period, the CH_4 (0.1–351.9 mg m^{-2} h^{-1}) and CO_2 emission fluxes (−19.1–352.2 mg m^{-2} h^{-1}) exhibited large inter-lake variations for the different trophic states (Table S3 and Fig. 3). The highest CH_4 and CO_2 emission fluxes were measured in Lake Chaohu (CH), which is hyper-eutrophic (Fig. 3). The mean CH_4 emission flux from the mesotrophic, eutrophic, middle-eutrophic, and hyper-eutrophic lakes was 0.1, 4.4, 12.0, and 130.4 mg m^{-2} h^{-1}, respectively (Table S3); thus, the mean CH_4 emission flux from hyper-eutrophic lakes was approximately 1000-, 30-, and 10-times that from mesotrophic, eutrophic and middle-eutrophic lakes, respectively. With a shift in the trophic state from mesotrophic to hyper-eutrophic, the studied lakes functioned as a CH_4 source, whereby eutrophication accelerated the emission of CH_4. In addition, the mean CO_2 emission flux from hyper-eutrophic lakes was approximately 30-, 20-, and 4-times that of from mesotrophic, eutrophic, and middle-eutrophic lakes, respectively. It is interesting that this differed to the trend of the CH_4 emissions, as only the hyper-eutrophic lakes functioned as a complete source for CO_2 (Fig. 3b).

The CH_4 and CO_2 emission fluxes had positive correlations with the *TLI* (Fig. S1). The CH_4 emission flux displayed an exponential increase with the *TLI* in the studied lakes ($R^2 = 0.67$, $p < 0.01$) (Fig. S1a); meanwhile, the CO_2 emissions flux also had a significant exponential correlation ($R^2 = 0.50$, $p = 0.024$) (Fig. S1b). This was best fitted by a nonlinear exponential function to show the relationships between the mean CH_4 and CO_2 emission fluxes and *TLI* ($R^2 > 0.99$) (Fig. 4). It is clear that the CH_4 and CO_2 emission fluxes increased with an increase in the *TLI*, and that the hyper-eutrophic lakes acted as a very large source of CH_4 and CO_2 emissions.

2.3.3 Relationship between CH_4 and CO_2 emissions and environmental parameters

The correlations between the CH_4 and CO_2 fluxes and physicochemical parameters of the overlying water were analysed (Table S2). The CO_2 emission flux was strongly and significantly correlated with the CH_4 emission flux ($p < 0.01$). The CH_4 and CO_2 fluxes were significantly correlated with the TN, NO_3^-, NH_4^+, and chl-*a* concentrations of the overlying water ($p < 0.05$). However, the DO and pH of the overlying water were both significantly negatively correlated with the CO_2 emission flux ($p < 0.05$). In addition, the TP and DOC concentrations of the overlying water were not significantly correlated with the CH_4 and CO_2 emission fluxes ($p > 0.05$). Further analysis revealed that ln(CH_4) and CO_2 emission fluxes had significant, positive linear correlations with the TN ($R^2 = 0.50$, $p = 0.001$ for ln(CH_4); $R^2 = 0.33$, $p = 0.015$ for CO_2) and chl-*a* concentration ($R^2 = 0.60$, $p < 0.001$ for ln(CH_4); $R^2 = 0.48$, $p = 0.002$ for CO_2) (Fig. 5). The parameter of ln(CH_4) exhibited a significant, negative linear correlation with the C:N ration of the overlying water ($R^2 = 0.52$, $p = 0.001$). However, there was no significant correlation between the CO_2 emission flux and the C:N ratio of the overlying water ($p = 0.104$).

Multiple stepwise regression models incorporating the variables of the overlying water were established for the CH_4 and CO_2 emission fluxes (Table 2). The results showed that only NH_4^+-N could be used to predict CH_4 emissions ($R^2 = 0.74$, $p < 0.01$). In addition, NH_4^+-N and pH could jointly predict CO_2 emissions based on given samples ($R^2 = 0.68$, $p < 0.01$). Obviously, NH_4^+ ($t_1 = 3.86$) was more positively correlated with CO_2 emissions than pH ($t_2 = -2.66$), which suggests that pH was only a minor explanatory variable compared with NH_4^+.

2.3.4 Abundance and community of methanogens and methanotrophs in different trophic lakes

Methanogenic archaea and methanotrophic bacteria community structures at the genus level are summarised in Fig. 6. The relative abundance of methanogenic archaea increased between the mesotrophic and hyper-eutrophic lakes (Fig. 6a). The total relative abundance of methanogens in mesotrophic, eutrophic, mid-eutrophic, and hypereutrophic

states were 0.03%, 0.35%, 0.94%, and 1.17%, respectively. These methanogens were classified into five orders: *Methanosarcinales, Methanomicrobiales, Methanocelleales*, *Methanofastidiosales*, and *Methanobacteriales*. *Methanobacterium* (genus of the *Methanobacteriales* order) were found in lakes of different trophic states, and the mesotrophic lakes possessed *Methanobacterium* as the only genus. Clearly, the relative abundances of the orders *Methanosarcinales* and *Methanomicrobiales* in the hyper-eutrophic and middle-eutrophic lakes were higher than those of the eutrophic and mesotrophic lakes.

The relative abundance of methanotrophs did not show an obvious trend as observed for the methanogens. The relative abundance of methanotrophs in the middle-eutrophic lakes (2.27%) was higher than that at the hyper-eutrophic (1.28%), eutrophic (0.47%), and mesotrophic (0.75%) states. Aerobic methanotrophs dominated the assemblages, whereas anaerobic methanotrophs (e.g. the phylum *NC10*) had a very low total abundance. The relative abundances of different methanotrophs in the mesotrophic lakes were higher than those in the eutrophic lakes.

2.4 Discussion

2.4.1 Nonlinear response of CH_4 emissions from lakes of different trophic states

In recent years, studies have reported that freshwater lakes are a potential source of CH_4 emissions (Yang et al., 2011). The loadings of C and N in lakes gradually accumulate, and eventually, a hypereutrophic lake functions as a fermentation “tank”, thus resulting in increased CH_4 emissions. Our results showed that the mean CH_4 emission flux from each of the sampled lakes (except those classified as mesotrophic) was higher than the global mean CH_4 emission flux from freshwater ecosystems during summer (Table S3) (Bastviken et al., 2011). In particular, the mean CH_4 emission flux for the hyper-eutrophic lakes was approximately 300 times higher than the global mean CH_4 emission flux for freshwater ecosystems. Although numerous studies have demonstrated that lake eutrophication induces CH_4 emissions (Sepulveda-Jauregui et al., 2018; Beaulieu et al.,

2019), these studies did not summarise the CH_4 emission pattern across lakes with different trophic states. The pattern of the CH_4 fluxes from the lakes in the present study was consistent with the hypothesis that the CH_4 emission flux increases as the trophic state shifts from mesotrophic to hyper-eutrophic. Surprisingly, compared with lakes of a lower level of eutrophication in this study, the CH_4 emission flux from hyper-eutrophic lakes was extremely high, thus indicating a nonlinear increase of CH_4 release with increasing eutrophication (Fig. S1a). Moreover, the CO_2 flux exhibited a very similar pattern to that of the CH_4 flux (Fig. S1b). As the *TLI* is robust means for quantifying the trophic state of lakes, it is possible to propose a nonlinear model to estimate the CH_4 and CO_2 emissions using the *TLI* (Fig. 4). Beaulieu et al. (2019) proposed a simplistic upscaling method to describe a global CH_4 emission rate without considering the driving mechanisms, which may cause large uncertainties with respect to estimated global CH_4 emissions. Given that lakes can have similar characteristics (i.e. latitudinal, geographic, and morphological conditions), our results indicate that multiple driving factors co-regulate CH_4 emissions, and that the pattern of CH_4 emissions follows a nonlinear increase with the increasing trophic level of lakes.

2.4.2 Environmental factors driving CH_4 emissions in shallow lakes

Variations in the organic matter content and redox conditions in lakes are key aspects for regulating the biological release of CH_4. First, it is necessary to emphasise that nutrient and organic matter overloading facilitates high CH_4 emissions. The lakes that were investigated in this study were classified into four trophic states, and the results showed that the mean CH_4 emission flux from mesotrophic lakes was significantly lower than that from the lakes of other trophic states (Table S3). This suggests that nutrients are the most basic substrate source for CH_4 production processes. Lake eutrophication is induced by the accumulation of excess nutrients in waterbodies, thereby leading to a large amount of nutrient and carbon fixation by excessive algal growth with subsequent contributions to the sedimentary organic pool after the algae collapse (Table 1 and S1) (Yan et al., 2017). This can also be confirmed by the decreased C:N ratio in the overlying water with the

increase of the *TLI* (Fig. 2) because autochthonous primary production in lakes has a very low C:N ratio (Meyers, 1994). Therefore, our results reveal the non-negligible contribution of autochthonous primary production (i.e. accumulated algae) to hyper-eutrophication in lakes and CH_4 emissions (Figs. 5b and 5c). This trend is consistent with previous studies that found that high aquatic primary productivity caused by the overloading of nutrients drives the increase in CH_4 emission fluxes (Huttunen et al., 2002; Bastviken et al., 2004; Furlanetto et al., 2012).

In several lakes, a positive correlation between $\ln(CH_4)$ and chl-*a* (Fig. 5b) was observed. It is known that chl-*a* can act as a proxy for algal productivity (Liikanen and Martikainen, 2003), which is consistent with Beaulieu et al. (2019), who showed that CH_4 emissions were positively correlated with productivity variables in lakes. For instance, the continual accumulation of algae blooms have been found to be a crucial factor that triggers higher emission CH_4 fluxes in eutrophic lakes (Yan et al., 2017). Correspondingly, it has been widely observed that large algae blooms always occur in the hypereutrophic lakes during the summer (Xu, et al., 2004; Chen, et al., 2014; Yan, et al., 2017). In hypereutrophic lakes, algae are a crucial driver for the accumulation of organic matter. For example, Xu et al. (2019b) found that at least 50% of the accumulated organic matter in Lake Taihu was from algae. Therefore, the overloading of nutrients and the subsequent algae growth are crucial drivers for CH_4 emissions. Ultimately, these relationships reflect the link between an increase in the organic substrate and enhanced rates of methanogenesis in shallow lakes.

The accumulation of organic substrates in lakes is bound to change the microenvironment of the lake. Correspondingly, the alteration of factors such as DO, pH, and temperature in microenvironments can affect the CH_4 emissions from freshwater lakes. It has been well documented that low DO and high temperature conditions facilitate the emission of CH_4 (Xing et al., 2005; Duc et al., 2010). In the present study, the highest DO concentrations in surface waters were observed in the mesotrophic lakes, which had the lowest mean CH_4 emission flux. A close relationship between DO and pH was

observed in this study ($p < 0.05$). Obviously, hypoxia and sufficient organic matter are prerequisites for fermentation. Subsequently, the processes of fermentation and acid production affect the pH levels in the water column, and accelerate oxygen consumption (Yan et al., 2017). These biotic processes involve methanogenesis. Therefore, the accumulated labile organic matter in eutrophic lakes is rapidly consumed with oxygen, which still leaves a large amount of substrate for methanogenesis.

In this study, the relative abundance of methanogens in the mesotrophic lakes was lower than that in the lakes with a higher level of eutrophication, which was in accordance with the CH_4 emissions (Fig. 6). The fermentation processes involved in methanogenesis are generally affected by the quality and quantity of organic matter that contribute to fermentation (Zhou et al., 2018). A recent study found that the quantity rather than the quality of organic matter was a limiting factor for CH_4 emissions, which suggests that autochthonous organic matter is a significant contributor to CH_4 emissions (Grasset et al., 2018). This is consistent with our study, whereby the lower CH_4 emissions were found in the mesotrophic lakes that contained a lower organic matter content than the lakes of a higher trophic state (Table 1).

The emission process of CH_4 is controlled by a combination of production by methanogens and oxidation by methanotrophs (Borrel et al., 2011). Aerobic and anaerobic methanotrophs had relatively high abundances in the middle-eutrophic lakes, especially in Lake Honghu (HH) (Fig. 6b). This is consistent with Yang et al. (2019) who found that high methanotroph abundances were induced by eutrophication. As a consumer of CH_4, methanotrophs significantly reduced the CH_4 emissions in the middle-eutrophic lakes in comparison to the hyper-eutrophic lakes, which had substantial CH_4 emissions and comparatively higher methanogens and lower methanotrophs abundances (Fig. 6). A high relative abundance of methanotrophs is likely to occur under high DO concentrations. Previous studies have considered that oxygen availability is a major factor affecting the regulation of methanotrophic activity (Borrel et al., 2011; Yang et al., 2019). In the present investigation, the DO concentration of the middle-eutrophic lakes was significantly

higher than that of the hyper-eutrophic lakes (Tale 1 and S1). Therefore, the high relative abundance of methanotrophs in the middle-eutrophic lake contributed to the process of CH_4 consumption, which is also consistent with previous studies (Yang et al., 2019). Moreover, the present study also suggests that the overloading of NH_4^+-N, which can easily occur under low oxygen conditions, contributed to the limitation of methanotrophic activity (Bosse et al., 1993). Therefore, the production and emission of CH_4 were determined by the abundances of methanogens and methanotrophs, which were affected by the surrounding redox conditions.

To explore the potential drivers of CH_4 and CO_2 emissions, a stepwise linear regression involving all environmental variables indicated that CH_4 and CO_2 emissions could be well-predicted by the NH_4^+-N concentration trend for lakes of different trophic states, as evidenced by their strong correlations (Table 2). This finding agrees with previous studies that showed that NH_4^+-N, CH_4, and CO_2 are simultaneously produced during mineralisation processes (Furlanetto et al., 2014; Yan et al., 2017). It is worth mentioning that the process of organic matter mineralisation involves the formation of NH_4^+-N, which is easily oxidised by methane monooxygenase and hence retards the CH_4 oxidation rate (Holmes et al., 1995; He et al., 2019b; Yan et al., 2019). During CH_4 oxidation, the accumulated and decomposed algae probably provide an important source of autochthonous organic matter in hyper-eutrophic lakes. Bastviken et al. (2015) suggested that anaerobic carbon mineralisation accounts for 20–60% of the overall mineralisation in aquatic ecosystems. Autochthonous organic matter, especially algae, are closely connected with CH_4 production (Chen et al., 2016). In addition, the decomposition, fermentation, and mineralisation processes also involve strong CO_2 emissions, which were significantly and positively correlated with the CH_4 emissions in this study ($p < 0.01$) (Table S2). Therefore, the availability of organic matter produced from nutrients is a primary factor for the CH_4 production that is linked to biotic processes.

2.4.3 Relationship between eutrophication and CH_4 emissions: Implications for

climate change

To date, many studies have discussed the impact and feedback of climate change on lake eutrophication processes. In particular, hypereutrophic lakes are known to play a crucial role as a sink for GHGs (Sepulveda-Jauregui et al., 2018; Beaulieu et al., 2019). Our findings evidence the change that occurs in CH_4 emissions with lake eutrophication, whereby a nonlinear model was proposed to describe the CH_4 emissions (Fig. 4) across a gradient from mesotrophic to hypertrophic lakes (and increasing *TLI*). The dramatic increase in CH_4 emissions from the hyper-eutrophic lakes is probably related to the simultaneous shift from a clear-water state to a turbid-water algae-dominated state. The results further emphasise that phytoplankton biomass, as induced by excess nutrients (Lau and Lane, 2002), is a potential facilitator driving increased CH_4 emissions in eutrophic lakes. The combination of our results with those of previous studies (Yan et al., 2017; Zhou et al., 2018; Yan et al., 2019) indicates that the algae decomposition process, which easily occurs in hyper-eutrophic lakes, provides abundant organic matter and suitable microenvironments for methanogenesis. The CH_4 emission flux from each lake of a different typical trophic state was estimated using our conceptual model based on the *TLI* index and CH_4 emission flux. Given that the mean *TLI* for the mesotrophic, eutrophic, middle-eutrophic, and hyper-eutrophic lakes were 45, 55, 65, and 75, respectively, the CH_4 emissions would increase by a factor of ~10 for each increase in the trophic level. Therefore, it is extremely important that an accurate model (incorporating key driving factors) can estimate the CH_4 emission flux from lakes with different trophic states. Further research regarding GHG emissions should consider a parameterised conceptual model for shallow lakes that includes potential drivers such as nutrients, sediment organic matter, and DO. Additionally, it should be noted that the model in the present study is only applicable during the summer and that CH_4 emissions most likely vary seasonally; hence, this aspect requires further study.

2.5 Conclusions

In this study, we investigated the CH_4 emission flux and environmental variables across different lakes along a trophic state gradient of the Yangtze River basin, China. This is the first study to elucidate the nonlinear response of the release of CH_4 from shallow lakes along a gradient of increasing eutrophication. An increase in the *TLI* of a lake by one level (*e.g.,* from mesotrophic to eutrophic) would correspond to a 10-fold increase in CH_4 emissions. This phenomenon is related to the fact that the accumulated nutrients and subsequent production of algae organic matter are the crucial drivers for the microbial community responsible for the CH_4 emissions from lakes. In addition, the decomposition of algae makes a significant contribution to the CH_4 emissions from eutrophic lakes, especially hyper-eutrophic lakes. Correspondingly, the NH_4^+ concentration in the water column can be used to predict the CH_4 emissions from lakes. Thus, our results strongly suggest that the eutrophication of lakes not only causes a deterioration in water quality, but also has a positive feedback effect on the global greenhouse effect.

2.6 References

Bastviken, D., Cole, J., Pace, M.L., Tranvik, L.J., 2004. Methane emissions from lakes: dependence of lake characteristics, two regional assessments, and a global estimate. Global Biogeochemical Cycles 18, 1-12.

Bastviken, D., Cole, J.J., Pace, M.L., Van de Bogert, M.C., 2008. Fates of methane from different lake habitats: Connecting whole-lake budgets and CH_4 emissions. Journal of Geophysical Research 113, 61-74.

Bastviken, D., Tranvik, L.J., Downing, J.A., Crill, P.M., Enrich-Prast, A., 2011. Freshwater methane emissions offset the continental carbon sink. Science 311, 50.

Beaulieu, J.J., DelSontro, T., Downing, J.A., 2019. Eutrophication will increase methane emissions from lakes and impoundments during the 21st century. Nature Communication 10, 1375.

Borrel, G., Jezequel, D., Biderre-Petit, C., Morel-Desrosiers, N., Morel, J.P., Peyret, P.,

Fonty, G., Lehours, A.C., 2011. Production and consumption of methane in freshwater lake ecosystems. Research in Microbiology 162, 832-847.

Bosse, U., Frenzel, P., Conrad, R., 1993. Inhibition of methane oxidation by ammonium in the surface layer of a littoral sediment. FEMS Microbiology Ecology 13, 123-134.

Carlson, R.E., 1997. A trophic state index for lakes. Limnology and Oceanography 22, 361-369.

Chen, Y., Liu, Q., 2014. On the horizontal distribution of algal-bloom in Chaohu Lake and its formation process. Acta. Mechanica sincia 30(5), 656-666.

Chen, Y., Dong, S., Wang, F., Gao, Q., Tian, X., 2016. Carbon dioxide and methane fluxes from feeding and no-feeding mariculture ponds. Environmental Pollution 212, 489-497.

Chen, Y., Jiang, X., Xiao, K., Shen, N., Zeng, R.J., Zhou, Y., 2017. Enhanced volatile fatty acids (VFAs) production in a thermophilic fermenter with stepwise pH increase - Investigation on dissolved organic matter transformation and microbial community shift. Water Research 112, 261-268.

Cole, J.J., Bade, D.L., Bastviken, D., Pace, M.L., Van de Bogert, M., 2010. Multiple approaches to estimating air-water gas exchange in small lakes. Limnology and Oceanography-Methods 8, 285-293.

DelSontro, T., Beaulieu, J.J., Downing, J.A., 2018. Greenhouse gas emissions from lakes and impoundments: upscaling in the face of global change. Limnology and Oceanography-Letter 3, 64–75.

Dunfield, P., Knowles, R., Dumont, R., Moore, T.R., 1993. Methane production and consumption in temperate and subarctic peat soils: Response to temperature and pH. Soil Biology and Biochemistry 25(3),321-326.

Duc, N.T., Crill, P., Bastviken, D., 2010. Implications of temperature and sediment characteristics on methane formation and oxidation in lake sediments. Biogeochemistry 100(1-3), 185-196.

Furlanetto, L.M., Marinho, C.C., Palma-Silva, C., Albertoni, E.F., FigueiredoBarros, M.P.,

Esteves, F.A., 2012. Methane levels in shallow subtropical lake sediments: dependence on the trophic status of the lake and allochthonous input. Limnologica 42, 151-155.

Gålfalk, M., Bastviken, D., Fredriksson, S., Arneborg, L., 2013. Determination of the piston velocity for water-air interfaces using flux chambers, acoustic Doppler velocimetry, and IR imaging of the water surface. Journal of Geophysical Research-Biogeosciences 118, 770-782.

Grasset, C., Mendonça, R., Saucedo, G.V., Bastviken, D., Roland, F., 2018. Large but variable methane production in anoxic freshwater sediment upon addition of allochthonous and autochthonous organic matter. Limnology and Oceanography 63(4), 1488-1501.

Gong, M., Yang, G., Zhuang, L., Zeng, E.Y., 2019. Microbial biofilm formation and community structure on low-density polyethylene microparticles in lake water microcosms. Environmental Pollution 252, 94-102.

Henckel, T., Roslev, P., Conrad, R., 2000. Effects of O_2 and CH_4 on presence and activity of the indigenous methanotrophic community in rice field soil. Environmental Microbiology 2(6), 666-679.

He, Z., Xu, S., Zhao, Y., Pan, X., 2019a. Methane emissions from aquous sedimets are influenced by complex interactions among microbes and environmental factors: A modeling study. Water Research 166, 115086.

He, Z., Wang, J., Hu, J., Yu, H., Jetten, M.S.M., Liu, H., Cai, C., Liu, Y., Ren, H., Zhang, X., Hua, M., Xu, X., Zheng, P., Hu, B., 2019b. Regulation of coastal methane sinks by a structured gradient of microbial methane oxidizers. Environmental Pollution 244, 228-237.

Holgerson, M.A., Raymond, P. 2016. Large contribution to inland water CO2 and CH4 emissions from very small ponds. Nature Geoscience 9, 222–226.

Holems, A.J., Costello, A., Lidstrom, M.E., Murrell, J.C, 1995. Evidence that participate methane monooxygenase and ammonia monooxygenase may be evolutionarily

related. FEMS Microbiology Letter 132, 203-208.

Huttunen, J.T., Väisänen, T.S., Hellsten, S.K., Heikkinen M., Nykänen, H., Jungner, H., Niskanen, A., Virtanen, M.O., Lindqvist, O.V., Nenonen, O.S., Martikainen, P.J., 2002. Fluxes of CH_4, CO_2, and N_2O in hydroelectric reservoirs Lokka and Porttipahta in the northern boreal zone in Finland. Global Biogeochemical Cycle 16(1), 3-1-3-17.

IPCC. 2014. Climate change 2014 synthesis report summary chapter for policymakers. Ipcc 31.

Lau, S.S.S., Lane, S.N., 2002. Biological and chemical factors influencing shallow lake eutrophication: a long-term study. Science of the Total Environment 228, 167-181.

Liikanen, A., Martikainen, P.J., 2003. Effect of ammonium and oxygen on methane and nitrous oxide fluxes across sedimentewater interface in a eutrophic lake. Chemosphere 52, 1287-1293.

Li, S., Bush, R.T., Santos, I.R., Zhang, Q., Song, K., Mao, R., Wen, Z., Lu, X., 2018. Large greenhouse gases emissions from China's lakes and reservoirs. Water Research 147, 13-24.

Liu, X., Shi, C., Xu, X., Li, X., Xu, Y., Huang, H., Zhao, Y., Zhou, Y., Shen, H., Chen, C., Wang, G., 2017. Spatial distributions of b-cyclocitral and b-ionone in the sediment and overlying water of the west shore of Taihu Lake. Science of the Total Environment 579, 430-438.

Lofton, D.D., Whalen, S.C., Hershey, A.E., 2014. Effect of temperature on methane dynamics and evaluation of methane oxidation kinetics in shallow Arctic Alaskan lakes. Hydrobiologia 721, 209-222.

Jin, X., 1995. Lake environment in China. Ocean Press, Beijing.

Juutinen, S., Rantakari, M., Kortelainen, P., Huttunen, J.T., Larmola, T., Alm, J., Silvola, J., Martikainen, P.J., 2009. Methane dynamics in different boreal lake types. Biogeosciences 6, 209-223.

Marotta, H., Pinho, L., Gudasz, C., Bastviken, D., Tranvik, L.J., Enrich-Prast, A., 2014.

Greenhouse gas production in low-latitude lake sediments responds strongly to warming. Nature Climate Change 4, 467-470.

Meyers, P.A., 1994. Preservation of elemental and isotopic source identification of sedimetary organic matter. Chemical Geology 114, 289-302.

Musenze, R.S., Fan, L., Grinham, A., Werner, U., Gale, D., Udy, J., Yuan, Z., 2016. Methane dynamics in subtropical freshwater reservoirs and the mediating microbial communities. Biogeochemistry 128, 233-255.

Ortiz-Llorente, M.J., Alvarez-Cobelas, M., 2012. Comparison of biogenic methane emissions from unmanaged estuaries, lakes, oceans, rivers and wetlands. Atmospheric Environment 59, 328-337.

Palma-Silva, C., Marinho, C.C., Albertoni, E.F., Giacomini, I.B., Barros, M.P.F., Furlanetto, L.M., Trinadada, C.R.T., Esteves, F., 2013. Methane emissions in two small shallow neotropical lakes: The role of temperature and trophic level. Atmospheric Environment 81, 373-379.

Rinta, P., Bastviken, D., van Hardenbroek, M., Kankaala, P., Leuenberger, M., Schilder, J., Stötter, T., Heiri, O., 2015. An inter-regional assessment of concentrations and $\delta^{13}C$ values of methane and dissolved inorganic carbon in small European lakes. Aquatic Science 77, 667-680.

Schilder, J., van Hardenbroek, M., Bodelier, P., Kirilova, E., Leuenberger, M., Lotter, A., Heiri, O., 2017. Trophic state changes can affect the importance of methane-derived carbon in aquatic food webs. Proceedings of the Royal Society B 284, 20170278.

Sepulveda-Jauregui, A., Hoyos-Santillan, J., Martinez-Cruz, K., Walter Anthony, K.M., Casper, P., Belmonte-Izquierdo, Y., Thalasso, F., 2018. Eutrophication exacerbates the impact of climate warming on lake methane emission. Science of the Total Environment 636, 411-419.

Stoddard, J.L., Sickle, J.V., Herlihy, A.T., Brahney, J., Paulsen, S., Peck, D.V., Mitchell, R., Pollard. A.I., 2016. Continental-scale increase in lake and stream phosphorus: are oligotrophic systems disappearing in the United States? Environmental Science

& Technology 50, 3409–3415.

Wu, L., Wu, X., Lin, S., Wu, Y., Tang, S., Zhou, M., Shaaban, M., Zhao, J., Hu, R., Kuzyakov, Y., Wu, J., 2018. Carbon budget and greenhouse gas balance during the initial years after rice paddy conversion to vegetable cultivation. Science of the Total Environment 2018, 627, 46-56.

Xing, Y., Xie, P., Yang, H., Ni, L., Wang, Y., Rong, K., 2005. Methane and carbon dioxide fluxes from a shallow hypereutrophic subtropical Lake in China. Atmospheric Environment 39(30), 5532-5540.

Xu, J., Zhang, M., Xie, P., 2007. Stable carbon isotope variations in surface bloom scum and subsurface seston among shallow eutrophic lakes. Harmful Algae 6(5), 679-685.

Xu, X., Zhou, Y., Han, R., Song, K., Zhou, X., Wang, G., Wang, Q., 2019a. Eutrophication triggers the shift of nutrient absorption pathway of submerged macrophytes: Implications for the phytoremediation of eutrophic waters. Journal of Environmental Management 239, 376-384.

Xu, J., Lyu, H., Xu, X., Li, Y., Li, Z., Lei, S., Bi, S., Mu, M., Du, C., Zeng, S., 2019b. Dual stable isotope tracing the source and composition of POM during algae blooms in a large and shallow eutrophic lake: All contributions from algae? Ecology Indictors 102, 599-607.

Yan, X., Xu, X., Ji, M., Zhang, Z., Wang, M., Wu, S., Wang, G., Zhang, C., Liu, H., 2019. Cyanobacteria blooms: A neglected facilitator of CH_4 production in eutrophic lakes. Science of the Total Environment 651, 466-474.

Yan, X., Xu, X., Wang, M., Wang, G., Wu, S., Li, Z., Sun, H., Shi, A., Yang, Y., 2017. Climate warming and cyanobacteria blooms: Looks at their relationships from a new perspective. Water Research 125, 449-457.

Yang, Y., Chen, J., Tong, T., Li, B., He, T., Liu, Y., Xie, S., 2019. Eutrophication influences methanotrophic activity, abundance and community structure in freshwater lakes. Science of the Total Environment 662, 863-872.

Yang, H., Xie, P., Ni, L., Flower, R.J., 2011. Underestimation of CH_4 emission from

freshwater lakes in China. Environmental Science & Technology 45, 4203-4204.

Yvon-Durocher, G., Allen, A.P., Bastviken, D., Conrad, R., Gudasz, C., St-pierre, A., Thanh-Duc, N., Giorgio, P.A., 2014. Methane fluxes show consistent temperature dependence across microbial to ecosystem scales. Nature 507, 488-491.

Zeng, Z., Guo, X., Xu, P., Xiao, R., Huang, D., Gong, X., Cheng, M., Yi, H., Li, T., Zeng, G., 2018. Responses of microbial carbon metabolism and fuction diversity induced by complex fugal enzymes in lignocelulosic waste composting. Science of the Total Environment 64, 539-547.

Zhang, J., Ni, W., Luo, Y., Stevenson, R.J., Qi, J., 2011. Respose of freshwater algae to water quality in Qinshan Lake within Taihu Watershed, China. Physics and Chemistry of the Earth 36, 360-365.

Zhuang, Q., Melack, J.M., Zimov, S., Walter, K.M., Butenhoff, C.L., Khalil, M.A.K., 2009. Global methane emissions from wetlands, rice paddies, and lakes. Eos, Transactions American Geophysical Union, 90, 37-38.

Zhou, Y., Xiao, Q., Yao, X., Zhang, Y., Zhang, M., Shi, K., Lee, X., Podgorski, D.C., Qin, B., Spencer, R.G.M., Jeppesen, E., 2018. Accumulation of terrestrial dissolved organic matter potentially enhances dissolved methane levels in eutrophic Lake Taihu, China. Environmental Science & Technology 52, 10297-10306.

Zhou, Y., Xu, X., Han, R., Li, L., Feng, Y., Yeerken, S., Song, K., Wang, Q., 2019. Suspended particles potentially enhance nitrous oxide (N_2O) emissions in the oxic estuarine waters of eutrophic lakes: Field and experimental evidence. Environmental Pollution 252, 1225-1234.

Tables and figures

Table 1 Abiotic variables of the water column and sediment in each type of eutrophic lake. Values are presented as the mean ± standard deviation.

Eutrophic state *TLI* (∑)	DO (mg L^{-1})	pH	TN (mg L^{-1})	NO_3^--N (mg L^{-1})	NH_4^+-N (mg L^{-1})	TP (mg L^{-1})	DOC (mg L^{-1})	chl-*a* (μg L^{-1})	STN (g kg^{-1})	STOC (g kg^{-1})	OM (g kg^{-1})
Mesotrophic (≤ 50)	8.2±0.8	7.9±0.6	0.6±0.1	0.1±0.1	0.3±0.1	0.1±0.1	5.6±0.4	7.1±1.8	0.9±0.5	28.6±13.5	49.2±23.1
Eutrophic (50 – 60)	8.0±1.1	8.3±0.8	1.2±0.2	0.2±0.2	0.5±0.2	0.2±0.2	6.5±2.2	15.6±4.9	1.5±0.4	36.0±17.5	62.1±30.1
Middle-eutrophic (60 – 70)	6.8±2.3	7.9±0.6	1.4±0.5	0.5±0.4	0.6±0.2	0.2±0.2	5.0±1.5	41.9±10.7	2.0±0.5	31.5±9.5	54.3±16.3
Hyper-eutrophic (> 70)	5.6±2.0	7.8±0.7	3.4±0.6	1.7±0.5	1.1±0.3	0.3±0.1	6.4±1.1	92.7±19.4	2.4±0.3	41.3±18.0	71.1±31.1

Table 2. Multiple stepwise linear regression model of CH_4 and CO_2 emission fluxes incorporating the variables of the overlying water

Parameters	Equations	Adj. R^2	*p*	Significance level		
				F-test	T-test	
				F	t_1	t_2
CH_4	$\ln(CH_4) = 7.181(NH_4^+\text{-N}) – 3.454$	0.74	< 0.01	43.37	6.59	-
CO_2	$CO_2 = 174.66(NH_4^+\text{-N}) – 60.51(pH) + 417.23$	0.68	< 0.01	15.05	3.86	−2.66

CH_4 (mg m^{-2} h^{-1}), CO_2 (mg m^{-2} h^{-1}), and NH_4^+-N (mg L^{-1}).

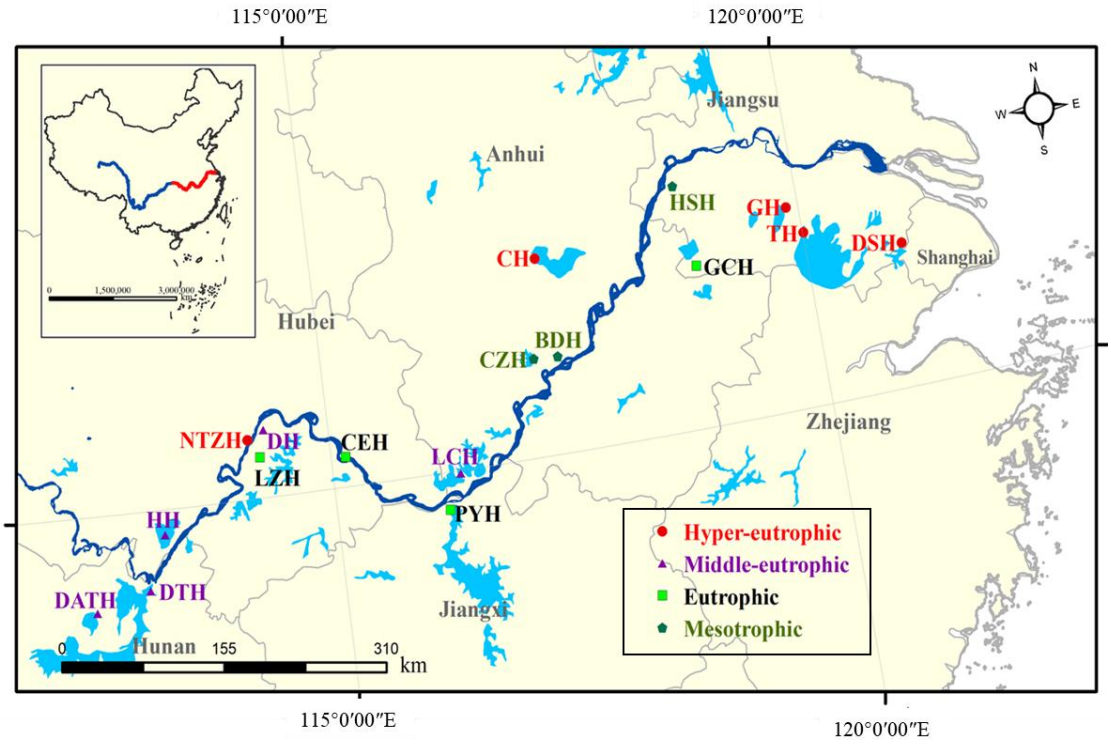

Fig. 1 Distribution of sampling sites in the middle and lower reaches of the Yangtze River basin, China. DSH: Lake Dianshang; TH: Lake Taihu; GH: Lake Gehu; GCH: Lake Gucheng; HSH: Lake Huashen; CH: Lake Chaohu; BDH: Lake Baidang; CZH: Lake Caizi; LGH: Lake Longgan; PYH: Lake Poyang; CEH: Lake Cehu; DH: Lake Donghu; LZH; Lake Liangzi; NTZH; Lake Nantaizi; HH: Lake Honghu; DTH; Lake Dongting; DATH: Lake Datong.

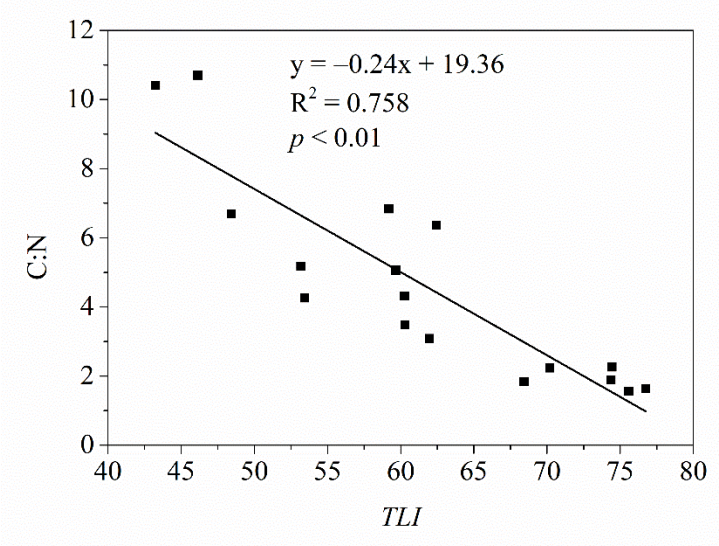

Fig. 2 Relationship between the *TLI* and C:N in the sampled lakes.

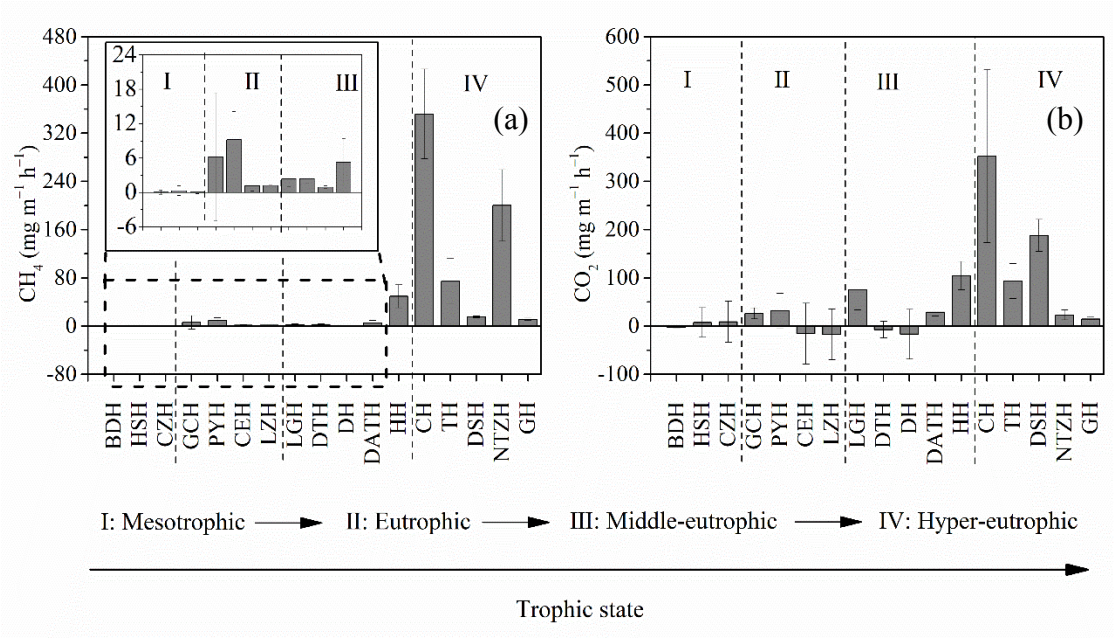

Fig. 3 Net CH_4 (a) and CO_2 (b) emissions at the water–air interface for the 17 sampled lakes. Values are as the mean ± standard deviation.

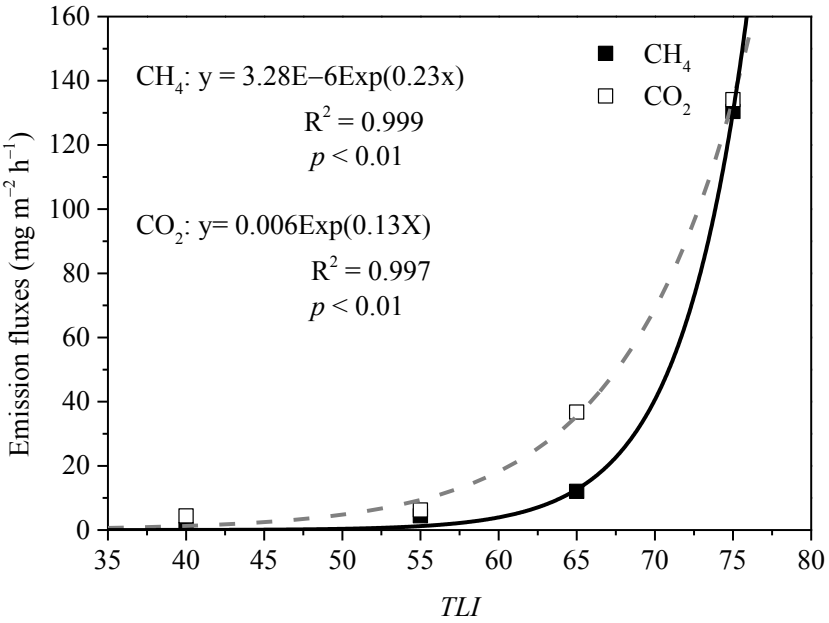

Fig. 4 Mean CH_4 (solid line) and CO_2 (dashed line) emissions for four categories of lakes (mesotrophic, eutrophic, middle-eutrophic, and hypereutrophic) based on their *TLI* values.

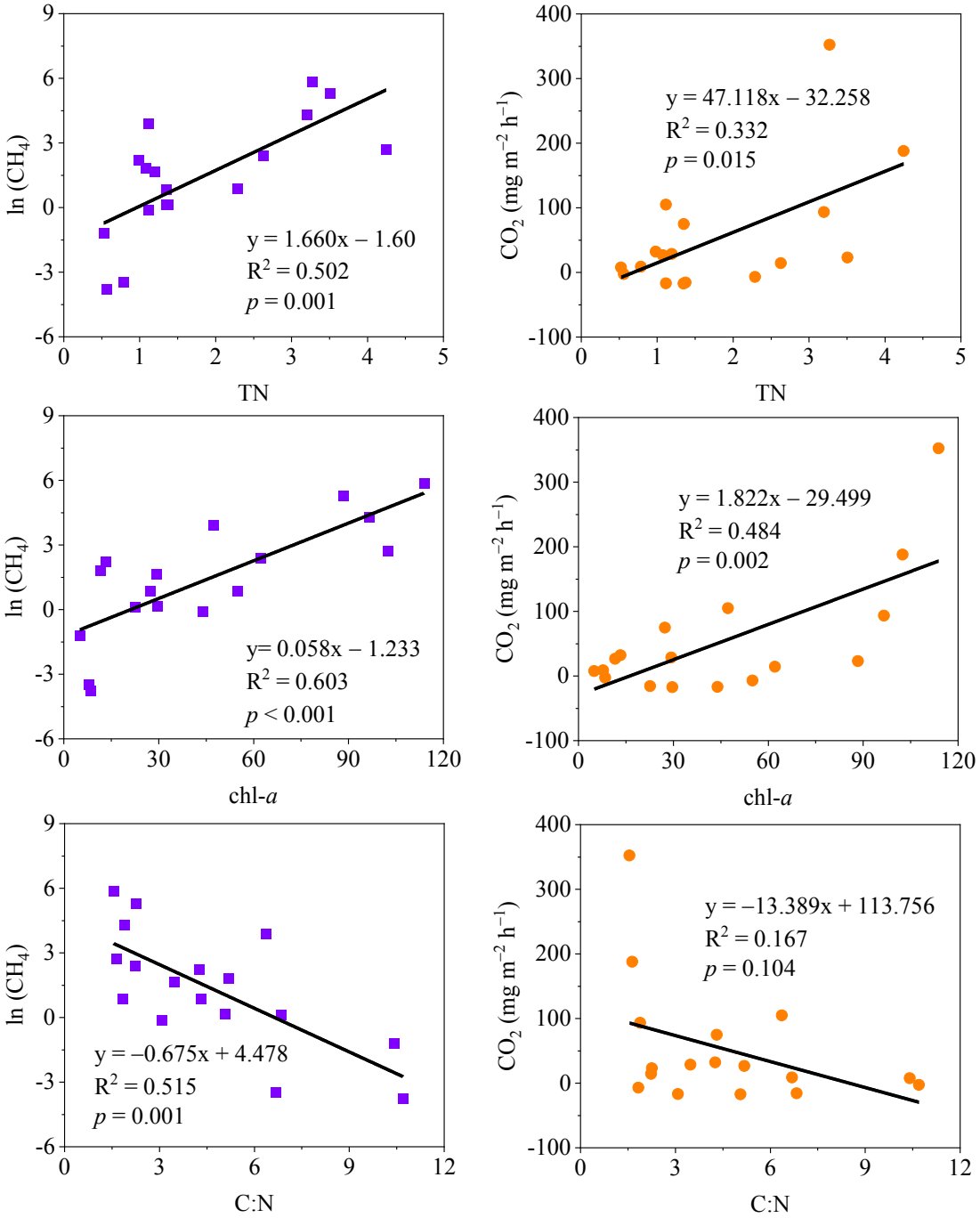

Fig. 5 Relationships between environmental factors and greenhouse gas (CH_4 and CO_2) emissions in shallow lakes.

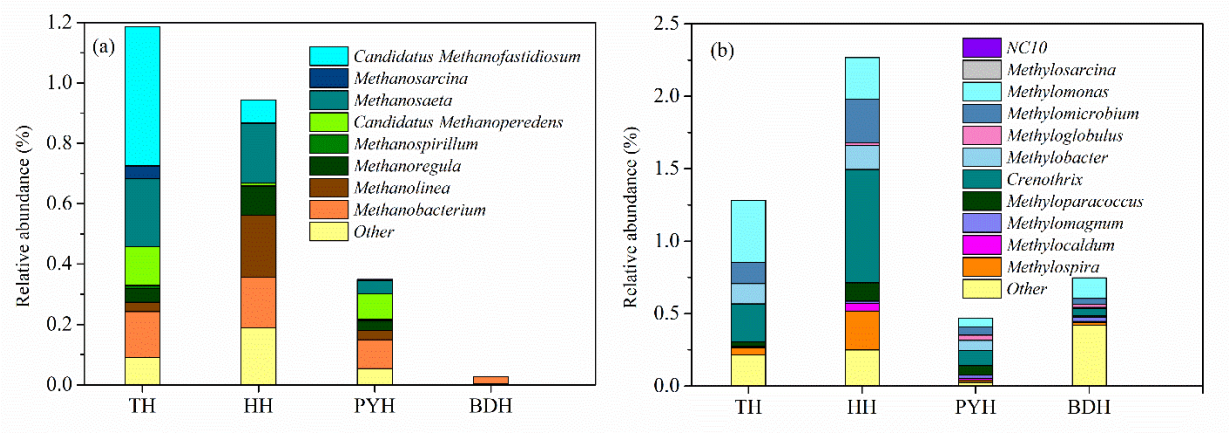

Fig. 6 Relative abundance of methanogen (a) and methanotroph (b) bacteria community compositions at the genus level in different trophic lakes. Lake Baidang (BDH), Lake Poyang (PYH), Lake Honghu (HH), and Lake Taihu (TH) represent mesotrophic, eutrophic, middle-eutrophic, and hyper-eutrophic lakes, respectively.

Supporting materials

Table S1 Physiochemical parameters of each lake in the middle and lower reaches of the Yangtze River region, China.

Lakes	TN (mg L^{-1})	TP (mg L^{-1})	NO_3^--N (mg L^{-1})	NH_4^+-N (mg L^{-1})	DOC (mg L^{-1})	chl-*a* (μg L^{-1})	Temperature (°C)	pH	DO (mg L^{-1})	*TLI*	Mean depth (m)	Eutrophic state
BDH	0.5	0.17	0.06	0.35	5.5	8.5	30.7	8.5	9.08	46.14	3.1	
HSH	0.6	0.12	0.04	0.34	6.0	5.0	30.4	7.8	7.46	43.26	< 7	Mesotrophic lake
CZH	0.8	0.04	0.26	0.32	5.3	7.8	29.4	7.3	8.00	48.43	3	
GCH	1.1	0.14	0.14	0.86	5.6	11.6	29.7	7.9	7.07	53.18	1.6	
PYH	1.0	0.13	0.52	0.45	4.2	13.3	28.6	7.6	6.95	53.43	5.1	Eutrophic lake
CEH	1.4	0.43	0.11	0.45	9.4	22.7	30.4	9.1	8.92	59.19	2	
LZH	1.2	0.04	0.10	0.35	6.8	29.7	29.6	8.9	8.91	59.66	3	
LGH	1.4	0.08	0.48	0.70	5.8	27.4	27.2	7.6	6.30	60.27	3.7	
DTH	2.3	0.13	1.18	0.45	4.2	55.0	28.2	8.0	9.20	68.43	5.5	
DH	1.1	0.16	0.47	0.44	3.4	44.0	28.7	8.7	9.25	61.96	2.5	Middle-eutrophic lake
DATH	1.3	0.46	0.39	0.69	4.2	29.4	27.4	8.1	4.72	60.30	2.6	
HH	1.1	0.16	0.18	0.77	7.1	47.3	27.1	7.2	4.59	62.44	1.3	
CH	3.3	0.31	1.52	1.34	5.1	113.9	31.3	7.4	5.41	75.59	2.9	
TH	3.2	0.32	1.77	0.93	6.0	96.6	29.6	7.3	3.93	74.38	1.9	
DSH	4.3	0.36	2.40	1.00	7.0	102.5	30.7	7.3	3.73	76.74	2.1	Hyper-eutrophic lake
NTZH	3.6	0.39	1.61	1.30	7.9	88.4	29.3	8.8	6.56	74.45	2	
GH	2.7	0.33	0.92	0.71	5.9	62.2	30.6	8.5	8.44	70.19	1.3	

Table S2 Correlations between variables and GHGs emission fluxes.

	CH_4	CO_2	TN	NO_3^-	NH_4^+	TP	chl-*a*	DOC	*TLI*	DO	pH
CH_4	1										
CO_2	0.749**	1									
TN	0.556*	0.582*	1								
NO_3^-	0.497*	0.591*	0.965**	1							
NH_4^+	0.789**	0.722**	0.786**	0.716**	1						
TP	0.344	0.269	0.587*	0.473	0.553*	1					
chl-*a*	0.689**	0.696**	0.941**	0.810**	0.533*	0.405	1				
DOC	0.096	0.000	0.236	0.115	0.219	0.377	0.143	1			
TLI	0.546*	0.545*	0.921**	0.843**	0.755**	0.566*	0.944**	0.169	1		
DO	-0.349	-0.657**	-0.486*	-0.549*	-0.663**	-0.425	-0.585*	-0.081	-0.408	1	
pH	-0.165	-0.587*	-0.158	-0.344	-0.280	0.158	-0.256	0.275	-0.067	0.691**	1

Significant correlation at the *$p < 0.05$ and **$p < 0.01$ levels.

Table S3 Mean CH_4 and CO_2 emission fluxes in each type of eutrophic lake

Types	Mesotrophic			Eutrophic			Middle-eutrophic			Hyper-eutrophic		
	Range	Mean	SD	Range	Mean	SD	Range	Mean	SD	Range	Mean	SD
CH_4 (mg m^{-2} h^{-1})	0.1-0.3	0.1	0.2	1.1-9.2	4.4	4.0	0.9-49.3	12.0	20.9	11.2-351.9	130.4	145.5
CO_2 (mg m^{-2} h^{-1})	−2.9-8.7	4.4	6.4	−17.5-31.9	6.2	26.6	−16.8-104.6	36.7	52.2	14.4-352.2	134.1	140.4

-)Exp(0.14x)

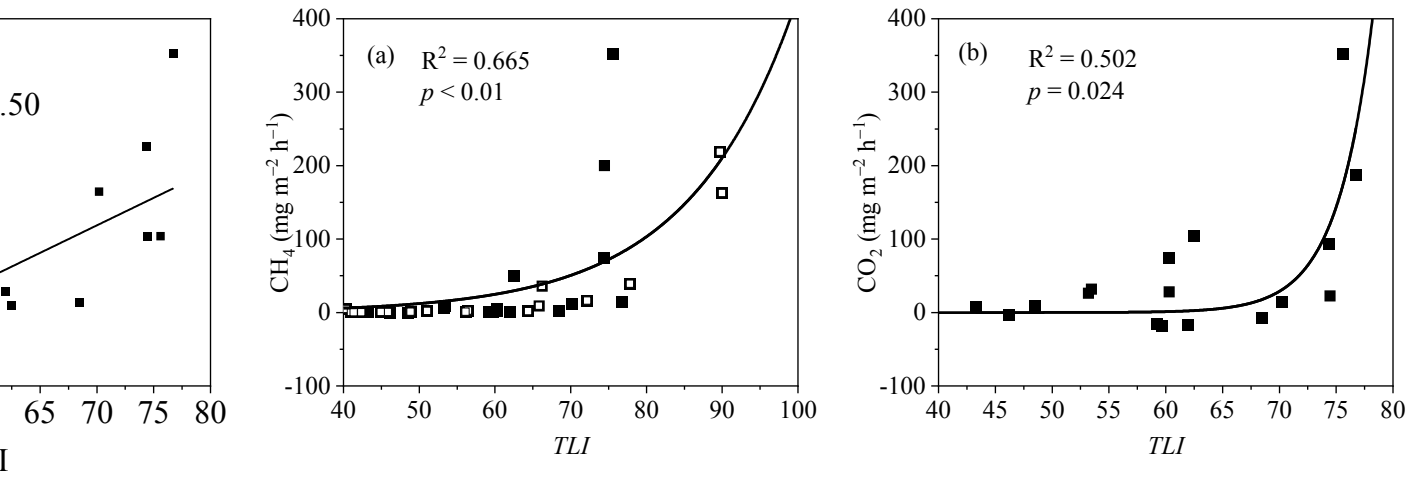

Fig. S1 Relationship between the *TLI* and CH_4 (a) and CO_2 (b) emission fluxes in shallow lakes. The solid points represent the data from this study, the hollow points represent the data from other studies[1].

[1]Reference:

Gonzalez-Valencia, R., Sepulveda-Jauregui, A., Martinez-Cruz, K.Hoyos-Santillan, J., Dendooven, L., Thalasso, F., 2014. Methane emissions from Mexican freshwater bodies: correlations with water pollution. Hydrobiologia 721(1), 9-22.

Martinez-Cruz, K., Gonzalez-Valencia, R., Sepulveda-Jauregui, A., Plascencia-Hernandez, F., Belmonte-Izquierdo, Y., Thalasso, F., 2017. Methane emission from aquatic ecosystems of Mexico City. Aquat. Sci. 79(1), 159-169.

Sepulveda-Jauregui, A., Walter Anthony, K. M., Martinez-Cruz, K., Greene, S., Thalasso, F., 2015. Methane and carbon dioxide emissions from 40 lakes along a north–south latitudinal transect in Alaska. Biogeosciences 12(11), 3197-3223.

Sepulveda-Jauregui, A., Hoyos-Santillan, J., Martinez-Cruz, K., Walter Anthony, K.M., Casper, P., Belmonte-Izquierdo, Y., Thalasso, F., 2018. Eutrophication exacerbates the impact of climate warming on lake methane emission. Sci. Total Environ. 636, 411-419.

Chapter 3: Suspended particles potentially enhance nitrous oxide (N_2O) emissions in the oxic estuarine waters of eutrophic lakes

3.1 Introduction

Rivers and lakes, which play the role of linking Earth's various layers, contain a large amount of nitrogen (N) from terrestrial ecosystems, and are potential to be a major storage reservoir and a short- to long-term sink within the N cascade (Galloway et al., 2004; Schmadel et al., 2018). Estuaries bridge the riverine and lacustrine ecosystems while carrying large amounts of land-based organic or inorganic materials into lakes, particularly particulate organic matter (Howarth et al., 2011; Zhou et al., 2018). The sources of suspended particles (SPS) in inland river-lake system are complex. A large amount of terrestrial particulate matter enters water bodies and is affected by various factors, such as human activity, soil erosion, and rainfall processes (Walling, 2005; Wetz et al., 2017; Woodward and Walling, 2007; Yao et al., 2016). Meanwhile, sediment resuspension occurs due to hydraulic disturbances and biological activities, causing particles to re-enter water columns (Chen et al., 2018; Huang and Liu, 2009; Maa et al., 1998). These SPS have recently been found to affect the physicochemical properties and biological processes of N in estuaries (Turner and Millward, 2002; Yao et al., 2016). A number of studies have focused on the N cycles of oceans and adjoining estuary ecosystems (Dalsgaard et al., 2003; Howarth et al., 2011; Lebreton et al., 2016). However, the potential effects of transporting matter in river estuaries of lake ecosystems with high SPS concentrations on the N cycle are still poorly understood.

SPS can adhere a large amount of aerobic heterotrophic microbes and inorganic ions (NH_4^+, Fe^{2+}, Mn^{2+}, and HS^-) to its surface, serving as the main attachment interface for micro-organic materials (Jeris and Owens, 1975; Ochs et al., 2010; Xia et al., 2004; Xia et al., 2009). The organic matter and reducing inorganic ions in the SPS are oxidised by micro-organisms, resulting in significantly lower DO concentrations in the SPS than

those of the surrounding water (Bianchi et al., 1992; Bonin et al., 1981; Falkowski et al., 2008; Jørgensen, 1977). To date, surface sediment is considered to be a hotspot for the formation of gaseous-N (including N_2 and N_2O) by denitrification in common shallow-lake ecosystems. However, recent studies have highlighted that a large fraction of the gaseous-N released from aquatic ecosystems can be produced in oxygenated water columns containing a high quantity of SPS (Garnier et al., 2006; Venkiteswaran et al., 2014; Yao et al., 2016). In the estuaries of the Yangtze River or Yellow River, the large amounts of SPS serve as a significant interface and an alternative zone for denitrification, and accelerate the N cycle of the aquatic ecosystem (Xia et al., 2017; Yao et al., 2016). The particular microenvironment at the SPS-interface provides a new N_2O production source (Liu et al., 2013; Xia et al., 2017). The release flux of N_2O in aquatic ecosystems may, therefore, be underestimated without consideration of the presence of SPS. Although the N cycle at the SPS-interface has received great attention (Lebreton et al., 2016; Ma et al., 2016), there is little understanding of the influence of SPS on N_2O emissions and their potential mechanisms in the estuaries of eutrophic lakes.

Unlike the aforementioned high turbid inorganic materials in the studied river estuaries, the SPS in the estuaries of eutrophic lakes mainly consist of organic matter derived from terrestrial leaf litter and autochthonous phytoplankton (Teeter et al., 2001). The different physic-chemical properties of SPS, including particle size, source and composition, may alter the mechanisms of N_2O production and release with microbial processes (Xia et al., 2017). We hypothesize that these organic-enriched SPS in the estuaries of eutrophic lakes potentially enhance the N_2O emissions. Laboratory simulations were simultaneously conducted to study the effect of SPS concentrations on N_2O emission characteristics. The objectives of this study are to provide more direct evidence via a simulation experiment about the relationship between N_2O emissions and SPS concentrations interpreted by the potential microbial mechanisms.

3.2 Material and methods

3.2.1 Microcosm system

To investigate whether SPS affected N_2O emissions, a set of double-Perspex closed chambers (inner diameter and height of 7 and 40 cm, respectively) containing water and SPS were designed. In order to ensure high microbial activities, these chambers were heated in a water bath and maintained at 25 °C, an optimized temperature for comparing N_2O emissions from different chambers in the same level. A stirring device with a polytetrafluoroethylene paddle was used to adjust the speed and ensure that the particles remained suspended in the water column. The chamber could maintain its atmospheric pressure at 0.5 atm for 24 h by applying pressure in a closed experiment. After removing particulates by a 200-mesh nylon sieve, 1 L of lake water from the lake region of Shatang River was added to each chamber. Then 0, 0.5, 1.5, 3, and 5 g of the homogenized sediments from the same place with lake water were added to different chambers. The NO_3^--N concentration of the water was adjusted to 4 mg L^{-1}, in consideration of sufficient substances for denitrification, by KNO_3 without NH_4^+-N. The total organic carbon (TOC) and TN contents of the sediments were 44.31 and 2.19 mg g^{-1}, respectively, and the NH_4^+-N and NO_3^--N contents were 94.58 and 15.70 μg g^{-1}, respectively. The headspace of 538 mL, reserved in each chamber, was open to the atmosphere for 30 min to purge the N_2O from the previous incubation period and maintain the oxygen saturation level during the experiment. At predetermined intervals, gas samples were collected using a gastight syringe to detect the N_2O and CO_2 concentrations during the incubation periods. The average N_2O or CO_2 emission rate = $(C_t\text{-}C_a)/t$ (Ct: the N_2O or CO_2 concentration at t day; C_a: the N_2O or CO_2 concentration in atmosphere; t: sampling days). Ten millilitres of water was collected using a syphon for NO_3^--N analysis. Water and gas samples were collected by sampling, and stored at 4 °C for less than 24 h before analysis.

3.2.2 Chemical analysis

3.2.2.1 Physicochemical properties of water and sediment

The water samples for chemical analysis, including TN, NO_3^--N, NH_4^+-N, and dissolved organic carbon (DOC), were discontinuously collected using a tube sampler and mixed thoroughly, with three replicates. The detailly methodology for testing the parameters can be found in Chapter 2. The SPS concentrations of overlying water were measured by using a Whatman GF/C 0.45-μm filter to weigh the dried weight that kept at 100 °C for 4 h. In the simulation system, the SPS concentrations of the chamber were determined by the moisture content via calculating weight difference between wet and dried samples.

3.2.2.2 N_2O and CO_2 concentration analysis

A syringe was used to extract gases for N_2O analysis using a 7890B Agilent gas chromatograph equipped with ECD (Electron Capture Detector) and a nickel catalyst methaniser. Greenhouse gas production was expressed as the cumulative production. The CO_2 produced in microcosm system was analysed using a 7890B Agilent gas chromatograph equipped with FID (Frame Ionization Detector). The gas chromatograph configurations detailly described by Shaaban et al. (Shaaban et al., 2016) were adopted for the gas concentration analysis.

3.2.3 Biological analysis

The microbial population analysis of SPS from each treatment was collected at the end of incubation experiments. DNA was extracted from the collected SPS samples using the MOBIO PowerSoil® DNA Isolation Kit (MOBIO, USA) according to the manufacturer's instructions. The DNA was stored at -20°C until analysis by PCR. The qPCR assay was performed using an ABI 7900HT real-time qPCR detection system (Applied Biosystems, Inc., USA). PCR amplification of *nir*K fragment, which encode for nitrite reductase of bacteria, was conducted using the F1aCu (5′-ATCATGGTScTGCCGCG-3′) and R3Cu (5′-GCCTCGATCAGRTTGTGGTT-3′) primers set. Each 20 μL reaction system consisted of 10 μL of SYBR Premix (Takara, China), 1 μL of DNA template or total DNA, 0.5 μL each of forward and reverse

primers, and 8 μL of sterile water. After an initial denaturation step at 95 °C for 30 s, 30 cycles of 95 °C denaturation (10 s), 55 °C annealing (40 s), 72 °C elongation (50 s) were followed by a final elongation step of 7 min at 72 °C. All plasmids containing the target genes were provided by Tyhygene Biotech Co., Ltd. and subjected to 10 × serial dilution to serve as DNA templates for the construction of standard curves ($R^2 > 0.999$).

3.2.4 Statistical analysis

Statistical analysis was conducted using the SPSS 19.0 software package (SPSS Inc., Chicago). Significant differences between treatments were tested by conducting a one-way ANOVA. The criteria of $p < 0.05$ and $p < 0.01$ were used to determine statistical significances at the 0.05 and 0.01 levels (two-tailed), respectively. The statistical significance of the results was determined by conducting a Duncan test at the 5% level.

3.3 Results

3.3.1 Physicochemical properties of water in microcosm system

The average DO concentration in water exceeded 7.0 mg L^{-1} in each treatment during the experimental periods, suggesting oxic conditions in the system (Fig. 1a). The DO concentrations decreased as the SPS concentrations increased when the SPS concentration increased from 0.5 to 5 g L^{-1}, the average DO concentration decreased from 8.15 to 7.60 mg L^{-1}. In contrast, the pH values exhibited a decreasing trend during the initial incubation periods. The pH values significantly decreased with 0 g L^{-1} SPS compared to the treatment with 5 g L^{-1} SPS ($p < 0.01$). The variations in the NO_3^--N concentrations of the microcosm system are shown in Fig. 1(c). The initial NO_3^--N concentration of the overlying water in all treatments was 4 mg L^{-1}. There was no significant change in the concentration of NO_3^--N during the first nine days under different SPS concentrations. In the treatments with 3 and 5 g L^{-1} of SPS, the NO_3^--N concentration significantly increased, with the highest concentrations reaching 5.22 and 7.12 mg L^{-1}, respectively. However, in the treatments with 0.5 and 1.5 g L^{-1} SPS, the

NO_3^--N concentrations first increased and then decreased, with minimum values of 3.58 and 3.34 mg L^{-1}, respectively. In the treatment with without SPS, the NO_3^--N concentration in the overlying water remained relatively stable at approximately 4.0 mg L^{-1} during the experimental periods.

3.3.2 N_2O emissions and denitrifying bacteria population in microcosm system

For all treatments with different SPS concentrations, the accumulated N_2O emission rates increased with the SPS concentrations (Fig. 2). When the SPS concentration increased from 0.5 to 5 g L^{-1}, the average N_2O emission rate increased from 4.78 to 10.89 μg m^{-3} d^{-1}. In the experimental system without SPS, the accumulated N_2O emission and average N_2O emission rate were 7.01 μg m^{-3} and 1.28 μg m^{-3} d^{-1}, respectively. For the experimental system with 3 g L^{-1} of SPS, the accumulated N_2O emission and average N_2O emission rate were higher than those of the other system, at 407.38 μg m^{-3} and 10.89 μg m^{-3} d^{-1}, respectively. As shown in Fig. 2b, the average N_2O emission rate increased linearly with the SPS concentrations (R^2 = 0.7018, $p < 0.05$), suggesting that the SPS concentration significantly affected the N_2O emissions. Similarly, with the increase of SPS concentrations, the positively correlated average CO_2 emission rate (R^2 = 0.855, $p < 0.05$) further indicated the strong microorganism activities in the microcosm system (Fig. 2c).

The characteristics of the denitrifying bacteria population in the SPS of all treatments with different SPS concentrations at the end of incubation was summarized in Fig. 3. The highest and lowest denitrifying bacteria populations were occurred in the treatments of 3 and 0.5 g L^{-1} SPS, respectively (Fig. 3a). Although the treatment of 5 g L^{-1} SPS was significantly lower than the treatment of 3 g L^{-1} SPS, the denitrifying bacteria population in the SPS displayed an increased tendency with the SPS concentrations. In addition, the liner response of average N_2O emission rates to the ln (denitrifying bacteria) (R^2 = 0.973, $p < 0.01$) (Fig. 3b), further indicated that the N_2O emissions was significantly affected by the denitrifying bacteria in the SPS.

3.4 Discussion

Our results revealed that high SPS concentrations can accelerate the emissions of N_2O from oxic water, particularly in estuarine regions with high SPS concentrations and N loadings. Coupled nitrification-denitrification occurs in wastewater treatment and natural micro-ecological systems, as aerobic microorganisms consume oxygen to generate a hypoxic microenvironment, and NO_3^--N is produced by nitrification (Walter et al., 2005; Xia et al., 2017). Correspondingly, the simulation experiment exhibited increasing NO_3^--N concentrations in the water after 12 days. Xia et al. (2017) reported that nitrifying bacteria appeared on the SPS-interface, as evidenced by the positive correlation between their abundance and the SPS concentration. The organic N in the SPS is the main form of N, and the main form of inorganic N is NH_4^+-N. Therefore, the nitrification of NH_4^+-N to NO_3^--N is an important process to supplement the NO_3^--N concentration in an oxic overlying water. In the chambers with SPS concentrations of 3 and 5 g L^{-1}, the concentrations of NO_3^--N increased from 4 mg L^{-1} to maximum concentrations of 5 and 7 mg L^{-1}, respectively (Fig. 1c). In addition, a decrease in the NO_3^--N concentration of the water column was observed with SPS concentrations of 0.5 and 1.5 g L^{-1}, and the concentrations of NO_3^--N in the water column increased with SPS concentrations of 3 and 5 g L^{-1}. These results indicated that the nitrification and denitrification processes occurred in the microcosm system. However, the denitrification was hardly observed in the chamber without SPS as there was almost no change in the level of NO_3^--N in the water column. Based on these observations, we speculate that the denitrification occurring on the SPS-interface in the water column is another important source of N_2O. It is confirmed by the findings that the denitrifying bacteria population in the SPS increased with the SPS concentrations (Fig. 3a). Additionally, the denitrifying bacteria population had a significantly positive correlation with N_2O emissions (Fig. 3b). Although N_2O emissions are controlled by multiple pathways, many studies suggest that they are primarily controlled by denitrification (Galloway et al., 2004; Yan et al., 2012; Yan et al., 2017). In addition,

the coupling of nitrification-denitrification on SPS accelerates N transfer and the emissions of N_2O in naturally oxic water. Hence, the SPS facilitates the conversion of N and also accelerates the emissions of N_2O in oxic water columns, which suggests that N_2O emissions were underestimated when the SPS concentrations and N loadings in aquatic ecosystems were high.

Currently, many studies have discussed the impact or feedback of climate change on cyanobacterial blooms (Yan et al., 2017) and eutrophic processes (Cole and Caraco, 2001; Wang et al., 2009) in shallow lakes, particularly those that are hypereutrophic. There are large external particle sources and waves accelerate the suspension of sediments in the estuaries of shallow lakes, resulting in high SPS concentrations and N loadings. Based on our experimental model to estimate the N_2O emissions fluxes in the estuaries of the hypereutrophic Taihu Lake, N_2O emissions are easily to be underestimated in estuarine regions, particularly in those of hypereutrophic lakes. Given the average TN concentration of 5.9 mg L^{-1}, SPS concentration of 0.344 g L^{-1} and DO concentration of 5.19 mg L^{-1} (Zhao et al., 2015), the estimated average N_2O emission flux is 114.37 μg m^{-2} h^{-1} in the estuarine region of shallow eutrophic lakes. In the case of Taihu Lake, the N_2O emissions are approximately 36.20 t yr^{-1} from its estuaries that are considered as a semicircle with a radius of 1 km and the total 23 main inflow rivers, which constitute an area of 36.13 km^2 (Zhao et al., 2015). However, the influences of anthropologic activities, climate change, N concentrations, hydrodynamic conditions, and the particle size and organic composition of SPS will significantly affect the N cycle and N_2O emissions, and thus require further study.

3.5 Conclusions

This study was the first to report N_2O emissions from a lacustrine estuary particularly that of a hypereutrophic shallow lake. The relationship between environmental factors and N_2O emissions was analysed and indicated that the concentrations of both N and SPS would accelerate the N cycle and facilitate the emission of N_2O from an oxic water column. Both N and SPS concentrations played an

important role in controlling N_2O emissions from the oxic water column, which should be considered in the future estimations of N_2O emissions from eutrophic lakes.

3.6 References

Bianchi, M., Marty, D., Teyssie, J.L., Fowler, S., 1992. Strictly aerobic and anaerobic bacteria associated with sinking particulate matter and zooplankton fecal pellets. Marine Ecology Progress 88, 55-60.

Bonin, D.J., Maestrini, S.Y., Leftley, J.W., 1981. Some processes and physical factors that affect the ability of individual species of algae to compete for nutrient partition. Canadian Bulletin of Fisheries & Aquatic Sciences 67, 292-309.

Chen, Y., Chen, N., Li, Y., Hong, H., 2018. Multi-timescale sediment responses across a human impacted river-estuary systems. Journal of Hydrology 560, 160-172.

Cole, J.J., Caraco, N.F., 2001. Emissions of Nitrous Oxide (N_2O) from a Tidal, Freshwater River, the Hudson River, New York. Environmental Science & Technology 35, 991-996.

Dalsgaard, T., Canfield, D.E., Petersen, J., Thamdrup, B., Acuña-González, J., 2003. N_2 production by the anammox reaction in the anoxic water column of Golfo Dulce, Costa Rica. Nature 422, 606-608.

Falkowski, P.G., Fenchel, T., Delong, E.F., 2008. The microbial engines that drive Earth's biogeochemical cycles. Science 320, 1034-1039.

Galloway, J.N., Dentener, F.J., Capone, D.G., Boyer, E.W., Howarth, R.W., Seitzinger, S.P., Asner, G.P., Cleveland, C.C., Green, P.A., Holland, E.A., 2004. Nitrogen cycles: Past, present, and future. Biogeochemistry 70, 153-226.

Garnier, J., Cébron, A., Tallec, G., Billen, G., Sebilo, M., Martinez, A., 2006. Nitrogen Behaviour and Nitrous Oxide Emission in the Tidal Seine River Estuary (France) as Influenced by Human Activities in the Upstream Watershed. Biogeochemistry 77, 305-326.

Howarth, R., Chan, F., Conley, D.J., Garnier, J., Doney, S.C., Marino, R., Billen, G., 2011. Coupled biogeochemical cycles: eutrophication and hypoxia in temperate

estuaries and coastal marine ecosystems. Frontiers in Ecology & the Environment 9, 18-26.

Huang, P., Liu, Z., 2009. The effect of wave-reduction engineering on sediment resuspension in a large, shallow, eutrophic lake (Lake Taihu). Ecological Engineering 35, 1619-1623.

Jørgensen, B.B., 1977. Bacterial sulfate reduction within reduced microniches of oxidized marine sediments. Marine Biology 41, 7-17.

Jeris, J.S., Owens, R.W., 1975. Pilot-scale, high-rate biological denitrification. Journal - Water Pollution Control Federation 47, 2043-2057.

Lebreton, B., Beseres Pollack, J., Blomberg, B., Palmer, T.A., Adams, L., Guillou, G.l., Montagna, P.A., 2016. Origin, composition and quality of suspended particulate organic matter in relation to freshwater inflow in a South Texas estuary. Estuarine, Coastal and Shelf Science 170, 70-82.

Liu, T., Xia, X., Liu, S., Mou, X., Qiu, Y., 2013. Acceleration of Denitrification in Turbid Rivers Due to Denitrification Occurring on Suspended Sediment in Oxic Waters. Environmental Science & Technology 47, 4053-4061.

Ma, X., Zhang, G.-L., Liu, S.-M., Wang, L., Li, P.-P., Gu, P.-P., Sun, M.-S., 2016. Distributions and fluxes of nitrous oxide in lower reaches of Yellow River and its estuary: Impact of water-sediment regulation. Estuarine, Coastal and Shelf Science 168, 22-28.

Maa, P.Y., Sanford, L., Halka, J.P., 1998. Sediment resuspension characteristics in Baltimore Harbor, Maryland. Marine Geology 146, 137-145.

Ochs, C.A., Capello, H.E., Pongruktham, O., 2010. Bacterial production in the Lower Mississippi River: importance of suspended sediment and phytoplankton biomass. Hydrobiologia 637, 19-31.

Schmadel, N.M., Harvey, J.W., Alexander, R.B., Schwarz, G.E., Moore, R.B., Eng, K., Gomezvelez, J.D., Boyer, E.W., Scott, D., 2018. Thresholds of lake and reservoir connectivity in river networks control nitrogen removal. Nature Communications

9.

Shaaban, M., Wu, Y., Peng, Q.A., Lin, S., Mo, Y., Wu, L., Hu, R., Zhou, W., 2016. Effects of dicyandiamide and dolomite application on N_2O emission from an acidic soil. Environmental Science Polluttion and Research 23, 6334-6342.

Teeter, A.M., Johnson, B.H., Berger, C., Stelling, G., Scheffner, N.W., Garcia, M.H., Parchure, T.M., 2001. Hydrodynamic and sediment transport modeling with emphasis on shallow-water, vegetated areas (lakes, reservoirs, estuaries and lagoons). Hydrobiologia 444, 1-24.

Turner, A., Millward, G.E., 2002. Suspended Particles: Their Role in Estuarine Biogeochemical Cycles. Estuarine Coastal & Shelf Science 55, 857-883.

Venkiteswaran, J.J., Rosamond, M.S., Schiff, S.L., 2014. Nonlinear response of riverine N_2O fluxes to oxygen and temperature. Environmental Science & Technology 48, 1566-1573.

Walling, D.E., 2005. Tracing suspended sediment sources in catchments and river systems. Science of the Total Environment 344, 159-184.

Walter, B., Haase, C., Räbiger, N., 2005. Combined nitrification/denitrification in a membrane reactor. Water Research 39, 2781-2788.

Wang, S., Liu, C., Yeager, K.M., Wan, G., Li, J., Tao, F., Lu, Y., Liu, F., Fan, C., 2009. The spatial distribution and emission of nitrous oxide (N_2O) in a large eutrophic lake in eastern China: anthropogenic effects. Science of the Total Environment 407, 3330-3337.

Wetz, M.S., Cira, E.K., Sterba-Boatwright, B., Montagna, P.A., Palmer, T.A., Hayes, K.C., 2017. Exceptionally high organic nitrogen concentrations in a semi-arid South Texas estuary susceptible to brown tide blooms. Estuarine, Coastal and Shelf Science 188, 27-37.

Woodward, J.C., Walling, D.E., 2007. Composite suspended sediment particles in river systems: their incidence, dynamics and physical characteristics. Hydrological Processes 21, 3601-3614.

Xia, X., Liu, T., Yang, Z., Michalski, G., Liu, S., Jia, Z., Zhang, S., 2017. Enhanced nitrogen loss from rivers through coupled nitrification-denitrification caused by suspended sediment. Science of the Total Environment 579, 47-59.

Xia, X.H., Yang, Z.F., Huang, G.H., Zhang, X.Q., Yu, H., Rong, X., 2004. Nitrification in natural waters with high suspended-solid content—A study for the Yellow River. Chemosphere 57, 1017-1029.

Xia, X.H., Yang, Z.F., Zhang, X.Q., 2009. Effect of suspended-sediment concentration on nitrification in river water: importance of suspended sediment-water interface. Environmental Science & Technology 43, 3681-3687.

Yan, W., Yang, L., Wang, F., Wang, J., Ma, P., 2012. Riverine N_2O concentrations, exports to estuary and emissions to atmosphere from the Changjiang River in response to increasing nitrogen loads. Global Biogeochemical Cycles 26, 1-15.

Yan, X., Xu, X., Wang, M., Wang, G., Wu, S., Li, Z., Sun, H., Shi, A., Yang, Y., 2017. Climate warming and cyanobacteria blooms: Looks at their relationships from a new perspective. Water Research 125, 449-457.

Yao, X., Zhang, L., Zhang, Y., Xu, H., Jiang, X., 2016. Denitrification occurring on suspended sediment in a large, shallow, subtropical lake (Poyang Lake, China). Environmental Polluttion 219, 501-511.

Zhao, Y., Xia, Y., Ti, C., Shan, J., Li, B., Xia, L., Yan, X., 2015. Nitrogen removal capacity of the river network in a high nitrogen loading region. Environmental Science & Technology 49, 1427-1435.

Zhou, Y., Xiao, Q., Yao, X., Zhang, Y., Zhang, M., Shi, K., Lee, X., Podgorski, D.C., Qin, B., Spencer, R.G.M., Jeppesen, E., 2018. Accumulation of Terrestrial Dissolved Organic Matter Potentially Enhances Dissolved Methane Levels in Eutrophic Lake Taihu, China. Environmental Science & Technology 52, 10297-10306.

Figures

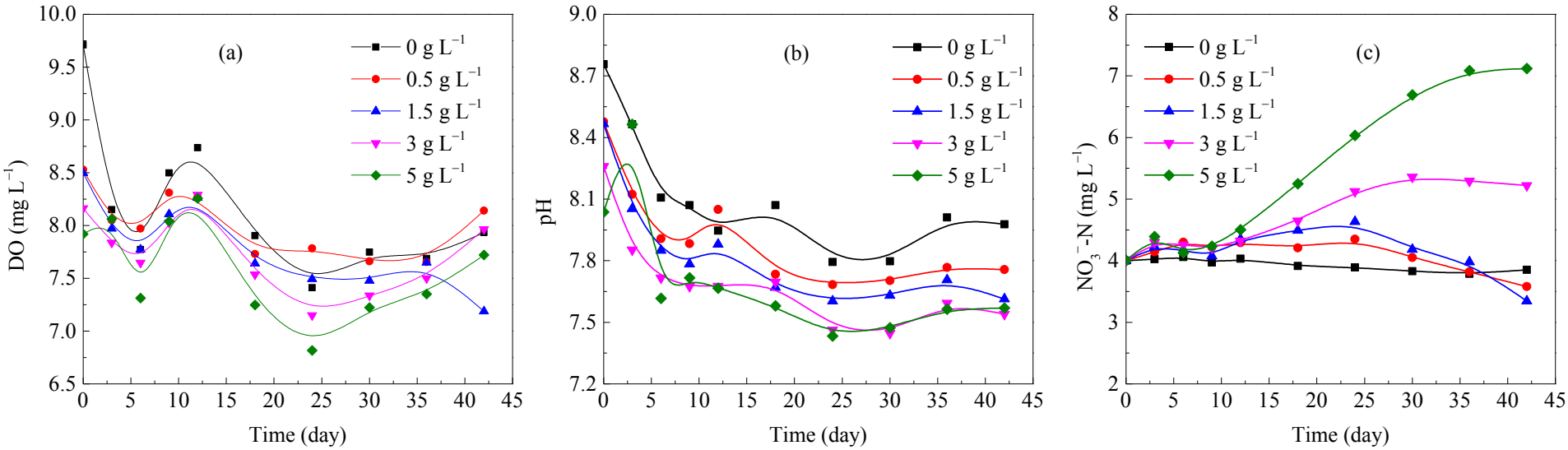

Fig. 1. Variations of physiochemical characteristics, (a) DO, (b) pH, and (c) NO_3^--N, of the overlying water during the incubation periods.

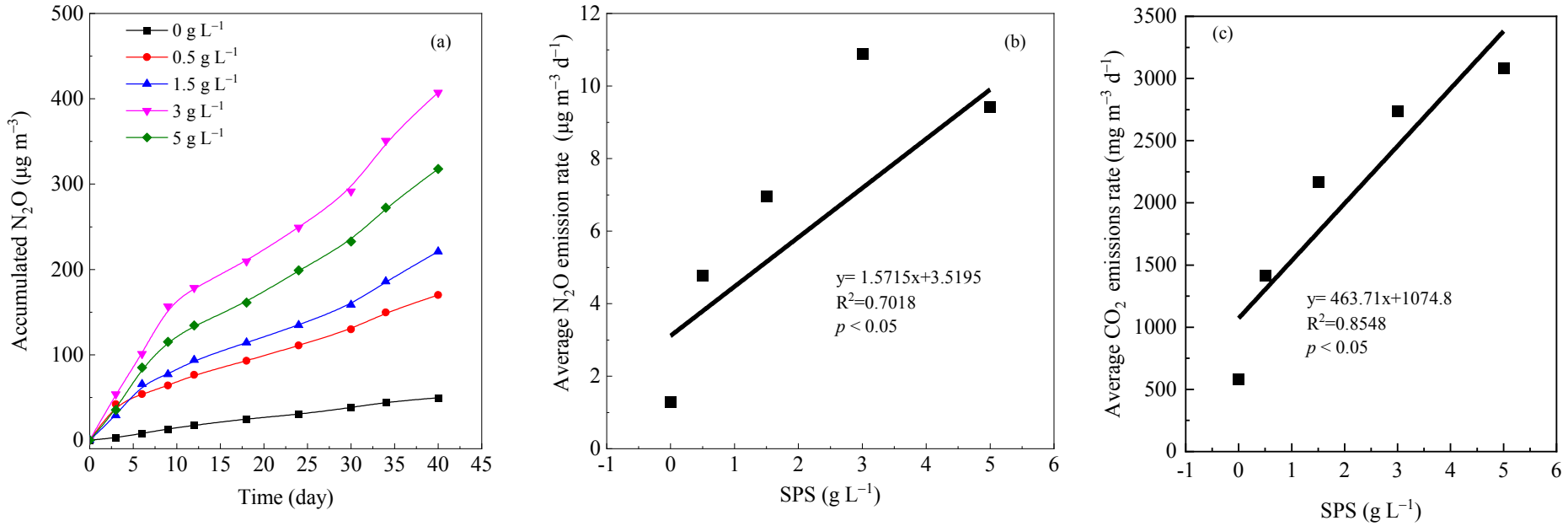

Fig. 2. Effect of the SPS concentration on the (a)N_2O emissions, (b) average N_2O emission rates, and (c) average CO_2 emission rates during the 42 days of incubation.

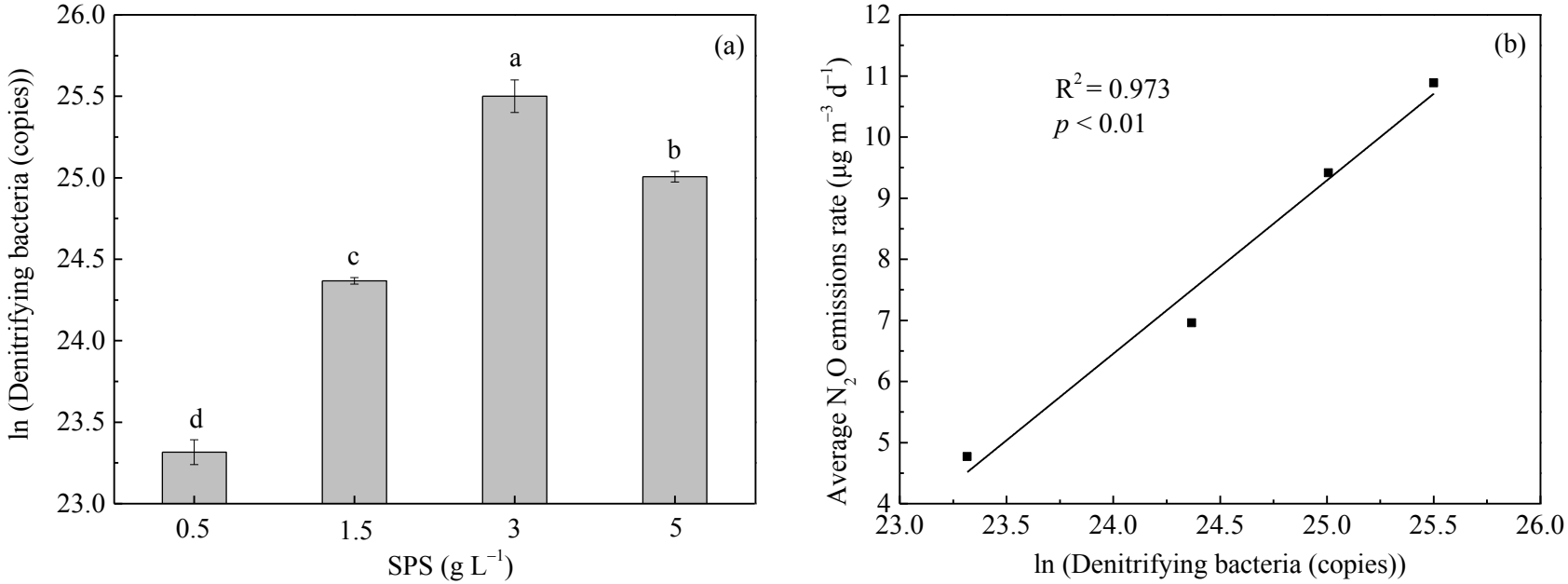

Fig. 3. The denitrifying bacteria population in SPS in incubation systems (a) and the relationship between the denitrifying bacteria population in SPS and N_2O emissions rate (b).

Chapter: 4 Characterization of N_2O emission in different trophic shallow lakes

4.1 Introduction

Nitrous oxide (N_2O) is an ozone-depleting and highly potent greenhouse gas (GHG) with a long half-life that contributes to global warming, in addition to carbon dioxide (CO_2) and methane (CH_4), in the stratosphere (Ravishankara et al., 2009). Atmospheric N_2O has increased by 20% from 1750 to 2018 and is steadily increasing at a rate of 0.2% per year (Tian et al., 2020). The IPCC reported that approximately 10% of anthropogenic N_2O sources are derived from freshwater and coastal marine systems (IPCC, 2013). Given that inland freshwater lakes are recipients of nutrients transported from terrestrial ecosystems to trigger uncertainty of GHG emissions (Wang et al., 2009; Zhou et al., 2020a), they function as N_2O hot spots where the high turnover of nitrogen (N) compounds. Hence, the N_2O emissions from aquatic ecosystems have received considerable attention (Beaulieu et al., 2011; Kortelainen et al., 2020). Although multiple factors such as nutrient composition, eutrophication, and temperature likely regulate N_2O emissions from freshwater lakes at regional and global scales, the dominant factors affecting N_2O emissions in freshwater lakes remain poorly understood (Kortelainen et al., 2020; Li et al., 2018; Yan et al., 2017). There is also a need to evaluate and quantify the N_2O emissions of freshwater lake ecosystems given that they are globally significant sources of N_2O (Lauerwald et al., 2019). Generally, understanding the mechanisms underlying variation in N_2O emissions from freshwater lakes can aid the development of policies to address global warming.

N_2O is mainly produced by a by-product from nitrification and an intermediate from denitrification (Wenk et al., 2016). Of these multiple sources, denitrification is thought to

be a main source of N_2O in aquatic ecosystems (Beaulieu et al., 2011; Li et al., 2019a; Salk and Ostrom, 2019). N_2O reduction, the final step of denitrification ($NO_3^- \rightarrow NO_2^- \rightarrow NO \rightarrow N_2O \rightarrow N_2$), is catalyzed by N_2O reductase, which is encoded by the *nosZ* gene (Yoon et al., 2016). Denitrification plays a critical role in determining N_2O emission fluxes, including whether aquatic ecosystems are N_2O sources or sinks. N_2O production is regulated by microbial community structure in aquatic ecosystems (Zhao et al., 2018; Zhao et al., 2019). Microbial community composition affects the amount of N_2O emissions, as some bacteria lack *nosZ* and nitrite reductase genes, which significantly contribute to N_2O consumption and production in natural ecosystems, respectively (Domeignoz-Horta et al., 2016). Among several environmental factors, nutrients, redox conditions, and temperature determine the microbial guilds involved in N_2O production and consumption (Hinshaw and Dahlgren, 2013; Xiao et al., 2019). Seasonal changes involve multiple environmental fluctuations that affect lacustrine microbial community structure (Song et al., 2012) and lead to uncertainty in the magnitude of N_2O emissions. N conversion rates and eutrophication progress are crucial for regulating final N forms (N_2 or N_2O) in aquatic ecosystems (Jiang et al., 2020; Salk and Ostrom, 2019; Zhu et al., 2020). Such N conversions are dynamic and dependent on eutrophication progress (Li et al., 2018; Liikanen et al., 2003). There is thus a need to understand the microbial processes that regulate N_2O sources or sinks in lakes of different trophic state and determine spatial heterogeneity in N_2O emissions.

Shallow lakes receive massive amounts of nutrients from anthropogenic activities, which potentially lead to changes in lake trophic state (Zhou et al., 2020a; Zhou et al., 2019). GHG emissions from eutrophic shallow lakes have also been surveyed, and this work has shed light on differences in N_2O emission fluxes among shallow lakes of different trophic state. In these surveys, the commonly used default emission factor (EF_{5r}) by the IPCC has been used (Maavara et al., 2019), which results in either an underestimation or overestimation of the N_2O budgets in freshwater ecosystems of

different trophic state (Zhang et al., 2020). For example, Xiao et al.(2019) indicated that the mean N_2O emission fluxes in the East and West zones of Lake Taihu (eutrophic and oligotrophic, respectively) were substantially different, which is partially caused by N flowing to the lake. In addition, N loadings regulate the distribution of denitrifying bacteria, which is often indicated by functional genes for N_2O production (*nirS* and *nirK*) and consumption (*nosZ*) (Huang et al., 2011; Zhao et al., 2018). High N flowing to eutrophic lakes increases algal growth, potentially enhancing N_2O emissions and N turnover rates (Yan et al., 2017; Zhu et al., 2020). However, the accumulation of algae alters the redox conditions favoring denitrification (Yan et al., 2017), and more severe anoxic conditions limit the supply of nitrogen oxides generated by nitrification required for denitrification (Zhu et al., 2020); these observations impede our understanding of the role of algae in N_2O emissions. Such correlations in eutrophic and hypereutrophic lakes have been extensively investigated (Lauerwald et al., 2019; Xiao et al., 2019); however, shallow lakes have been poorly studied. In particular, no studies have compared N_2O emission fluxes among lakes of different trophic state (Salk and Ostrom, 2019). The trophic state of lakes leads to uncertainty in N_2O emission estimates (Kortelainen et al., 2020), yet the relationship between N_2O emission fluxes and the trophic state of lakes is not entirely decoupled. Studies of the N_2O emissions of lacustrine trophic states on a biogeographic scale could help enhance our understanding of their potential to act as sources of N_2O emissions.

Approximately 0.9% of China is covered with lakes. There are a total of 2,693 lakes (> 1.0 km^2), about one-third of which are shallow lakes located in the middle and lower reaches of the Yangtze River basin (Ma et al., 2011). To enhance our understanding of the relationship between N_2O emissions and eutrophication in shallow lakes in the Yangtze River basin, we characterized spatiotemporal variation in N_2O emission fluxes and its underlying mechanisms in 17 lakes along a trophic state gradient at a biogeographic scale. We constructed a model to predict the N_2O emission patterns in shallow lakes of different

trophic state. The aims of this study were to (i) identify N_2O emission patterns in shallow lakes of different trophic state; (ii) characterize differences in the main microorganisms and functional genes for N_2O emissions in the sediments in shallow lakes of different trophic state; (iii) evaluate the relationship between environmental variables and N_2O emissions to reveal the main drivers of N_2O emissions; and (iv) elucidate the role of algae on N_2O emissions in shallow lakes. The results of this study enhance our ability to accurately predict N_2O emission patterns from shallow lakes.

4.2 Material and methods

4.2.1 Field survey

4.2.1.1 Lakes of different trophic state

This study designated 17 sampling shallow lakes (< 7 m deep) in the middle and lower reaches of the Yangtze River basin. Lakes were sampled in the winter (November) of 2017 and summer (August and September) of 2018. Lake Taihu, Lake Guchenghu, Lake Chaohu, and Lake Donghu were sampled in winter 2017. Because river inflow affects the environmental conditions of lakes (Zhou et al., 2019), all sampling sites were located more than 1 km away from the mouth of inflow rivers. Based on the trophic level index (*TLI*) (see Chapter 2.2.4 for a description of how *TLI* was calculated), these lakes were classified into four trophic states: mesotrophic ($30 < TLI \leq 50$), eutrophic ($50 < TLI \leq 60$), middle-eutrophic ($60 < TLI \leq 70$), and hyper-eutrophic ($TLI > 70$) (Fig. 1) (Zhou et al., 2020b).

4.2.1.2 Heavy algae-accumulated and light algae-accumulated zones in Lake Taihu

Lake Taihu is a eutrophic lake that has experienced frequent and intensive cyanobacteria blooms since the 1980s (Qin et al., 2010). To characterize N_2O emission fluxes with or without algae accumulation, three typical zones (from west to east) in Lake Taihu, heavy algae-accumulated (Zone A and B), transitional (Zone C), and light algae-

accumulated zones (Zone D), were studied (Fig. 1c). Sampling was conducted in summer (July) and winter (November) in 2019. The physicochemical parameters of the surface water and N_2O emission fluxes were investigated.

4.2.2 Sample collection and analysis

At each sampling event, vertical samples (*i.e.*, overlying water (20 cm below the water level), surface sediment (0–10 cm), and gas samples) were collected in triplicate. The *in situ* dissolved oxygen (DO), temperature, and pH were measured with DO, temperature, and pH probes (HQ3d, HACH, USA) on-site, respectively. To measure dissolved N_2 concentrations in summer, a water sample from a glass water sampler (1 L) was slowly drained from the bottom and transferred to a sample vial (12 mL) through a silicone tube with minimal turbulence. The silicone tube was placed in the bottom of the vial to avoid the ingress of atmospheric N_2. Next, 60 μL of saturated $HgCl_2$ solution (0.5% v/v final concentration) was added to the sample vial to inhibit microbial activity. These samples were stored in an ice cooler on-site and immediately transported to the laboratory in a cooler at 4ºC. Water samples for chemical analyses, including total nitrogen (TN), total phosphorus (TP), NO_3^--N, NH_4^+-N, dissolved organic carbon (DOC), and chlorophyll-*a* (chl-*a*), were tested using previously described procedures (Zhou et al., 2019). Briefly, TN and TP were measured using an ultraviolet spectrophotometry method and an ammonium molybdate spectrophotometric method, respectively. NO_3^- and NH_4^+ concentrations were measured by a water flow analyzer (Auto Analyzer 3, Seal, Germany), and the DOC concentration was determined using an elemental analyzer (Flash EA 1112, CE Instruments, Italy). Chl-*a* was quantified by extraction in 95% ethanol and measuring the absorbance at 630, 645, 663, and 750 nm using a UV-vis spectrophotometer (UV-6100, Mapada, China).

4.2.3 Tested and calculated N_2O emission fluxes

N_2O emission flux was estimated by a floating static chamber (Cole et al., 2010; Gålfalk et al., 2013). The headspace gas was collected between 11:00 and 14:00 using three floating static chambers (size: 38.5 cm × 30.5 cm × 18.5 cm) following a previously described procedure (Zhou et al., 2019). During each gas sampling event, six gas samples were collected at 10-min intervals for 1 h via a static chamber. The gas chromatography (7890B Agilent) configuration described by Shaaban et al. (2018) was used to measure the N_2O concentration. The detailed methods for calculating N_2O emission fluxes are described in our previous study (Zhou et al., 2019). N_2O emission flux estimated by the floating static chamber method was calculated using Eq. (1):

$$F = \frac{V}{A} \times \frac{dC}{dt}, \quad (1)$$

where F is the N_2O emission flux (μg m^{-2} h^{-1}); V (m^3) and A (m^2) are the static chamber volume and surface area, respectively; and dC/dt is the time derivative of the N_2O concentration (μg m^{-3} h^{-1}).

4.2.4 Dissolved N_2 concentration and excess dissolved N_2 concentration

Dissolved N_2 was measured by a membrane inlet mass spectrometer system (MIMSS) with a probe inlet (HPR-40, Hiden Analytical Co.) using the N_2:Ar method described in a previous study (Chen et al., 2014). N_2:Ar ratios were calculated based on the quadrupole instrument signal (N_2 and Ar pressures at a detector) and calibrated using air-equilibrated water standards (Weiss, 1970). The dissolved N_2 concentrations of triplicate water samples were analyzed, and excess dissolved N_2 concentrations (ΔN_2) were calculated following previously described methods (Chen et al., 2014). ΔN_2 (μmol L^{-1}) was calculated using Eq. (2):

$$\Delta N_2 = N_{2\,(water)} - N_{2(eq)}, \quad (2)$$

where $N_{2(water)}$ is the dissolved N_2 concentration in water measured by MIMSS, and $N_{2(eq)}$ is the concentration expected if the water were in equilibrium with the atmosphere. Both

were estimated following previously described methods (Weiss, 1970; Weiss and Price, 1980).

4.2.5 Predication of N_2O emission fluxes based on the IPCC model

A predictive model was used to determine the N_2O emission factor (EF_{5r}) as recommended in the IPCC-2019 guidelines. The dissolved N_2O concentration (μg-N L^{-1}) was estimated using Eq. (3):

$$N_2O\text{-}N = NO_3^-\text{-}N \times EF_{5r}, \qquad (3)$$

where EF_{5r} is 0.26% according to the IPCC-2019 default value (IPCC, 2019), and NO_3^--N (μg-N L^{-1}) represents the concentration measured in a water column. N_2O emission fluxes (F', μg m^{-2} h^{-1}) were calculated by the dissolved N_2O concentration using the two-layer model of diffusive gas exchange, which is given as Eq. (4)

$$F' = k \times (C_w - C_{eq}), \qquad (4)$$

where C_w, is obtained from Eq. 3 and is the dissolved N_2O concentration in water estimated by the EF_{5r}; C_{eq} is the N_2O concentration in water that is in equilibrium with the atmosphere at the *in situ* air pressure and temperature; k is the gas transfer coefficient (m d^{-1}) and was normalized to the Schmidt number of 600, as described in the Supporting Materials (Cole and Caraco, 1998).

4.2.6 DNA extraction, high-throughput sequencing, and real-Time qPCR analysis

Biomass for the sediment microbial community analysis was collected from lakes of different trophic state. DNA was extracted from the collected biomass using the DNA Isolation Kit (MOBIO, USA) per the manufacturer's instructions. The concentration and purity of DNA were measured using a microvolume UV-VIS spectrophotometer (NanoDrop^{TM} One^{C}, Thermo Fisher Scientific, USA), and the extracted DNA was stored at −20ºC before further analysis. 16S rRNA gene high-throughput sequencing was conducted using an Illumina MiSeq platform (Magigene Biotechnology Co. Ltd.,

Guangzhou, China). The primers used for high-throughput sequencing were modified 515F (5′-GTGYCAGCMGCCGCGGTAA-3′) and 806R (5′-GGACTACHVGGGTWTCTAAT-3′) targeting the V3 and V4 hypervariable regions of both bacterial and archaeal 16S rRNA genes (Zhou et al., 2020b). Given that the *nirK* and *nirS* genes and the *nosZ* gene encode enzymes for N_2O production and consumption in denitrification, respectively (Zhao et al., 2018), the abundances of these three genes were analyzed. 16S rRNA gene abundances were quantified by real-time quantitative PCR (qPCR) with reported primer sets (Table S3). The PCR conditions for the amplification of *nirK, nirS*, and *nosZ* were described in a previous study (Chen et al., 2017).

4.2.7 Statistical analysis

Statistical analyses were conducted using SPSS 19.0 (SPSS Inc., Chicago, USA). Significant differences among lakes were determined by one-way analysis of variance (ANOVA). The thresholds for statistically significant and highly statistically significant were $p < 0.05$ and $p < 0.01$ (two-tailed), respectively. The Kolmogorov-Smirnov test was conducted to determine if the data were normally distributed. The built-in exponential model of Origin 2019 software (OriginLab Inc., USA) was carried out to assess the relationship between N_2O emission fluxes and *TLI*.

4.3 Results

4.3.1 *In situ* N_2O emission fluxes in lakes of different trophic state

The *TLI* of the examined lakes ranged from 44.0 to 69.7 and from 43.3 to 76.7 in the summer and winter, respectively (Fig. S1). The hyper-eutrophic sampling sites were not included in the winter dataset. Among these examined lakes, the ranges of N_2O emission fluxes were –1.0–53.0 μg m^{-2} h^{-1} and 0.4–102.9 μg m^{-2} h^{-1} in summer and winter, respectively, indicating a high degree of variation in N_2O emission fluxes (Table S1 and Fig. 2). In addition, all examined lakes were N_2O sources, with the exception of

mesotrophic lakes in summer. The mean N_2O emission fluxes of the middle-eutrophic lakes in winter (50.4 μg m^{-2} h^{-1}) were higher than those of the hyper-eutrophic (39.1 μg m^{-2} h^{-1}) and middle-eutrophic (7.4 μg m^{-2} h^{-1}) lakes in summer (Table S1). Overall, the N_2O emission fluxes gradually increased as *TLI* increased (Fig. 2a).

The lacustrine N_2O emission fluxes in both winter and summer were positively correlated with *TLI* (Fig. 2a). The N_2O emission fluxes exponentially increased with the *TLI*s of the sampled lakes (adj. $R^2 = 0.85$, $p < 0.01$ in summer; adj. $R^2 = 0.63$, $p < 0.01$ in winter). There was a non-linear relationship between the net N_2O emission fluxes and *TLI* (adj. $R^2 = 0.36$, $p < 0.01$) (Fig. 2b). The N_2O emission fluxes increased as the *TLI* of lakes increased, and the increase was more pronounced in hypertrophic lakes. In addition, N_2O emission fluxes were predicted based on the EF_{5r} [Equation (3)]. There was a nonlinear exponential relationship between the predicted N_2O emission fluxes and *TLI* (adj. $R^2 = 0.80$, $p < 0.01$) (Fig. 2b). These fluxes were higher than the observed values, especially in the hyper-eutrophic lakes in summer (*TLI* > 70) (Fig. S2).

4.3.2 Dissolved N_2 concentration in shallow lakes

Mean dissolved N_2 concentrations across all lakes in summer ranged from 403.3 μmol L^{-1} to 443.8 μmol L^{-1} and exhibited a unimodal relationship with *TLI* (Fig. 3a). Among these examined lakes, the lowest dissolved N_2 concentration was observed in hyper-eutrophic lakes. There was a significant unimodal relationship between the dissolved N_2 concentration and *TLI* ($p < 0.001$). The excess dissolved N_2 (ΔN_2), which was obtained by subtracting dissolved N_2 from the saturated concentration, was consistently positive (8.1–16.1 μmol L^{-1}) in summer, indicating N_2 oversaturation. The trend of N_2 oversaturation as a function of *TLI* was consistent with dissolved N_2 (Fig. 3).

4.3.3 Relationship between environmental factors and N_2O emission fluxes

The Pearson correlations between N_2O emission fluxes and environmental

parameters of the overlying water were analyzed in different seasons (Table S4). The N_2O emission fluxes were significantly and positively correlated with TN, NO_3^--N, and *TLI* ($p < 0.01$). The correlation between chl-*a* and N_2O emission fluxes varied seasonally, and the correlation was stronger in summer. ΔN_2 was negatively correlated with N_2O emission fluxes, TN, NO_3^--N, and chl-*a* in summer ($p < 0.05$). There was a negative correlation between DO concentrations and N_2O emission fluxes ($p < 0.05$) in summer, and this correlation was not observed in winter and over the entire year ($p > 0.05$) (Table S4). The overlying water DO was higher in winter (> 7 mg L^{-1}) than in summer (Fig. S1b). During the survey period, the temperature of the overlying water ranged from 9.5°C to 15.1°C and 27.1°C to 31.3°C in winter and summer, respectively (Fig. S1c). The temperature was negatively correlated with N_2O emission fluxes in both summer and winter ($p < 0.05$, Table S5). N_2O emission fluxes showed significant and positive linear correlations with TN (adj, $R^2 = 0.797$, $p < 0.01$ in winter; adj. $R^2 = 0.908$, $p < 0.01$ in summer), NO_3^--N (adj. $R^2 = 0.787$, $p < 0.01$ in winter; adj. $R^2 = 0.826$, $p < 0.01$ in summer), and NH_4^+-N (adj. $R^2 = 0.39$, $p = 0.039$ in winter; adj. $R^2 = 0.484$, $p = 0.01$ in summer) (Fig. 4). In addition, there was a significant negative linear correlation between *TLI* and the C:N ratio (adj. $R^2 = 0.649$, $p < 0.001$) (Fig. S3). There was a strong nonlinear correlation between N_2O emission fluxes and the C:N ratio (adj. $R^2 = 0.414$, $p < 0.001$) (Fig. S5).

A multiple stepwise regression model incorporating the physicochemical variables of the overlying water was established for N_2O emission fluxes (Table 1). The results showed that TN and TP concentrations can predict N_2O emission fluxes in summer (adj. $R^2 = 0.94$, $p < 0.001$). TN ($t_1 = 10.80$) was more strongly positively correlated with N_2O emission fluxes than TP ($t_2 = 2.93$), which indicated that TN was an important parameter determining N_2O emission fluxes in summer. In addition, TN, chl-*a*, and NO_3^--N could jointly predict N_2O emission fluxes (adj. $R^2 = 0.96$, $p < 0.001$) in winter, demonstrating that both TN (6.11) and chl-*a* (–6.56) are important parameters determining N_2O emission fluxes in winter. TN (12.83) and chl-*a* (–4.07) were important variables predicting N_2O

emission flux in lakes (adj. $R^2 = 0.86$, $p < 0.01$).

4.3.4 Microbial community structure and denitrifier abundances in lakes of different trophic state

Relative abundances of microbes were obtained at the phylum level in summer and winter (Fig. 5). Overall, the top 15 phyla made up more than 80% of microbial communities in all lake sediments. The following six phyla accounted for over 60% of the total population in summer: *Proteobacteria*, *Chloroflexi*, *Bacteroidetes*, *Acidobacteria, Verrucomicrobia,* and *Planctomycetes*; those in the winter were *Proteobacteria, Bacteroidetes, Acidobacteria, Nitrospirae, Planctomycetes,* and *Verrucomicrobia.* The most abundant phylum was *Proteobacteria*, which had relative abundances in hyper-eutrophic, middle-eutrophic, eutrophic, and mesotrophic lakes of 30.6–44.2%, 32.3–42.4%, 31.8–39.9%, and 32.0–46.4%, respectively. *Proteobacteria* (26.4–43.4%) was also common in all lakes in winter. Among the six dominant phyla, the relative abundances of *Chloroflexi* were 2.8–5.7% in winter and 4.7–15.9% in summer; the relative abundances of *Nitrospirae* were 2.3–9.7% in winter and 0.1–4.1% in summer.

The *nirS* gene abundances in winter (0.66×10^7–3.67×10^7 copies g^{-1}-sediment) were lower than those in summer (2.70×10^7–7.62×10^8 copies g^{-1}-sediment) (Fig. S5). By contrast, no significant difference was observed for *nirK* gene abundances in winter (0.36×10^7–2.29×10^7 copies g^{-1}-sediment) and summer (0.06×10^7–2.06×10^7 copies g^{-1}-sediment). The *nirS*/*nirK* ratio was greater than 1, indicating that the *nirS*-type denitrifiers were consistently more abundant than *nirK*-type denitrifiers in these shallow lakes (Fig. 6a). The ratios were 9–48 times higher in summer than in winter. In addition, the *nirS*/*nirK* ratio increased as *TLI* increased in summer and winter ($p < 0.05$). *nirS*/*nirK* and N_2O emission fluxes were also positively correlated (Fig. S6a). The abundance of *nosZ*, which encodes an enzyme for N_2O consumption, varied from 0.31×10^7 copies g^{-1}-sediment to 2.88×10^7 copies g^{-1}-sediment in winter, which was lower than that in

summer (0.53×10^7–7.02×10^7 copies g^{-1}-sediment) (Fig. S5). Variation in the ratios of (*nirK* + *nirS*)/*nosZ* was lower among the shallow lakes in winter (0.8–9.5) than in summer (2.9–12.3) (Fig. 6b). The ratio of (*nirK* + *nirS*)/*nosZ* was positively correlated with *TLI* ($p = 0.022$) and N_2O emission flux (Fig. S6b). Further analysis revealed the relationship between the spatial distribution of these denitrifying genes and multiple environmental factors (Fig. 7). A redundancy analysis (RDA) showed that the first two axes explained 60.38% of the variation in the denitrifying genes. The samples of the examined lakes were well separated among the different seasons. The RDA between the denitrifying gene abundances and environmental parameters indicated that temperature was an important factor affecting gene abundances. Among the tested parameters, *nirS* and *nosZ* abundances were sensitive to temperature compared with *nirK*. The dissimilarity in the abundance of denitrifying genes in lakes of different trophic state was greater in summer than in winter. The abundance of *nirS* was positively correlated with *TLI*, and the abundance of *nosZ* was marginally correlated with *TLI*.

4.3.5 Characterization of N_2O emissions in the heavy algae-accumulated and light algae-accumulated zones in Lake Taihu

The N loading and chl-*a* concentrations were higher in the heavy algae-accumulated zones (Zones A and B) than in the light algae-accumulated zone (Zone D) (Table S2). The N_2O emissions fluxes were characterized in summer and winter in the two typical zones in Lake Taihu. The N_2O emission fluxes were significantly higher in the heavy algae-accumulated zones (Zones A and B) and transitional zone (Zone C) than in the light algae-accumulated zone (Zone D). The N_2O emission fluxes were location-dependent and varied from 42.16–136.63 μg m^{-2} h^{-1} in the heavy algae-accumulated zones (Zones A and B), 21.35–31.89 μg m^{-2} h^{-1} in the transitional zone (Zone C), and 3.7–4.71 μg m^{-2} h^{-1} in the light algae-accumulated zone (Zone D) (Fig. 8). These fluxes in the algae-accumulated zones were significantly different in summer and winter ($p < 0.05$), and

differences were not significant in Zone C ($p = 0.076$) and Zone D ($p = 0.677$). There was an exponential relationship between *TLI* and N_2O emission fluxes (Fig. S7) (adj. $R^2 = 0.55$, $p < 0.05$).

4.4 Discussion

4. 4.1 Nonlinear N_2O emission patterns

Shallow lakes are potential sources of N_2O emissions and have been extensively studied (Kortelainen et al., 2020; Lauerwald et al., 2019; McCrackin and Elser, 2011). Previous studies have documented variation in N_2O emissions across lakes of different trophic state (Kortelainen et al., 2020; Salk and Ostrom, 2019); nevertheless, predicting N_2O emission fluxes from shallow lakes remains a challenge. This study showed that the net N_2O emission fluxes in lakes located in the Yangtze River basin, which spans 1000 km, displayed spatial and temporal heterogeneity determined by lake trophic state (Fig. 2). Consistent with previous studies (Salk and Ostrom, 2019; Xiao et al., 2019; Zhou et al., 2020a), these findings indicate that eutrophic lakes in the Yangtze River basin are sources of N_2O emissions. The patterns of N_2O emission fluxes in the shallow lakes were not completely consistent with the results of previous studies and depended on eutrophication progress. The N_2O emission fluxes in the eutrophic and middle-eutrophic lakes (Table S1) were similar to the global median value of N_2O emission flux in lakes, whereas the mean N_2O emission flux in the hyper-eutrophic lakes was 8.7–11.2 times higher than the global median value (Hu et al., 2016). Shallow lakes in a mesotrophic state in summer were N_2O sinks (Fig. 2 and Table S1); these findings expand our knowledge regarding the prerequisites for freshwater lakes to act as either N_2O sinks or sources (Lauerwald et al., 2019). Our study underscores the significance of lake trophic state in determining N_2O emission fluxes, which is supported by the correlation between net N_2O emission flux and trophic state (Fig. 2a). Whether lakes of different trophic state act as N_2O sources or sinks can be predicted based on this correlation.

The major contribution of this study is the exponential model based on *TLI*, which could provide a robust means for quantifying lake trophic state; this model can be used to predict the N_2O emissions from lakes. This model represents an improvement over previous approaches for estimating N_2O emission fluxes because previous approaches do not consider differences in lake trophic state (Lauerwald et al., 2019). This model can be used to assess N_2O emission fluxes in shallow lakes of different trophic state. The N_2O emission fluxes and *TLI* were well fitted in summer (adj. $R^2 = 0.85$) and winter (adj. $R^2 = 0.63$). However, the coefficient of determination was low (adj. $R^2 = 0.36$) when all data (*i.e.*, summer and winter) were incorporated into the model, which is likely explained by the large differences in N_2O emission fluxes in winter and summer (Fig. 2). Therefore, seasonal differences in N_2O emission fluxes in shallow lakes should also receive consideration (Kortelainen et al., 2019; Miao et al., 2020). Given the limited data on seasonal differences and the limited number of shallow lakes investigated, more data on N_2O emission fluxes are required to verify the credibility of the model.

4.4.2 Potential drivers of N_2O emissions

Our results revealed that reactive N accumulation plays a major role in regulating lake trophic state levels and the biological N cycle and promotes N_2O emissions via denitrification in shallow lakes. Degradation and metabolism were similar among shallow lakes despite variation in trophic state. *Proteobacteria* was identified as a predominant phylum based on the 16S rRNA gene analysis, and it was commonly detected in lakes of different trophic state (Fig. 5) (Li et al., 2019b); *Proteobacteria* might potentially contribute to degradation and metabolism (Huang et al., 2019). Previous studies have indicated that copiotrophic groups such as *Proteobacteria* and *Bacteroidetes* with high growth rates tend to thrive in nutrient-rich conditions (Fierer et al., 2012). The overlying water and sediments likely stored abundant nutrients that could be used by microorganisms in shallow lakes. In addition, nutrient abundance is an important factor

affecting the microorganisms responsible for N conversion (Saarenheimo et al., 2015; Zhang et al., 2019). The denitrifying genes varied greatly among the different trophic lakes and seasons (Figs. 6 and S5). These results suggest that denitrification is an important source of N_2O emissions in shallow eutrophic lakes, which is consistent with the results of previous studies (Beaulieu et al., 2011; Zhang et al., 2020). This is also confirmed by the stronger correlation of N_2O emission flux with NO_3^- than with NH_4^+ (Fig. 4) and the negative correlation between DO and N_2O emission fluxes (Table S4). The significant relationship between *TLI* and (*nirK* + *nirS*)/*nosZ* (p = 0.022), which indicates the relative abundance of N_2O producers relative to N_2O consumers, suggests that N_2O production may be greater than N_2O consumption in hyper-eutrophic lakes (Fig. 6b) (Zhao et al., 2018). Higher net N_2O emission fluxes were observed in hyper-eutrophic lakes because of their higher nutrient availability and (*nirK* + *nirS*)/*nosZ* (Kortelainen et al., 2020). These findings might explain the close relationship between lake trophic state and N_2O emission flux.

N availability drives eutrophication, and the subsequent accumulation of algae alters the redox conditions favoring denitrification (Yan et al., 2017; Zhu et al., 2020) and increases N_2O emissions in shallow lakes. In freshwater ecosystems, N loadings significantly contribute to N_2O emissions via denitrification (Kortelainen et al., 2020; Mulholland et al., 2008), which explains the high N_2O emission fluxes observed in eutrophic lakes when N loading was high (Figs. 2 and 4). A stepwise linear regression model indicated that TN and chl-*a* (algal density) are important parameters explaining N_2O emissions (Table 1). Following algal accumulation, algal decay alters redox conditions and releases organic matter *in-situ* (Yan et al., 2017; Zhu et al., 2020). Moreover, algal blooms result in low DO concentrations and the accumulation of organic matter in hyper-eutrophic lakes (Yan et al., 2017; Zhou et al., 2020b; Zhu et al., 2020). For example, algal accumulation in Lake Taihu accounts for >50% of the organic matter (Xu et al., 2019). A C:N ratio lower than 8 indicates that organic matter is mainly derived

from autochthonous inputs (Meyers, 1994; Yan et al., 2017). The negative correlation between C:N ratio and *TLI* (Fig. S3) indicates that algal accumulation and decomposition alter the physicochemical conditions in shallow lakes. Therefore, the contribution of algal decomposition should receive increased consideration when exploring the relationship between N_2O emission fluxes and chl-*a*. Our results indicated that N_2O emission fluxes and the C:N ratio were negatively correlated ($p < 0.001$) (Fig. S5). Algal decomposition results in oxygen consumption and thus a low DO concentration, which is favorable for denitrification (Zhu et al., 2020). This observation is consistent with the negative correlation between DO and chl-*a* (Tables S4 and S5). These findings might potentially explain the roles of decomposed algae in stimulating N_2O emissions via consumed oxygen in eutrophic shallow lakes.

Temperature is an important variable determining denitrifier abundance and structure in both seasons (Figs. 6 and 7); the effect of temperature was also manifested by the differences in N_2O emissions among seasons (Fig. 2). This pattern is similar to a previous study of 87 boreal lakes in Finland showing that N_2O emissions peaked in winter (Kortelainen et al., 2020). Among enzymes responsible for denitrification, N_2O reductase is most sensitive to changes in temperature (Kortelainen et al., 2020; Veraart et al., 2011; Zhou et al., 2020c). Our previous study indicated that *nosZ* in N_2O-reducing bacteria is strongly related to temperature (Zhou et al., 2020c). In addition, N_2O reduction activity is inhibited by oxygen exposure, which increases N_2O emissions (Song et al., 2019). Low temperature increased the oxygen concentration (Fig. S1), and the relationship between the ratio of *nirS* to *nirK* with *TLI* varied in winter (slope: 0.08) and summer (slope: 1.11) ($p < 0.05$) (Fig. 6a). Given that the algae in lakes gradually declined in winter concomitant with increasing DO concentrations (Fig. S1 and Table S1), N_2O emission fluxes in lakes increased in winter (Fig. 2a) (Miao et al., 2020). In summer, algal decay further decreased the oxygen concentration. Previous studies have shown that *nirK* only achieves high abundances in conditionally oxygen-exposed environment (Huang et al., 2011), whereas

nirS genes have been more commonly detected in anoxic locations (Knapp et al., 2009). The observation that the N_2O emission fluxes, *nirS*/*nirK*, and (*nirS*+*nirK*)/*nosZ* showed more significant positive relationships in winter than in summer suggests that the N_2O emission fluxes in summer were also affected by other factors (Fig. S6). The dramatic difference between hyper-eutrophic lakes in winter and summer was in the frequency of algal blooms in hyper-eutrophic lakes in summer. The algae regulating N_2O emission fluxes in shallow lakes are discussed in the subsequent section. In sum, low temperature associated with abundant N favored N_2O accumulation via control oxygen concentrations and limit N_2O reduction activity.

4.4.3 The dual-impact of algae in N_2O emissions

N_2O emissions were highest, and the chl-*a* concentration low, in Zone B in contrast to Zone A in a heavy algae-accumulated zone of Lake Taihu (Fig. 8 and Table S2). This result is inconsistent with the finding that algal accumulation, reflected by *TLI*, stimulated N_2O emissions in a non-linear exponential manner in the other tested lakes (Fig. S7). In heavy algae-accumulated zones, lower N_2O emissions, indicated by the high chl-*a* concentration, likely stem from algal accumulation, which suppresses denitrification activities caused by the decrease in N_2O production. Recently, Zhu et al. (2020) reported that algal accumulation may inhibit denitrification during algal blooms in summer. Consistent with this finding, a unimodal relationship between *TLI* and excess dissolved N_2 (ΔN_2) in summer was observed (Fig. 3b), which indicated higher complete denitrification (*i.e.*, including N_2O consumption) rates in the eutrophic lakes (Chen et al., 2014; Wang et al., 2018). In summer, the highest gene abundances of *nirK*, *nirS*, and *nosZ* were observed in eutrophic and middle-eutrophic lakes rather than in hyper-eutrophic lakes (Fig. S5). Although more abundant N is available in hyper-eutrophic lakes, the complete denitrification rates may be lower in hyper-eutrophic lakes than in eutrophic lakes in summer. This pattern potentially stems from the abundance of algal biomass in

the hyper-eutrophic lakes, as release of algal debris eventually leads to reductive conditions (Table S2). The decay of excess algal biomass could create favorable conditions for denitrification where organic carbon is present under hypoxic or anoxic conditions. However, hypoxia limits nitrification, which leads to a deficiency in the supply of NO_3^- for denitrification (Small et al., 2014; Zhu et al., 2020). This effect is supported by previous work in zones with accumulated algae in Lake Taihu showing that the NH_4^+ concentration in sediments is two or three orders of magnitude higher than the NO_3^- concentration (Yan et al., 2019). Our results are also consistent with this observation (Table S2). In addition, chl-*a* (as a negative factor) and TN together predicted the N_2O emission fluxes (Table 1). Algal accumulation and decomposition create hypoxic conditions that limit nitrification by converting NH_4^+ into NO_3^-, eventually suppressing the ensuing denitrification. In addition, hypoxic conditions favor complete denitrifying bacteria for mitigating N_2O emissions. These results further explain why higher N_2O emission fluxes of shallow lakes were observed in winter rather than in summer (Figs. 2a and 8). Therefore, these evidences indicated that algal accumulation played a dual role in stimulating and impeding N_2O emissions, especially in hyper-eutrophic lakes.

4.4.4 Implications from eutrophic progress

In aquatic ecosystems, excessive N loadings drive eutrophication and promote N_2O emissions in water bodies (Zhao et al., 2015). Meanwhile, the nutrient overload induces algae growth in shallow lakes, forming an anoxic or microaerobic micro-environment favoring N_2O production by algae accumulation (Zhu et al., 2020). In this study, a nonlinear exponential increase in N_2O emission flux as a function of *TLI* in shallow lakes of different trophic state was observed (Fig. 2). Eutrophic lakes had high N_2O emission fluxes, which is consistent with the relationship between lake trophic state and CH_4 emission fluxes (Zhou et al., 2020b). The common trends indicate that increases in GHG emissions stem from eutrophication. The predicted N_2O emission fluxes based on the

IPCC EF_{5r} overestimated the observed fluxes but also exhibited a non-linear exponential increase with *TLI* (Fig. 2b). Xiao et al. (2019) reported that the N_2O emission factor in Lake Taihu was 0.18%, which is lower than the value of EF_{5r} based on the reported IPCC value. The overestimation by the IPCC default value indicates the need to calibrate an N_2O emission factor in shallow lakes depending on the eutrophic state. Pronounced differences between the predicted and observed N_2O emission fluxes were observed in hyper-eutrophic lakes where the abundance of algae impeded N_2O emissions. The high abundance of algae in summer compared with winter indicates that the degree to which N_2O emission flux was overestimated in summer was different from that in winter (Fig. S2). Algal decomposition made the redox conditions favorable for denitrification but unfavorable for nitrification because of an insufficient supply of NO_3^-. The retained nitrogen is absorbed by the newly grown algae (Zhu et al., 2020). In non-limited N, algal decay leads to low-oxygen conditions, which enhances denitrification and further stimulates N_2O emissions. Therefore, algae should be considered a nitrogen "pool" that maintains nitrogen in lakes. In such situations where algae pools N, lower N_2O emissions stemming from the suppression of nitrification do not contribute to the reduction in global N_2O emissions from lakes but potentially leads to substantial N_2O emissions from hyper-eutrophic state lakes when conditions for nitrification are suitable. We suggest that overestimation was possibly caused by the "dual role" of the algae because they help re-regulate denitrification to mitigate N_2O emissions. Estimation of flux by the two-layer model was one order of magnitude lower than that estimated by static chamber methods (Duchemin et al., 1999). Given that the two different methods plausibly overestimated or underestimated the N_2O emission fluxes in shallow lakes, an intensive survey of an N_2O emission factor in hyper-eutrophic lakes will be conducted in a follow-up study.

4.5 Conclusions

We performed a series of field measurements and characterized the N_2O emissions

in shallow lakes of different trophic state in the Yangtze River basin. The results of this study are detailed below.

- The N_2O emission fluxes of shallow lakes were most strongly affected by lake trophic state, suggesting that estimation of N_2O emission fluxes should consider lake trophic state.
- The nonlinear model incorporating trophic state levels can describe the N_2O emissions from a shallow lake.
- The predicted N_2O emission fluxes based on the IPCC EF_{5r} overestimated the observed fluxes, particularly those in hyper-eutrophic lakes.
- Nutrient-rich conditions and algal accumulation were key factors determining N_2O emission fluxes in shallow lakes, and algal accumulation played a dual role in stimulating and impeding N_2O emissions, especially in hyper-eutrophic lakes.
- Changes in season accompanied the appearance and disappearance of algae and altered N_2O emission fluxes, especially in hyper-eutrophic lakes.

4.6 References

Beaulieu, J.J., Tank, J.L., Hamilton, S.K., Wollheim, W.M., Hall, R.O., Jr., Mulholland, P.J., Peterson, B.J., Ashkenas, L.R., Cooper, L.W., Dahm, C.N., Dodds, W.K., Grimm, N.B., Johnson, S.L., McDowell, W.H., Poole, G.C., Valett, H.M., Arango, C.P., Bernot, M.J., Burgin, A.J., Crenshaw, C.L., Helton, A.M., Johnson, L.T., O'Brien, J.M., Potter, J.D., Sheibley, R.W., Sobota, D.J., Thomas, S.M., 2011. Nitrous oxide emission from denitrification in stream and river networks. Proceedings of the National Academy of Sciences of the United States of America 108, 214-219.

Chen, N., Chen, Z., Wu, Y., Hu, A., 2014. Understanding gaseous nitrogen removal through direct measurement of dissolved N_2 and N_2O in a subtropical river-reservoir system. Ecological Engineering 70, 56-67.

Chen, R., Deng, M., He, X., Hou, J., 2017. Enhancing nitrate removal from freshwater pond by regulating carbon/nitrogen ratio. Frontiers in Microbiology 8, 1712.

Cole, J.J., Bade, D.L., Bastviken, D., Pace, M.L., Van de Bogert, M., 2010. Multiple approaches to estimating air-water gas exchange in small lakes. Limnology and Oceanography: Methods 8, 285-293.

Cole, J.J., Caraco, N.F., 1998. Atmospheric exchange of carbon dioxide in a low-wind oligotrophic lake measured by the addition of SF6. Limnology and Oceanography 43, 647-656.

Domeignoz-Horta, L.A., Putz, M., Spor, A., Bru, D., Breuil, M.C., Hallin, S., Philippot, L., 2016. Non-denitrifying nitrous oxide-reducing bacteria - An effective N_2O sink in soil. Soil Biology and Biochemistry 103, 376-379.

Duchemin, E., Lucotte, M., Canuel, R., 1999. Comparison of static chamber and thin boundary layer equation methods for measuring greenhouse gas emissions from large water bodies. Environmental Science & Technology 33, 350-357.

Fierer, N., Lauber, C.L., Ramirez, K.S., Zaneveld, J., Bradford, M.A., Knight, R., 2012. Comparative metagenomic, phylogenetic and physiological analyses of soil microbial communities across nitrogen gradients. ISME Journal 6, 1007-1017.

Gålfalk, M., Bastviken, D., Fredriksson, S., Arneborg, L., 2013. Determination of the piston velocity for water-air interfaces using flux chambers, acoustic Doppler velocimetry, and IR imaging of the water surface. Journal of Geophysical Research: Biogeosciences 118, 770-782.

Hinshaw, S.E., Dahlgren, R.A., 2013. Dissolved nitrous oxide concentrations and fluxes from the eutrophic San Joaquin River, California. Environmental Science & Technology 47, 1313-1322.

Hu, M., Chen, D., Dahlgren, R.A., 2016. Modeling nitrous oxide emission from rivers: a global assessment. Global Change Biology 22, 3566-3582.

Huang, S., Chen, C., Yang, X., Wu, Q., Zhang, R., 2011. Distribution of typical

denitrifying functional genes and diversity of the *nir*S-encoding bacterial community related to environmental characteristics of river sediments. Biogeosciences 8, 3041-3051.

Huang, W., Chen, X., Wang, K., Chen, J., Zheng, B., Jiang, X., 2019. Comparison among the microbial communities in the lake, lake wetland, and estuary sediments of a plain river network. Microbiologyopen 8, e00644.

IPCC In: Stocker T.F. et al (Eds)., 2013. Climate change 2013: the physical science basis. Contribution of working group I to the fifth assessment report of the Intergovernmental Panel on Climate Change. Cambridge University Press, New York. Cambridge University Press, New York.

IPCC, In: Calvo, Buendia, E.; Tanabe, K.; Kranjc, A.; Baasansuren, J.; Fukuda, M.; Ngarize, S.; Osako, A.; Pyrozhenko, Y.; Shermanau, P.; Federici, S.; (Eds.), 2019. Refinement to the 2006 IPCC guidelines for national greenhouse gas inventories, Volum 4. IPCC, Switzerland, Kanagawa, JAPAN. Chapter 11.

Jiang, X., Gao, G., Zhang, L., Tang, X., Shao, K., Hu, Y., Cai, J., 2020. Role of algal accumulations on the partitioning between N_2 production and dissimilatory nitrate reduction to ammonium in eutrophic lakes. Water Research 183, 116075.

Knapp, C.W., Dodds, W.K., Wilson, K.C., O'Brien, J.M., Graham, D.W., 2009. Spatial heterogeneity of denitrification genes in a highly homogenous urban stream. Environmental Science & Technology 43, 4273-4279.

Kortelainen, P., Larmola, T., Rantakari, M., Juutinen, S., Alm, J., Martikainen, P.J., 2020. Lakes as nitrous oxide sources in the boreal landscape. Global Change Biology 26, 1432-1445.

Lauerwald, R., Regnier, P., Figueiredo, V., Enrich‐Prast, A., Bastviken, D., Lehner, B., Maavara, T., Raymond, P., 2019. Natural Lakes are a minor global source of N_2O to the atmosphere. Global Biogeochemical Cycles 33, 1564-1581.

Li, Q., Wang, F., Yu, Q., Yan, W., Li, X., Lv, S., 2019a. Dominance of nitrous oxide

production by nitrification and denitrification in the shallow Chaohu Lake, Eastern China: Insight from isotopic characteristics of dissolved nitrous oxide. Environmental Pollution 255, 113212.

Li, S., Bush, R.T., Santos, I.R., Zhang, Q., Song, K., Mao, R., Wen, Z., Lu, X.X., 2018. Large greenhouse gases emissions from China's lakes and reservoirs. Water Research 147, 13-24.

Li, Y., Sun, Y., Zhang, H., Wang, L., Zhang, W., Niu, L., Wang, P., Wang, C., 2019b. The responses of bacterial community and N_2O emission to nitrogen input in lake sediment: Estrogen as a co-pollutant. Environmental Research 179, 108769.

Liikanen, A., Huttunen, J.T., Murtoniemi, T., Tanskanen, H., Vaisanen, T., Silvola, J., Alm, J., Martikainen, P.J., 2003. Spatial and seasonal variation in greenhouse gas and nutrient dynamics and their interactions in the sediments of a boreal eutrophic lake. Biogeochemistry 65, 83-103.

Ma, R., Yang, G., Duan, H., Jiang, J., Wang, S., Feng, X., Li, A., Kong, F., Xue, B., Wu, J., Li, S., 2011. China’s lakes at present: Number, area and spatial distribution. Science China Earth Sciences 54, 283-289.

Maavara, T., Lauerwald, R., Laruelle, G.G., Akbarzadeh, Z., Bouskill, N.J., Van Cappellen, P., Regnier, P., 2019. Nitrous oxide emissions from inland waters: Are IPCC estimates too high? Global Change Biology 25, 473-488.

McCrackin, M.L., Elser, J.J., 2011. Greenhouse gas dynamics in lakes receiving atmospheric nitrogen deposition. Global Biogeochemical Cycles 25, 1-12.

Meyers, P.A., 1994. Preservation of elemental and isotopic source identification of sedimentary organic matter. Chemical Geology 114, 289-302.

Miao, Y., Huang, J., Duan, H., Meng, H., Wang, Z., Qi, T., Wu, Q.L., 2020. Spatial and seasonal Variability of nitrous oxide in a large freshwater lake in the lower reaches of the Yangtze River, China. Science of Total Environment 721, 137716.

Mulholland, P.J., Helton, A.M., Poole, G.C., Hall, R.O., Hamilton, S.K., Peterson, B.J.,

Tank, J.L., Ashkenas, L.R., Cooper, L.W., Dahm, C.N., 2008. Stream denitrification across biomes and its response to anthropogenic nitrate loading. Nature 452, 202-205.

Qin, B., Zhu, G., Gao, G., Zhang, Y., Wei, L., Paerl, H.W., Carmichael, W.W., 2010. A drinking water crisis in Lake Taihu, China: Linkage to climatic variability and lake management. Environmental Management 45, 105-112.

Ravishankara, A.R., Daniel, J.S., Portmann, R.W., 2009. Nitrous oxide (N_2O): the dominant ozone-depleting substance emitted in the 21st century. Science 326, 123-125.

Saarenheimo, J., Tiirola, M.A., Rissanen, A.J., 2015. Functional gene pyrosequencing reveals core proteobacterial denitrifiers in boreal lakes. Frontiers in Microbiology 6, 674.

Salk, K.R., Ostrom, N.E., 2019. Nitrous oxide in the Great Lakes: insights from two trophic extremes. Biogeochemistry 144, 233-243.

Shaaban, M., Wu, Y., Khalid, M.S., Peng, Q.A., Xu, X., Wu, L., Younas, A., Bashir, S., Mo, Y., Lin, S., Zafar-Ul-Hye, M., Abid, M., Hu, R., 2018. Reduction in soil N_2O emissions by pH manipulation and enhanced *nosZ* gene transcription under different water regimes. Environmental Pollution 235, 625-631.

Small, G.E., Cotner, J.B., Finlay, J.C., Stark, R.A., Sterner, R.W., 2014. Nitrogen transformations at the sediment–water interface across redox gradients in the Laurentian Great Lakes. Hydrobiologia 731, 95-108.

Song, K., Kang, H., Zhang, L., Mitsch, W.J., 2012. Seasonal and spatial variations of denitrification and denitrifying bacterial community structure in created riverine wetlands. Ecological Engineering 38, 130-134.

Song, X., Ju, X., Topp, C.F.E., Rees, R.M., 2019. Oxygen regulates nitrous oxide production directly in agricultural soils. Environmental Science & Technology 53, 12539-12547.

Tian, H., Xu, R., Canadell, J.G., Thompson, R.L., Winiwarter, W., Suntharalingam, P., Davidson, E.A., Ciais, P., Jackson, R.B., Janssens-Maenhout, G., Prather, M.J., Regnier, P., Pan, N., Pan, S., Peters, G.P., Shi, H., Tubiello, F.N., Zaehle, S., Zhou, F., Arneth, A., Battaglia, G., Berthet, S., Bopp, L., Bouwman, A.F., Buitenhuis, E.T., Chang, J., Chipperfield, M.P., Dangal, S.R.S., Dlugokencky, E., Elkins, J.W., Eyre, B.D., Fu, B., Hall, B., Ito, A., Joos, F., Krummel, P.B., Landolfi, A., Laruelle, G.G., Lauerwald, R., Li, W., Lienert, S., Maavara, T., MacLeod, M., Millet, D.B., Olin, S., Patra, P.K., Prinn, R.G., Raymond, P.A., Ruiz, D.J., van der Werf, G.R., Vuichard, N., Wang, J., Weiss, R.F., Wells, K.C., Wilson, C., Yang, J., Yao, Y., 2020. A comprehensive quantification of global nitrous oxide sources and sinks. Nature 586, 248-256.

Veraart, A.J., de Klein, J.J.M., Scheffer, M., 2011. Warming can boost denitrification disproportionately due to altered oxygen dynamics. PLoS One 6.

Wang, G., Wang, J., Xia, X., Zhang, L., Zhang, S., McDowell, W.H., Hou, L., 2018. Nitrogen removal rates in a frigid high-altitude river estimated by measuring dissolved N_2 and N_2O. Science of the Total Environment 645, 318-328.

Wang, S., Liu, C., Yeager, K.M., Wan, G., Li, J., Tao, F., Lu, Y., Liu, F., Fan, C., 2009. The spatial distribution and emission of nitrous oxide (N_2O) in a large eutrophic lake in eastern China: anthropogenic effects. Science of the Total Environment 407, 3330-3337.

Weiss, R.F., 1970. The solubility of nitrogen, oxygen and argon in water and seawater. Deep Sea Research and Oceanographic Abstracts 17, 721-735.

Weiss, R.F., Price, B.A., 1980. Nitrous-oxide solubility in water and seawater. Marine Chemistry 8, 347-359.

Wenk, C.B., Frame, C.H., Koba, K., Casciotti, K.L., Veronesi, M., Niemann, H., Schubert, C.J., Yoshida, N., Toyoda, S., Makabe, A., Zopfi, J., Lehmann, M.F., 2016. Differential N2O dynamics in two oxygen-deficient lake basins revealed by stable

isotope and isotopomer distributions. Limnology and Oceanography 61, 1735-1749.

Xiao, Q., Xu, X., Zhang, M., Duan, H., Hu, Z., Wang, W., Xiao, W., Lee, X., 2019. Coregulation of nitrous oxide emissions by nitrogen and temperature in China's third largest freshwater lake (Lake Taihu). Limnology and Oceanography 64, 1070-1086.

Xu, J., Lyu, H., Xu, X., Li, Y., Li, Z., Lei, S., Bi, S., Mu, M., Du, C., Zeng, S., 2019. Dual stable isotope tracing the source and composition of POM during algae blooms in a large and shallow eutrophic lake: All contributions from algae? Ecological Indicators 102, 599-607.

Yan, X., Xu, X., Ji, M., Zhang, Z., Wang, M., Wu, S., Wang, G., Zhang, C., Liu, H., 2019. Cyanobacteria blooms: A neglected facilitator of CH_4 production in eutrophic lakes. Science of the Total Environment 651, 466-474.

Yan, X., Xu, X., Wang, M., Wang, G., Wu, S., Li, Z., Sun, H., Shi, A., Yang, Y., 2017. Climate warming and cyanobacteria blooms: Looks at their relationships from a new perspective. Water Research 125, 449-457.

Yoon, S., Nissen, S., Park, D., Sanford, R.A., Loffler, F.E., 2016. Nitrous oxide reduction kinetics distinguish bacteria harboring clade I *nosZ* from those harboring clade II *nosZ*. Applied and Environmental Microbiology 82, 3793-3800.

Zhang, W., Li, H., Xiao, Q., Jiang, S., Li, X., 2020. Surface nitrous oxide (N_2O) concentrations and fluxes from different rivers draining contrasting landscapes: Spatio-temporal variability, controls, and implications based on IPCC emission factor. Environmental Pollution 263, 114457.

Zhang, Y., Ji, G., Wang, C., Zhang, X., Xu, M., 2019. Importance of denitrification driven by the relative abundances of microbial communities in coastal wetlands. Environmental Pollution 244, 47-54.

Zhao, S., Wang, Q., Zhou, J., Yuan, D., Zhu, G., 2018. Linking abundance and community of microbial N_2O-producers and N_2O-reducers with enzymatic N_2O production potential in a riparian zone. Science of the Total Environment 642, 1090-1099.

Zhao, S., Zhou, J., Yuan, D., Wang, W., Zhou, L., Pi, Y., Zhu, G., 2019. *Nir*S-type N_2O-producers and *nos*Z II-type N_2O-reducers determine the N_2O emission potential in farmland rhizosphere soils. Journal of Soils and Sediments 20, 461-471.

Zhao, Y., Xia, Y., Ti, C., Shan, J., Li, B., Xia, L., Yan, X., 2015. Nitrogen removal capacity of the river network in a high nitrogen loading region. Environmental Science & Technology 49, 1427-1435.

Zhou, Y., Xiao, Q., Zhou, L., Jang, K.S., Zhang, Y., Zhang, M., Lee, X., Qin, B., Brookes, J.D., Davidson, T.A., Jeppesen, E., 2020c. Are nitrous oxide emissions indirectly fueled by input of terrestrial dissolved organic nitrogen in a large eutrophic Lake Taihu, China? Science of the Total Environment 722, 138005.

Zhou, Y., Song, K., Han, R., Riya, S., Xu, X., Yeerken, S., Geng, S., Ma, Y., Terada, A., 2020a. Nonlinear response of methane release to increased trophic state levels coupled with microbial processes in shallow lakes. Environmental Pollution 265, 114919.

Zhou, Y., Suenaga, T., Qi, C., Riya, S., Hosomi, M., Terada, A., 2020c. Temperature and oxygen level determine N_2O respiration activities of heterotrophic N_2O-reducing bacteria: Biokinetic study. Biotechnology and Bioengineering.

Zhou, Y., Xu, X., Han, R., Li, L., Feng, Y., Yeerken, S., Song, K., Wang, Q., 2019. Suspended particles potentially enhance nitrous oxide (N_2O) emissions in the oxic estuarine waters of eutrophic lakes: Field and experimental evidence. Environmental Pollution 252, 1225-1234.

Zhu, L., Shi, W., Van Dam, B., Kong, L., Yu, J., Qin, B., 2020. Algal accumulation decreases sediment nitrogen removal by uncoupling nitrification-denitrification in shallow eutrophic lakes. Environmental Science & Technology 54, 6194-6201.

Table and Figures

Table 1. Validity of the multiple stepwise regression model for N_2O emission fluxes incorporating variables of the overlying water

Season	Parameters	Equations	Variables	Adj. R^2	*p*	Significance level			
						F-test	T-test		
						F	t_1	t_2	t_3
Summer	N_2O	$N_2O = 14.33(TN) – 10.45$	TN	0.91	$p < 0.001$	158.86	12.60		
		$N_2O = 12.36(TN) + 27.99(TP) – 13.13$	TN, TP	0.94	$p < 0.001$	123.95	10.80	2.93	
Winter	N_2O	$N_2O = 21.04(TN) – 13.44$	TN	0.80	$p < 0.001$	56.11	7.49		
		$N_2O = 32.06(TN) – 1.79(\text{chl-}a) – 1.09$	TN, chl-*a*	0.90	$p < 0.001$	60.65	8.76	–3.62	
		$N_2O = 20.68(TN) – 2.04(\text{chl-}a) + 22.55(NO_3^-\text{-N}) + 3.13$	TN, chl-*a*, NO_3^--N	0.96	$p < 0.001$	112.69	6.11	–6.56	0.61
Summer + Winter	N_2O	$N_2O = 18.93(TN) – 13.80$	TN	0.79	$p < 0.001$	110.56	10.52		
		$N_2O = 23.45(TN) – 0.33(\text{chl-}a) – 12.03$	TN, chl-*a*	0.86	$p < 0.001$	74.08	12.83	–4.07	

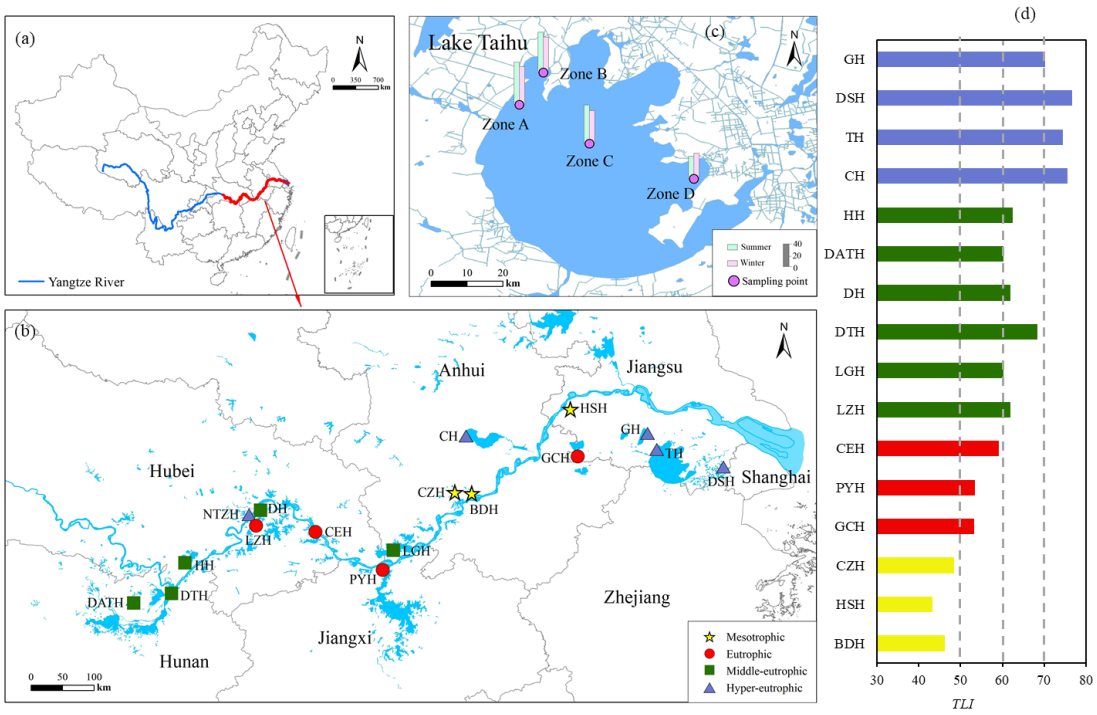

Fig. 1 Distribution of sampling sites (b) in the middle and lower reaches of the Yangtze River basin, China. Sampling sites (c) in the heavy algae-accumulated zone (Zone A and B), transitional zone (Zone C), and light algae-accumulated zone (Zone D) of Lake Tahui. The graph on the right (d) shows the *TLI* of each lake in summer. DSH: Lake Dianshang; TH: Lake Taihu; GH: Lake Gehu; GCH: Lake Gucheng; HSH: Lake Huashen; CH: Lake Chaohu; BDH: Lake Baidang; CZH: Lake Caizi; LGH: Lake Longgan; PYH: Lake Poyang; CEH: Lake Cehu; DH: Lake Donghu; LZH; Lake Liangzi; NTZH; Lake Nantaizi; HH: Lake Honghu; DTH; Lake Dongting; DATH: Lake Datong.

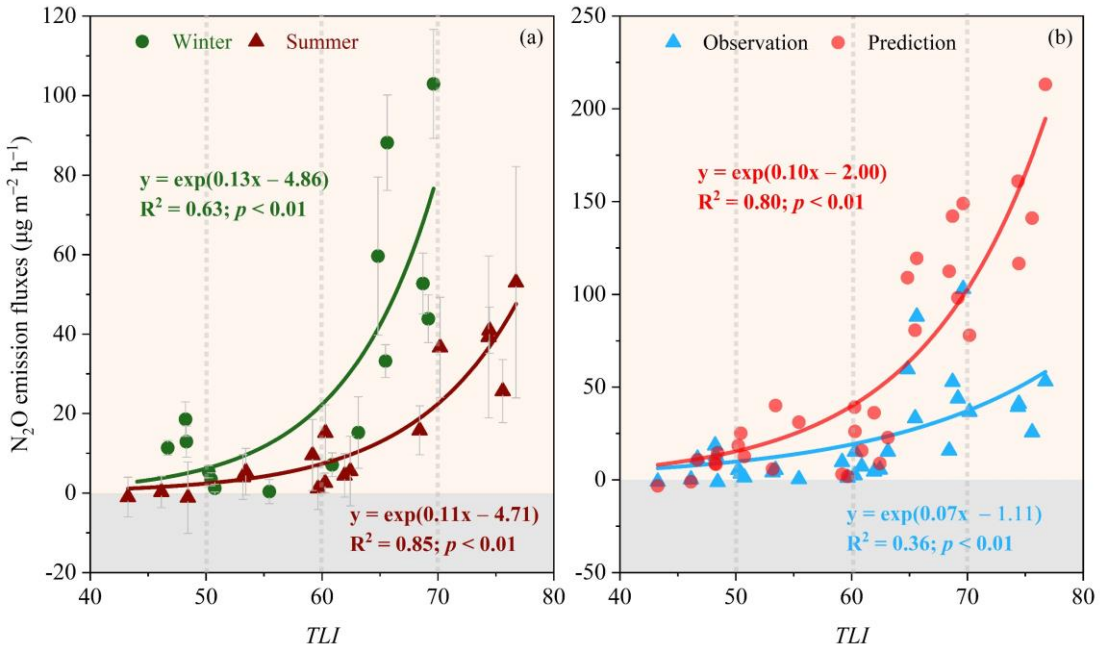

Fig. 2. Net N_2O emissions (a) in lakes of different trophic status during the winter (2017) and summer (2018). The plots (b) show the predicted N_2O emission fluxes based on the EF_{5r} of the IPCC default value (0.26%). Note that the *TLI* ranges for mesotrophic, eutrophic, middle-eutrophic, and hypereutrophic states are 40–50, 50–60, 60–70, and > 70, respectively.

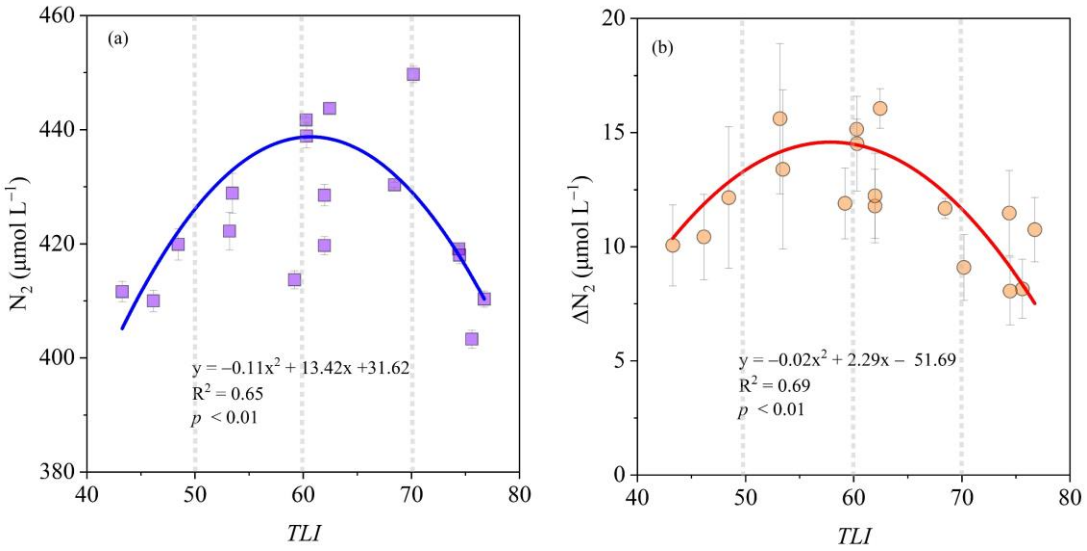

Fig. 3. The relationship between *TLI* and (a) dissolved N_2 concentration as well as (b) excess dissolved N_2 concentration (ΔN_2) in shallow lakes in summer (2018). Note that

the *TLI* ranges for mesotrophic, eutrophic, middle-eutrophic, and hypereutrophic states are 40–50, 50–60, 60–70, and > 70, respectively.

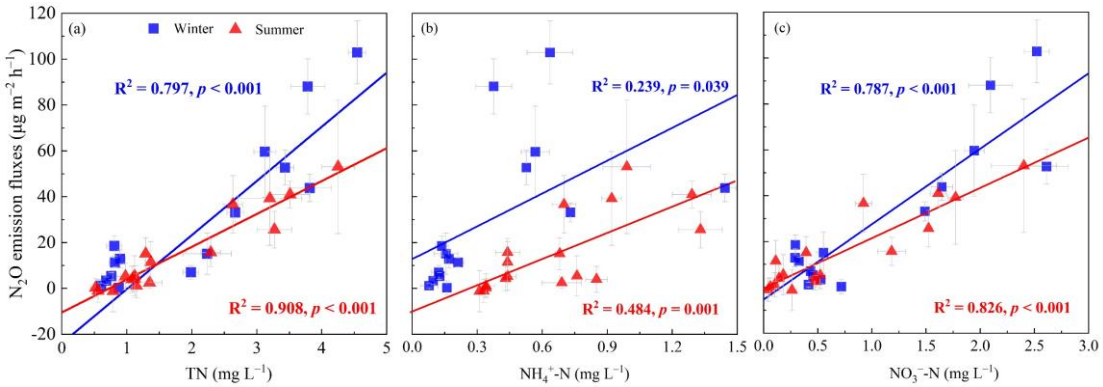

Fig. 4. Relationship between net N_2O emission fluxes and TN (a), NH_4^+-N (b), and NO_3^--N (c) in winter (2017) and summer (2018) of shallow lakes.

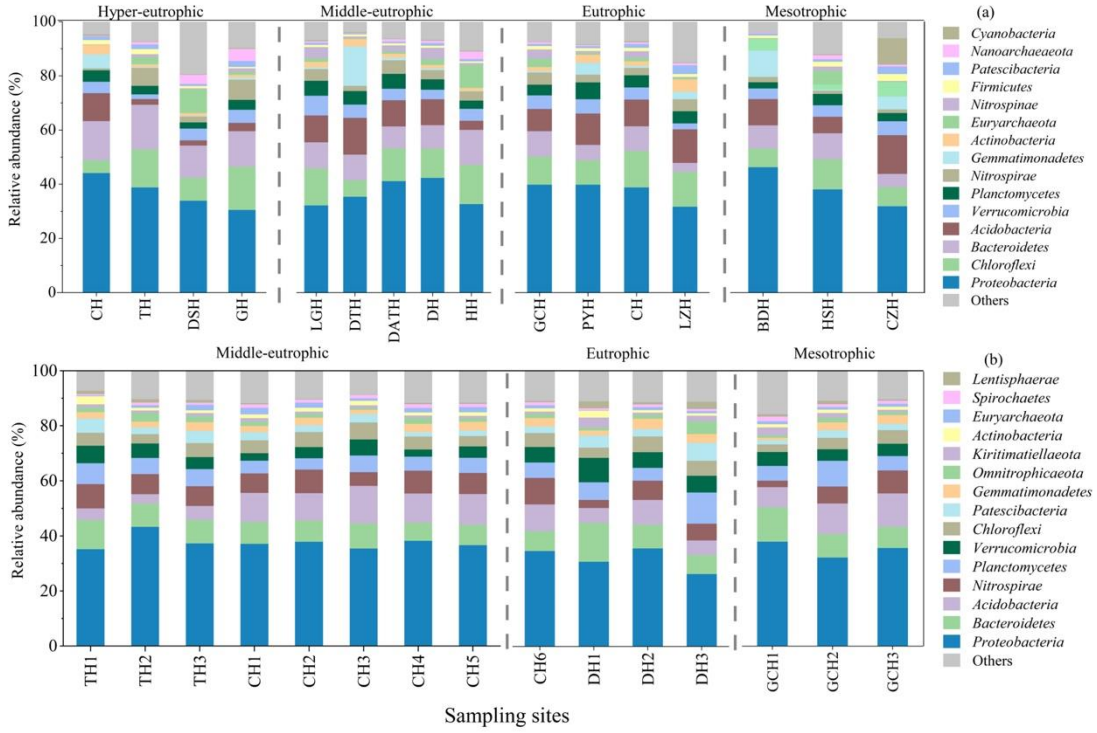

Fig. 5. Relative abundances of 16S rRNA gene-based microbial taxa for each sample at the phylum level in (a) summer (2018) and (b) winter (2017). The 15 most abundant phyla are shown.

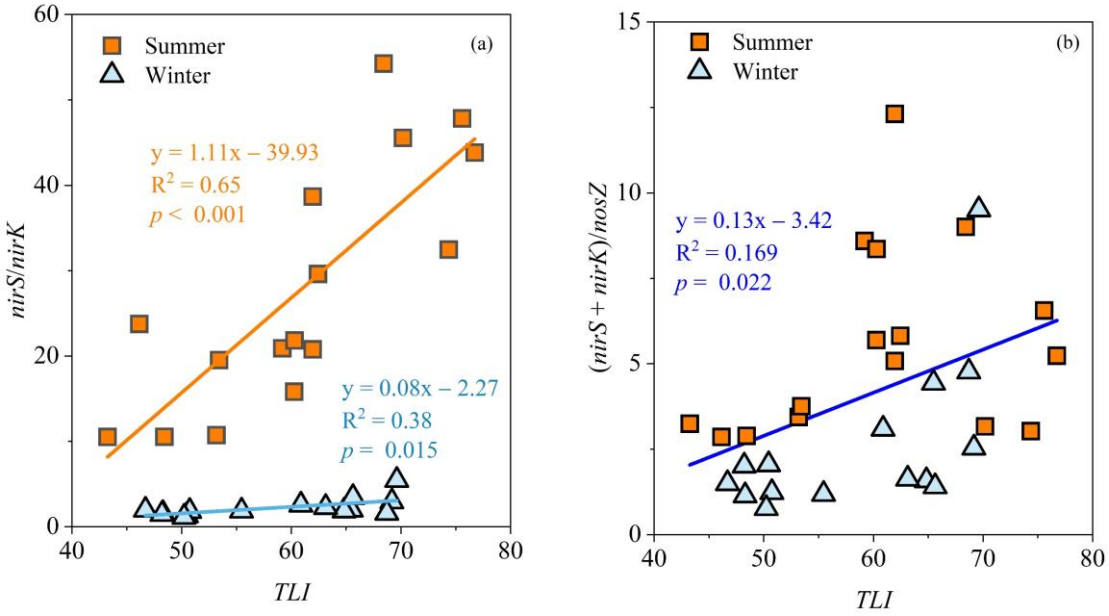

Fig. 6. The relationship between *TLI* and ratio of (a) *nirS*/*nirK* as well as (b) (*nirS* + *nirK*)/*nosZ*.

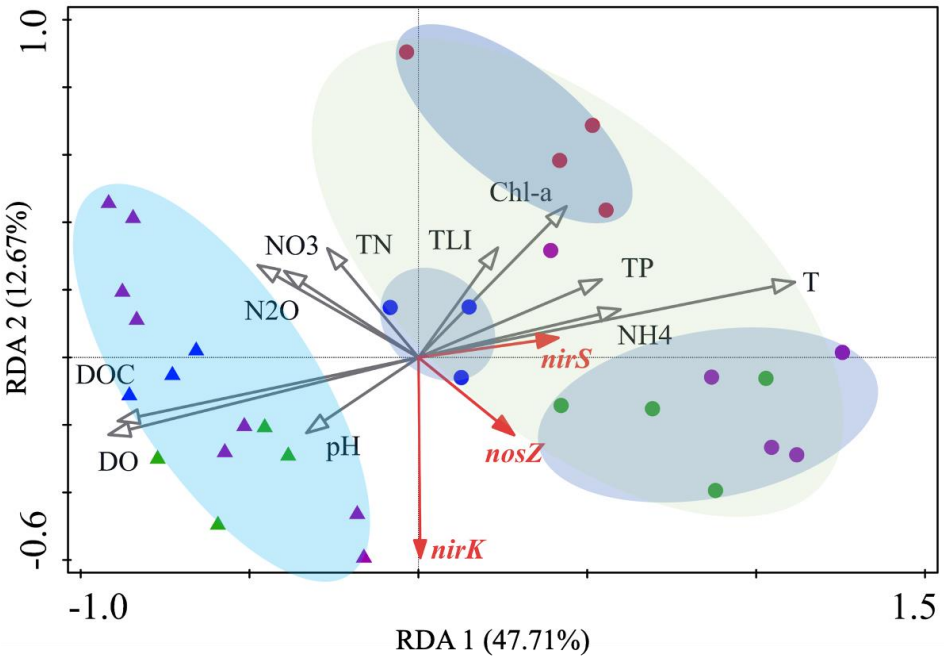

Fig. 7 Redundancy analysis (RDA) biplots of gene abundances and their relationship with environmental factors. The circle and triangle points correspond to samples taken in summer and winter, respectively. The trophic states of mesotrophic, eutrophic, middle-eutrophic, and hyper-eutrophic are represented by green, blue, violet, and red points,

respectively.

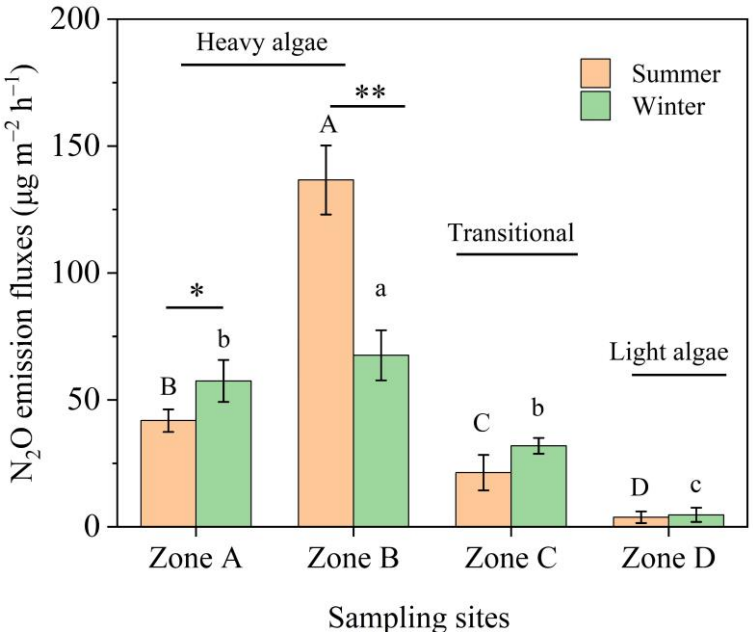

Fig. 8. Seasonal N_2O emission fluxes in heavy algae-accumulated (Zones A and B), transitional (Zone C), and light algae-accumulated (Zone D) zones in Lake Taihu. Significant differences were performed at the *$p < 0.05$ and **$p < 0.01$ levels.

Supporting information of material and methods

S1. Calculation of the gas transfer coefficient (*k*)

k is the gas transfer coefficient (m d^{-1}) and was normalized to a Schmidt number of 600, which is given as Eq. (4):

$$k = k_{600} \times \left(\frac{S_c}{S_{c600}}\right)^{-n}, \quad (5)$$

where S_c is the Schmidt number of a given gas at a given temperature and water density; S_{c600} is the Schmidt number 600 at a temperature of 20°C; *n* is the Schmidt coefficient, which is either 2/3 for wind speeds < 3.6 m s^{-1} or 1/2 for wind speeds > 3.6 m s^{-1}; k_{600} is the gas transfer coefficient adjusted to Schmidt number 600, which can be calculated by the wind speed (Cole and Caraco 1998):

$$k_{600} = 2.07 + 0.215 \times U_{10}^{1.7}, \quad (6)$$

where U_{10} is the wind speed at a 10-m height. The wind speed data (U_{10}) were obtained from nearby weather stations, which are available at the China Meteo

[References]

Carlson, R.E., 1997. A trophic state index for lakes. Limnology and Oceanography 22, 361-369.

Jin, X., 1995. Lake environment in China. Ocean Press, Beijing.

Zhang, J., Ni, W., Luo, Y., Stevenson, R.J., Qi, J., 2011. Response of freshwater algae to water quality in Qinshan Lake within Taihu watershed, China. Physics and Chemistry of the Earth 36, 360-365.

Cole, J.J., Caraco, N.F., 1998. Atmospheric exchange of carbon dioxide in a low-wind oligotrophic lake measured by the addition of SF6. Limnology and Oceanography 43: 647-656.

Table S1. Summary of the parameters of the overlying water and net N_2O emission fluxes in the different seasons. Data in parentheses indicate the mean values of each parameter.

Season	Eutrophic state *TLI*	TN (mg L^{-1})	NO_3^--N (mg L^{-1})	NH_4^+-N (mg L^{-1})	TP (mg L^{-1})	DOC (mg L^{-1})	chl-*a* (μg L^{-1})	N_2O emission fluxes (μg m^{-2} h^{-1})
Summer	Mesotrophic (≤50)	0.5-0.6 (0.6)	0.04-0.26 (0.1)	0.32-0.35 (0.3)	0.04-0.17 (0.1)	5.3-6.0 (5.6)	5.0-8.5 (7.1)	–1.0-0.3 (–0.6)
	Eutrophic (50-60)	1.0-1.4 (1.2)	0.10-0.52 (0.2)	0.35-0.86 (0.5)	0.04-0.43 (0.2)	4.2-9.4 (6.5)	11.6-29.7 (15.6)	4.0-9.5 (7.0)
	Middle-eutrophic (60-70)	1.1-2.4 (1.4)	0.39-1.18 (0.5)	0.44-0.70 (0.6)	0.08-0.46 (0.2)	3.4-7.1 (5.0)	27.4-44.0 (41.9)	1.6-15.8 (7.4)
	Hyper-eutrophic (≥70)	2.7-4.3 (3.4)	0.92-2.4 (1.7)	0.71-1.34 (1.1)	0.31-0.39 (0.3)	5.1-7.9 (6.4)	62.2-113.9 (92.7)	25.7-53.0 (39.1)
Winter	Mesotrophic (≤50)	0.8-0.9 (0.9)	0.29-0.33 (0.3)	0.14-0.21 (0.2)	0.02-0.03 (0.02)	12.8-14.0 (13.5)	5.6-7.2 (6.4)	11.7-18.6 (14.3)
	Eutrophic (50-60)	0.6-0.9 (0.7)	0.32-0.72 (0.5)	0.08-0.16 (0.1)	0.05-0.15 (0.09)	6.3-13.4 (8.5)	10.4-20.4 (14.4)	0.4-5.4 (2.6)
	Middle-eutrophic (60-70)	2.0-4.6 (3.2)	0.44-2.62 (1.7)	0.12-1.44 (0.6)	0.07-0.18 (0.13)	8.4-14.6 (10.6)	19.5-36.7 (27.4)	7.1-102.9 (50.4)

Table S2. Average constituent values of the overlying water in the different zones in Lake Taihu. The abbreviations Hy, Mi, and Me represent the hypereutrophic, middle-eutrophic, and mesotrophic states, respectively.

Sampling site	Classification	Season	*TLI*	Trophic state	TN (mg L^{-1})	NO_3^--N (mg L^{-1})	NH_4^+-N (mg L^{-1})	TP (mg L^{-1})	DOC (mg L^{-1})	chl-*a* (μg L^{-1})	DO (mg L^{-1})	pH	T (°C)
Zone A	Heavy algae-accumulated zone	Summer	77.72	Hy	4.2 ± 0.2	0.13 ±0.04	4.20 ± 0.12	0.47 ± 0.02	11.2 ± 1.3	120.0 ± 23.2	1.6 ± 0.2	7.46 ± 0.18	31.2
		Winter	69.69	Mi	3.4 ± 0.2	0.05 ± 0.01	1.00 ± 0.03	0.13 ± 0.01	13.8 ± 0.7	43.9 ± 11.7	7.1 ±0.2	7.81 ± 0.11	11.1
Zone B	Heavy algae-accumulated zone	Summer	73.39	Hy	4.9 ± 0.8	0.36 ± 0.04	0.13 ± 0.01	0.48 ± 0.13	7.5 ± 1.4	51.8 ± 13.5	6.5 ± 0.5	8.38 ± 0.08	32.1
		Winter	64.51	Mi	3.1 ± 0.2	1.88 ± 0.13	0.52 ± 0.03	0.14 ± 0.03	12.2 ± 1.0	21.5 ± 3.7	8.5 ± 0.5	8.10 ± 0.05	9.8
Zone C	Transitional zone (Lake center)	Summer	70.65	Hy	3.7 ± 0.7	0.04 ± 0.01	0.02 ± 0.01	0.13 ± 0.08	5.6 ± 0.7	45.9 ± 11.6	7.3 ± 0.2	8.65 ± 0.11	30.2
		Winter	60.23	Mi	2.4 ± 0.1	1.95 ± 0.35	0.48 ± 0.09	0.21 ± 0.02	10.5 ± 0.6	14.6 ± 3.5	11.0 ± 0.3	8.25 ± 0.21	9.7
Zone D	Light algae-accumulated zone	Summer	41.08	Me	0.4 ± 0.2	0.04 ± 0.01	0.01 ± 0.01	0.13 ± 0.10	5.8 ± 1.2	4.9 ± 4.2	10.4 ± 0.4	8.62 ± 0.08	31.5
		Winter	46.34	Me	0.7 ± 0.2	0.29 ± 0.20	0.07 ± 0.11	0.03 ± 0.03	12.1 ± 1.3	6.3 ± 4.4	11.5 ± 0.5	8.53 ± 0.12	10.9

Table S3 Primer sequences used for sequencing and qPCR analysis

Primer	Target	Sequence (5′- 3′)	Annealing temperature (°C)	Amplification size (bp)	References
16SrRNA-F	16S rRNA	CGGTGAATACGTTCYCGG	An initial denaturation at 95℃ for 5min, followed by 40 cycles of 95℃ for 30s, 55℃ 30s and 72℃ 30s.	142	He et al., 2017
16SrRNA-R		GGHTACCTTGTTACGACTT			
cd3aF	*nirS*	GTSAACGTSAAGGARACSGG	An initial denaturation at 95℃ for 5min, followed by 40 cycles of 95℃ for 30s, 55℃ 30s and 72℃ 30s.	426	Zhang et al., 2018
R3cd		GASTTCGGRTGSGTCTTGA			
nirKFlaCu	nirK	ATCATGGTSCTGCCGCG	An initial denaturation at 95℃ for 5min, followed by 40 cycles of 95℃ for 30s, 55 ℃ 30s and 72℃ 1min	473	Henry et al., 2006
nirKR3Cu		GCCTCGATCAGRTTGTGGTT			
nosZ2F	*nosZ*	CGCRACGGCAASAAGGTSMSSGT	An initial denaturation at 95℃ for 5min, followed by 40 cycles of 95℃ for 30s, 60℃ 30s and 72℃ 1min.	276	Henry et al., 2006
nosZ2R		CAKRTGCAKSGCRTGGCAGAA			

[References]

Henry, S., Bru, D., Stres, B., Hallet, S., Philippot, L., 2006. Quantitative detection of the *nosZ* gene, encoding nitrous oxide reductase, and comparison of the abundances of 16S rRNA, *narG, nirK, and nosZ* genes in soils. Applied Environmental Microbiology 72, 5181-5189.

He, X., Xu, Y., Chen, J., Ling, J., Li, Y., Huang, L., Zhou, X., Zheng, L., 2017. Evolution of corresponding resistance genes in the water of fish tanks with multiple stresses of antibiotics and heavy metals. Water Research 124, 29-48.

Zhang, H., Zhao, Z., Chen, S., Kang, P., Wang, Y., Feng, J., Jia, Y., Yan, M., Wang, Y., Xu, L., 218. *Paracoccus versutus* KS293 adaptation to aerobic and anaerobic denitrification: insights from nitrogen removal, functional gene abundance, and proteomic profiling analysis. Bioresource. Technology 260, 321-328.

Table S4 Pearson correlations between variables and N_2O emission fluxes in summer and winter, respectively. Text in blue and black represent winter and summer, respectively. Note that N_2O denotes N_2O emission flux.

	N_2O	N_2	ΔN_2	*TLI*	TN	NO_3^-	NH_4^+	TP	DOC	chl-*a*	C:N	DO	pH	T
N_2O	1	-0.100	-0.511*	0.740**	0.901**	0.897**	0.545*	0.625*	-0.037	0.578*	-0.675**	-0.184	-0.396	-0.478
TLI	0.848**	0.044	-0.354	1	0.944**	0.859**	0.705**	0.737**	-0.022	0.942*	-0.901**	-0.221	-0.434	-0.535*
TN	0.956**	-0.190	-0.527*	0.915**	1	0.914*	0.733**	0.697**	-0.005	0.833**	-0.857**	-0.280	-0.507	-0.552*
NO_3^-	0.915**	-0.223	-0.487*	0.847**	0.967**	1	0.647**	0.811*	-0.051	0.801**	-0.757	-0.220	-0.389	-0.373
NH_4^+	0.719**	-0.141	-0.283	0.742**	0.786**	0.710**	1	0.483	0.208	0.730**	-0.555*	-0.593*	-0.652**	-0.251
TP	0.708**	-0.081	-0.330	0.548*	0.587*	0.587*	0.485*	0.553*1	-0.278	0.712**	-0.735**	0.165	-0.001	-0.128
DOC	0.266	-0.238	-0.164	0.178	0.236	0.236	0.066	0.219	0.3371	0.014	0.391	-0.660**	-0.722**	-0.368
Chl-*a*	0.865**	-0.178	-0.503*	0.939**	0.941**	0.908**	0.810**	0.533*	0.143	1	-0.800**	-0.257	-0.401	-0.359
C:N	-0.707**	-0.232	0.146	-0.870**	-0.770**	-0.761**	-0.630**	-0.425	0.195	-0.761**	1	-0.006	0.144	0.330
DO	-0.515*	-0.011	-0.174	-0.446	-0.502*	-0.537*	-0.662*	-0.406	-0.101	-0.535*	0.382	1	0.908**	0.287
pH	-0.109	-0.017	-0.281	-0.064	-0.175	-0.307	-0.278	0.184	0.248	-0.214	0.152	0.691**	1	0.595*
T	0.322	-0.711**	-0.734**	0.071	0.311	0.253	0.115	0.229	0.274	0.248	0.128	0.166	0.168	1

Significant correlation at the *$p < 0.05$ and **$p < 0.01$ levels.

Table S5 Pearson correlations between variables and N_2O emission fluxes in two seasons. Note that N_2O denotes N_2O emission flux.

	N_2O	*TLI*	TN	NO_3^-	NH_4^+	TP	DOC	chl-*a*	C:N	DO	pH	T
N_2O	1											
TLI	0.627**	1										
TN	0.890**	0.865**	1									
NO_3^-	0.888**	0.757**	0.931**	1								
NH_4^+	0.375*	0.687**	0.611**	0.483**	1							
TP	0.252	0.525**	0.362**	0.278	0.527**	1						
DOC	0.246	-0.090	0.143	0.170	-0.193	-0.357*	1					
Chl-*a*	0.320	0.831**	0.607**	0.528**	0.694**	0.599**	-0.294	1				
C:N	-0.485**	-0.810**	-0.691**	-0.570**	-0.625**	-0.511**	0.498**	-0.606**	1			
DO	0.026	-0.350	-0.163	-0.075	-0.692**	-0.511**	0.356*	-0.586**	0.349	1		
pH	-0.159	-0.287	-0.313	-0.287	-0.597**	-0.087	0.064	-0.419*	0.255	0.52**	1	
T	-0.356*	0.091	-0.196	-0.284	0.361*	0.49**	-0.765**	0.410*	-0.312	-0.667**	-0.247	1

Significant correlation at the *$p < 0.05$ and **$p < 0.01$ levels.

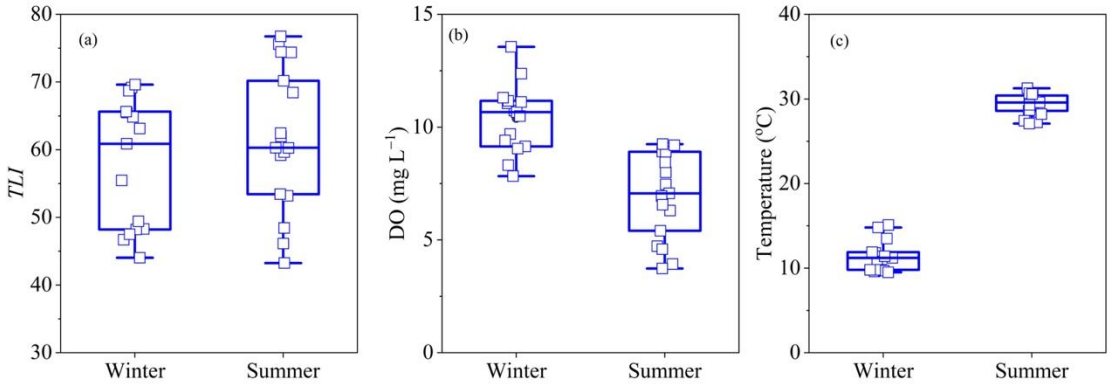

Fig. S1. (a) *TLI*, (b) DO, and (c) temperature of examined lakes in winter (2017) and summer (2018).

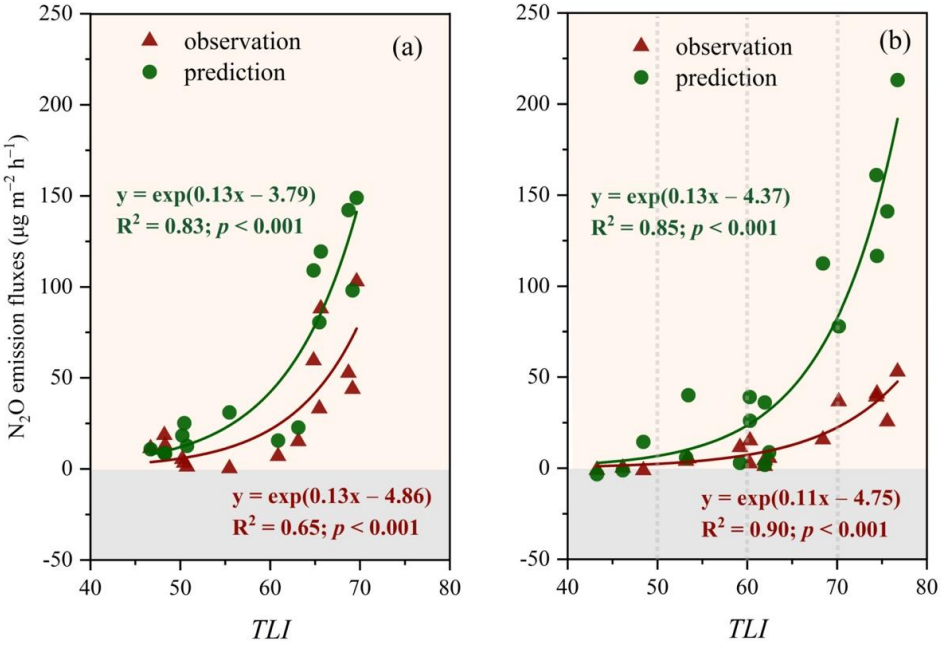

Fig. S2. Observation (red triangle) and prediction (green circle) of N_2O emission fluxes in (a) winter (2017) and (b) summer (2018). Note that the *TLI* ranges for mesotrophic, eutrophic, middle-eutrophic, and hypereutrophic states are 40–50, 50–60, 60–70, and > 70, respectively.

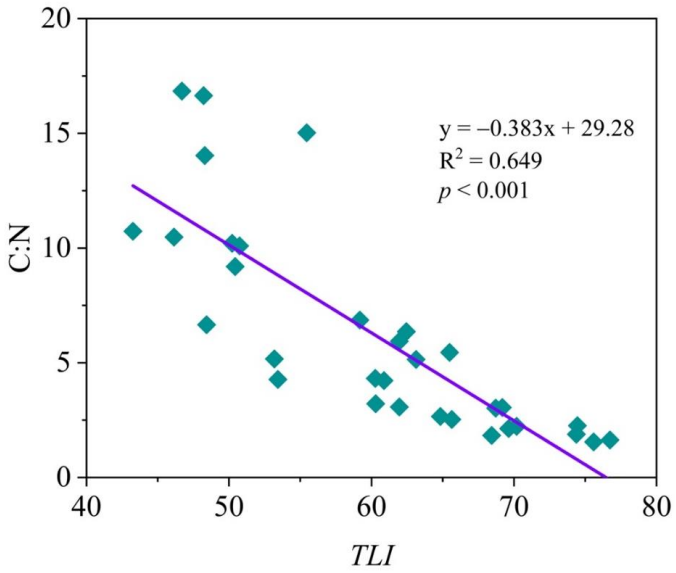

Fig. S3. The relationship between *TLI* and ratio of C:N in shallow lakes in winter (2017) and summer (2018).

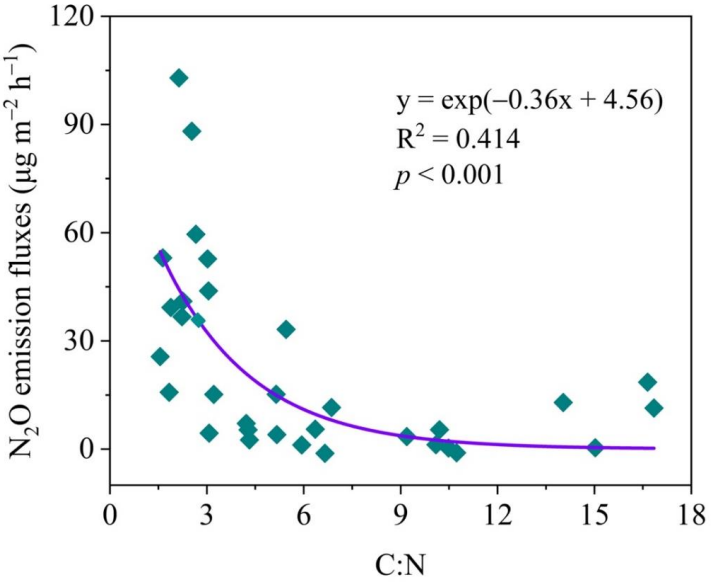

Fig. S4. The relationship between the ratio of C:N and N_2O emission fluxes in shallow lakes in winter (2017) and summer (2018).

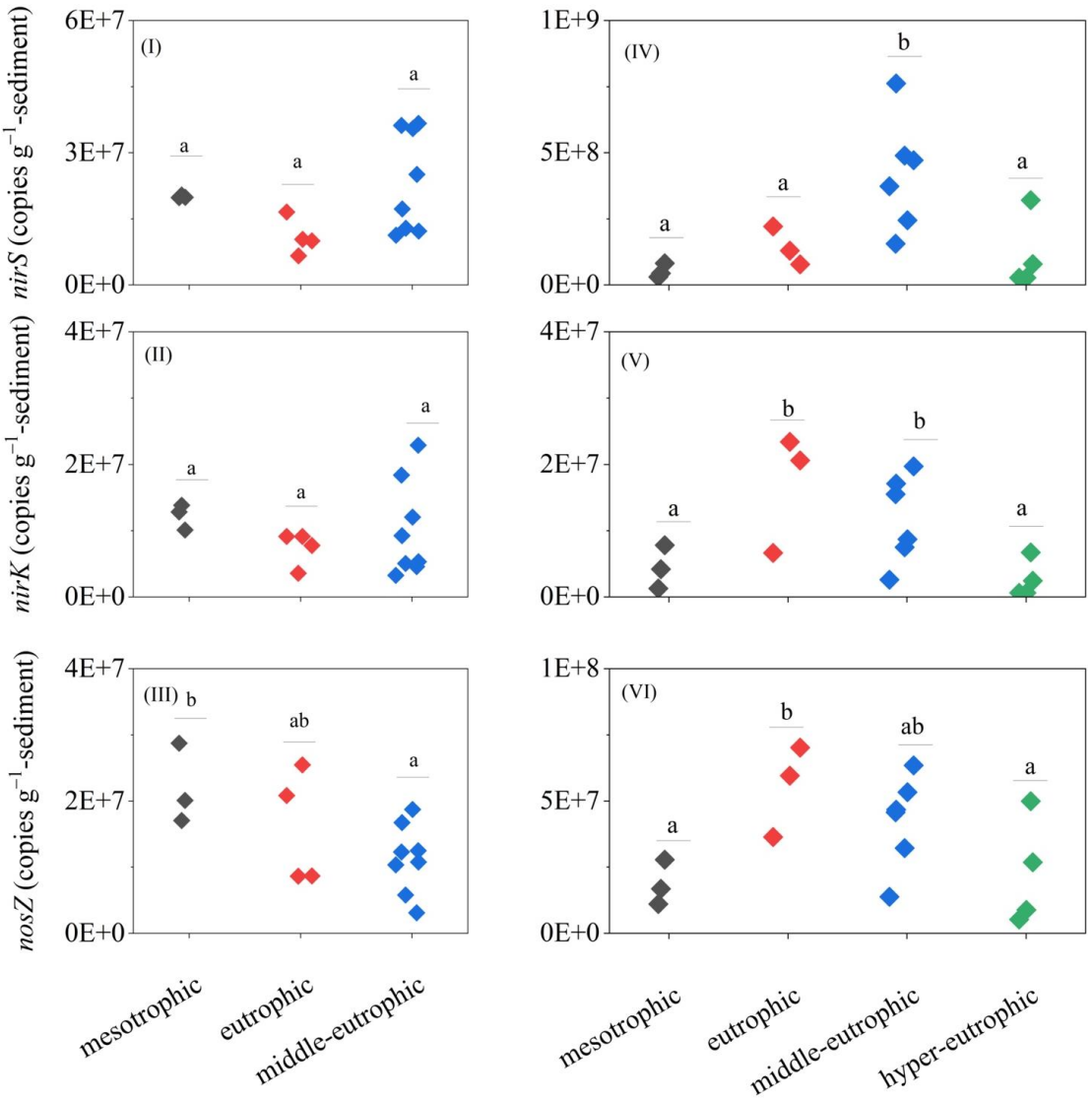

Fig. S5 Seasonal distribution (I–III: winter; IV–VI: summer) of denitrifying gene abundances, including N_2O producers (*nirS* and *nirK* genes) and N_2O reducers (*nosZ*), in different trophic levels. Lowercase letters indicate significant differences. The statistical analyses were performed using the Duncan test at the 5% level.

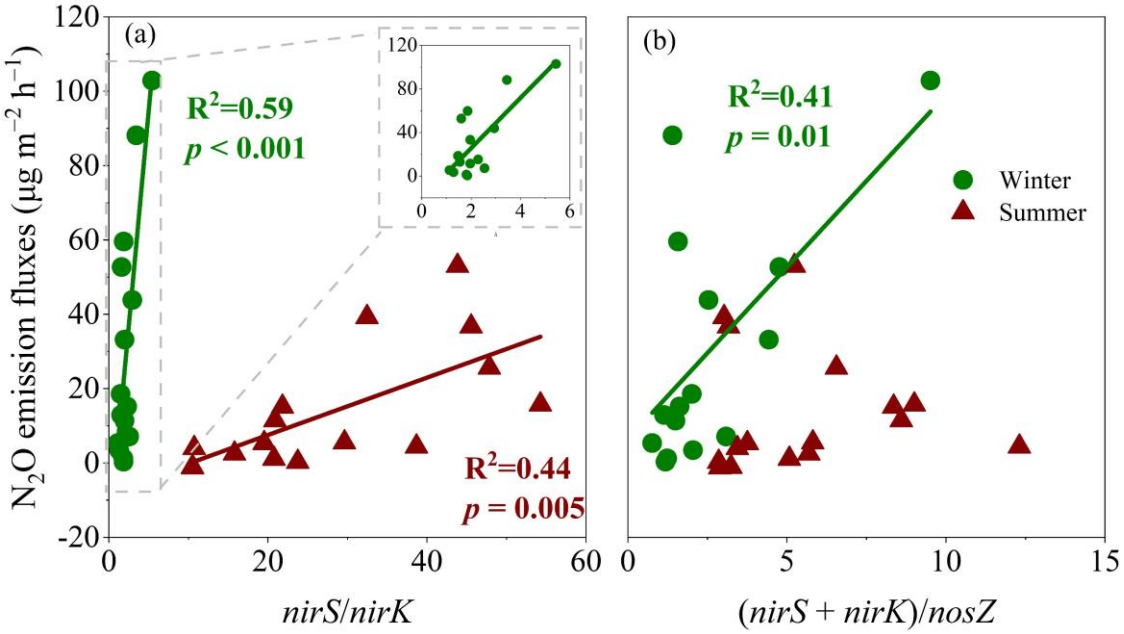

Fig. S6 Relationship between N_2O emission fluxes and (a) *nirS*/*nirk* as well as (b) (*nirK* + *nirS*)/*nosZ*.

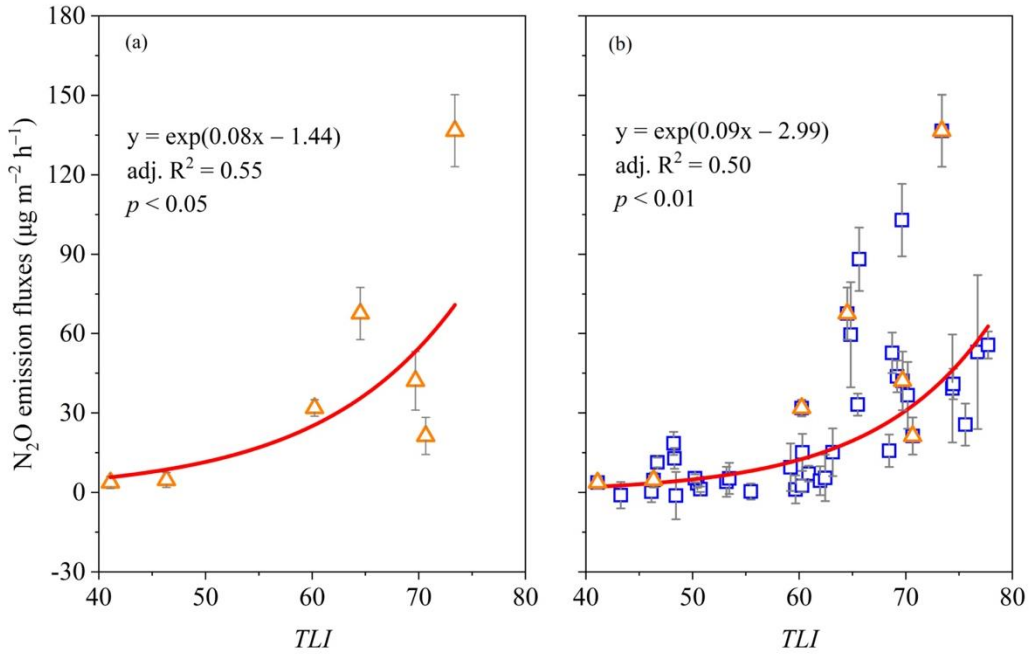

Fig. S7 Relationship between the N_2O emission fluxes and *TLI* in (a) Lake Taihu and (b) all shallow lakes. The triangles and squares correspond to Lake Taihu and other lakes, respectively.

Chapter 5: Effects of temperature and oxygen on N_2O respiration activities of heterotrophic N_2O-reducing bacteria

5.1 Introduction

Nitrous oxide (N_2O) emission into the atmosphere is one cause of ozone depletion and climate change (IPCC, 2014). The atmospheric N_2O concentration has increased by 20%, from 270 ppb in 1750 to 331 ppb in 2018, and this increasing trend has continued by 0.2% per year (Tian et al., 2020). Wastewater treatment plants (WWTPs), which receive and remove dissolved nitrogen constituents, are a source of N_2O emissions (Peng et al., 2014). The amount of N_2O emitted from WWTPs was as high as 108 Mt carbon dioxide (CO_2) equivalents in 2010, accounting for 3.4% of the estimated annual global N_2O emissions (IPCC, 2014). A recent report indicated that N_2O emissions from WWTPs have increased by 44% from 1990 to 2014 (US EPA, 2016). It is therefore essential to reduce the N_2O-footprint of WWTPs by developing a strategy to mitigate N_2O emissions.

N_2O is a byproduct of nitrification and an intermediate of heterotrophic denitrification, which act as an N_2O source and sink, respectively (Jones et al., 2013; Read-Daily et al., 2016). There are multiple pathways of N_2O production, including biological and abiotic processes (Wunderlin et al., 2012; Terada et al., 2017). N_2O reduction to N_2 gas is mediated by N_2O reductase (N_2OR), harbored by N_2O-reducing bacteria (N_2ORB) (Zumft and Kroneck, 2006). This pathway represents a pivotal role in wastewater treatment to mitigate N_2O emissions (Kim et al., 2020), strongly dependent on the intrinsic N_2O reduction capacity of N_2ORB. Therefore, understanding the physiologies of N_2ORB and developing N_2O mitigation strategies has attracted more attention in recent years (Yoon et al., 2016; Conthe et al., 2018a; Hallin et al., 2018; Suenaga et al., 2019).

Owing to differences in the N_2OR amino acid sequences (similarity <50%) and the protein-translocation pathways, N_2ORB harboring a functional *nos*Z gene can be

classified into either clade I or clade II (Jones et al., 2013; Sanford et al., 2012; Yoon et al., 2016). Whereas some clade II type N_2ORB display a higher affinity for N_2O than clade I type N_2ORB (Yoon et al., 2016; Suenaga et al., 2018a), research on N_2ORB biokinetics of N_2O consumption toward an effective strategy to reduce N_2O emissions is limited (Yoon et al., 2016; Suenaga et al., 2018a; Yoon et al., 2019). Therefore, more knowledge of N_2ORB physiologies concerning N_2O reduction is required.

Oxygen level is a crucial factor to determine the rates of N_2O production and consumption (Kinh et al., 2017; Massara et al., 2017). Under an anoxic environment, heterotrophic N_2ORB switch their dominant metabolism from O_2- to N_2O-dependent respiration (Miyahara et al., 2010; Suenaga et al., 2018a), but favor O_2 respiration under aerobic conditions (Qu et al., 2016). The transition from anoxic to oxic conditions triggers N_2O emissions due to the inhibition of N_2OR in the presence of oxygen (Read-Daily et al., 2016); however, returning from oxic to anoxic conditions reactivates N_2OR. N_2OR activity recovery and oxygen tolerance levels likely differ among N_2ORB. Previous work demonstrated that the betaproteobacterium *Azospira* sp. strain I13 displays a rapid recovery of N_2O reduction activity and is tolerant of O_2 inhibition (Suenaga et al., 2018a). A mechanistic enzymatic model has been proposed to interpret N_2OR activity after O_2 exposure (Zheng and Doskey, 2015). Nevertheless, the mechanism of the recovery of N_2O reduction activity after O_2 exposure has yet to be systematically studied.

Seasonal temperature variations change the microbial activities in WWTPs (Poh et al., 2015; Massara et al., 2017; Li et al., 2018), potentially associated with N_2O production and emission (Abdalla et al., 2009; Vasilaki et al., 2019). Lower temperatures retard N_2OR activities, causing higher N_2O emissions via denitrification from 20°C to 5°C (Adouani et al., 2015). Therefore, the temperature effect on N_2O consumption by N_2ORB is essential but has not yet been investigated. Particularly, whether or not the temperature dependence differs with *nos*Z clade types or bacterial species remains unclear.

To expand our understanding of N_2ORB biokinetics at various temperatures, a pure culture-based investigation will allow us to elucidate N_2ORB physiologies without the interference of other bacteria. Systematic analysis of pure culture biokinetics after an O_2 exposure event at various temperatures will demonstrate the potential of N_2ORB as an N_2O sink with changing environmental conditions. The objectives of this study are to (1) investigate the characteristics of O_2 and N_2O consumption kinetics at different temperatures; (2) determine O_2 inhibition constants at different temperatures; and (3) elucidate the recovery of N_2O reduction activity after O_2 exposure at different temperatures. Microrespirometric analysis of N_2O dynamics by a microrespiration system and mathematical modeling are employed in this study. The outcomes will indicate how N_2ORB exert an N_2O sink, leading to the development of a strategy to mitigate N_2O emissions.

5.2 Materials and methods

5.2.1 Targeted N_2ORB and culture conditions

Four different heterotrophic bacteria harboring either clade I or II type *nosZ* (listed in Table S1) were subjected to biokinetic investigations. The two isolates affiliated to the genus *Azospira* are denitrifiers possessing clade II type *nosZ*, whereas those of genera *Pseudomonas* and *Paracoccus* are canonical clade I type *nosZ* denitrifying bacteria. These *Azospira* isolates, previously acquired from a bioreactor, were chosen as they have a proven high affinity for N_2O (Suenaga et al., 2019). Contrarily, *Ps. stutzeri* and *Pa. denitrificans* were chosen as they are often used as model denitrifying bacteria (Jiang et al., 2020; Kim et al., 2020) and also are detected in WWTPs (Wang et al., 2014a; Huang et al., 2020; Han et al., 2020). All strains harbor a full set of denitrifying functional genes, according to their genomes on NCBI (www.ncbi.nlm.nih.gov/; Details can be found in Table S1). These strains, stored in a deep freezer (−80°C), were aerobically pre-grown in the nutrient medium (pH 7.0) consisting of 5 g L^{-1} NaCl, 5 g L^{-1} Bacto Peptone, and 3 g L^{-1} OxoidTM Lab-Lemco

meat extract, at 30°C with a shaking speed 150 rpm. This medium favors the resuscitation of stored bacteria for subsequent biokinetic experiments and avoids bacterial cell aggregation (Suenaga et al., 2018a and 2019). The incubation time was preliminarily optimized by the growth curves of the tested bacteria, as shown in Fig. S1. After reaching the respective exponential growth and early stationary phases, the pre-cultured bacterial suspension was collected and washed twice with 0.05 × PBS by centrifugation at 5,000 rpm for 5 min and then resuspended in a medium composed of 100 mg L^{-1} KH_2PO_4, 6.6 mg L^{-1} NaCl, 8.20 mg L^{-1} $MgSO_4 \cdot 7H_2O$, 13.4 mg L^{-1} KCl, 115 mg L^{-1} NH_4Cl, 188 mg L^{-1} $NaHCO_3$, and 1 ml L^{-1} trace element solution (Suenaga et al., 2018a). The OD_{600} value of the cell suspension was measured by a UV-vis spectrophotometer to confirm if the cell density was in an appropriate range. Prior to the experiment summarized in the next section, the pH of the experimental medium was adjusted to 7.5 with 1 mol L^{-1} HCl. All the media were sterilized before use.

5.2.2 N_2O respiration experiment

Whole-cell O_2 and N_2O consumption kinetics of the tested bacteria were estimated with a laboratory-scale microrespiration system equipped with O_2 and N_2O microsensors (Unisense, Aarhus, Denmark). The system, consisting of Clark-type N_2O and O_2 microsensors, a double-port chamber (10 ml), and stirrers installed in a sensor stand (Fig. S2), allowed the online monitoring of dissolved O_2 and N_2O concentrations (Suenaga et al., 2018a). The chamber was filled with the bacterial cell suspension and then injected with approximately 20 μL of a concentrated N_2O solution (25 mmol L^{-1}) and 25 μL acetate (250 mmol L^{-1}) as the sole carbon source in the experiment (Suenaga et al., 2018a). The excess acetate supply allowed N_2O to be the sole limiting substrate. Acetate was used because it cannot be fermented, excluding the possibility of fermentation. Prior to the experiment, the OD_{600} values of cell suspension were adjusted in the chamber to ensure the same cell density was used at each temperature. The N_2O and acetate addition ensured the working concentrations of 50 μmol L^{-1} and 625 μmol L^{-1}. For all experiments, oxygen was not intentionally scavenged but present in the

experimental medium. The acetate concentration was in excess for the following stoichiometric relations:

$4N_2O + CH_3COO^- \rightarrow 4N_2 + CO_2 + HCO_3^- + H_2O$

$2O_2 + CH_3COO^- \rightarrow CO_2 + HCO_3^- + H_2O$

This condition ensures preferential O_2 consumption, followed by N_2O consumption by each assigned N_2ORB (an example shown in Fig. S3). The addition of the concentrated N_2O solution was repeated until a comparable profile of a time-lapse N_2O concentration was attained (Fig. S3). To achieve a completely mixed condition in the chamber, a glass-coated stirrer bar was stirred at 600 rpm for 5 min immediately after the injection of both N_2O and acetate, and then the rotation speed of the stirrer bar was adjusted to 400 rpm for the duration of each experiment. The N_2O solution was spiked to adjust the N_2O concentration to approximately 50 μmol L^{-1} after the N_2O was depleted in the chamber. Subsequently, each bacterial suspension was applied for batch assays in triplicate. The incubation time was 6–8 h for the two *Azospira* strains and *Ps. stutzeri*, and 12–16 h for *Pa. denitrificans*. After each experiment, the cell suspension (total volume of 1 ml) was immediately taken from the chamber and fixed with a 2% glutaraldehyde solution. The suspension was filtered, and the captured cells on the filter were enumerated under microscopy (BZ-8100, Keyence, Osaka, Japan) as described elsewhere (Lunau et al., 2005). More than 500 cells (20–25 view fields), higher than the recommended cell numbers (400 cells) by Lanau et al. (2005), were counted. The batch experiments for each bacterium were conducted at 15°C, 25°C, 30°C, and 35°C in a water bath to evaluate the temperature effects on N_2O consumption dynamics.

5.2.3 Analysis of N_2O respiration by N_2ORB

By using the microrespiration system, changes in O_2 and N_2O concentrations over time, as shown in Fig. S3, are expressed as Eq. (1). The maximum cell-specific O_2 and N_2O consumption rates ($V_{max,\ O2}$ and $V_{max,\ N2O}$) and the whole-cell half-saturation constants of O_2 and N_2O ($K_{m,\ O2}$ and $K_{m,\ N2O}$) were determined by the equation of the whole-cell Michaelis-Menten kinetics in Eq. (2) and shown in Fig. S4:

$$V = \frac{dS}{dt} = \frac{S_t - S_{t+\Delta t}}{\Delta t} \quad (1)$$

$$V = \frac{V_{max} \times S}{K_m + S} \times X \quad (2)$$

where S_t and $S_{t+\Delta t}$ are the O_2 or N_2O concentrations (μmol L^{-1}) at the time points t and $t+\Delta t$ (Δt represents the time interval between two points; Δt = 1.39–2.78 × 10^{-3} h), respectively (Suenaga et al., 2018a). V_{max} and K_m are the cell-specific maximum consumption rates [μmol (cell h)$^{-1}$] and whole-cell half-saturation constants (μmol L^{-1}), respectively. X is the bacterial cell density (cell L^{-1}). For the comparison of the O_2 and N_2O respiration activities among N_2ORB, the specific affinities for O_2 and N_2O (a_0 [L (cell h)$^{-1}$)]) were independently calculated according to Eq. (3) (Kits et al., 2017; Suenaga et al., 2018a):

$$a_0 = \frac{V_{max}}{K_m} \quad (3)$$

The activation energies for O_2 and N_2O were calculated by the Arrhenius equation described in Eq. (4) (Holtan-Hartwig et al., 2002):

$$\ln V_{max} = \left(-\frac{E_a}{R}\right)\left(\frac{1}{T}\right) + \ln A \quad (4)$$

where E_a is the activation energy (J mol^{-1}); R is the gas constant of 8.314 J (mol K)$^{-1}$; and A is the pre-exponential factor. An Arrhenius plot was drawn to calculate E_a for the temperature dependence on O_2 and N_2O respiration rates, as previously reported (Rahman et al., 2019). The temperature coefficient Q_{10} for O_2 and N_2O, defined as the factor by which the maximum respiration rate increases with a temperature increase in 10°C, was calculated with Eq. (5):

$$Q_{10} = \left(\frac{k_2}{k_1}\right)^{\frac{10}{(T_2 - T_1)}} \quad (5)$$

where k_2 and k_1 are the rate constants of O_2 or N_2O consumption, T_2 and T_1, respectively.

The effect of O_2 concentration on N_2O consumption rate was parameterized according to previous research (Ni et al., 2011). The non-competitive inhibition heterotrophic denitrification model was applied to estimate O_2 inhibition constants [K_I (μmol L^{-1})] and incorporated into Eq. (6) (von Schulthess et al., 1994):

$$\frac{dS}{dt} = \frac{V_{max,\ N2O} \times S_{N2O}}{K_{m,\ N2O} + S_{N2O}} \times \frac{K_I}{K_I + S_{O2}} \qquad (6)$$

K_I was determined by minimizing the coefficient of determination as follows:

$$R^2 = 1 - \frac{\sum (S_{exp} - S_{model})^2}{\sum (S_{exp} - \overline{S_{exp}})^2} \qquad (7)$$

where S_{exp} and S_{model} are the experimental and simulated N_2O concentrations, respectively; and $\overline{S_{exp}}$ is the average value.

5.2.4 Analysis of the activity recovery of N_2O respiration by N_2ORB

To quantitatively describe the activity recovery of N_2O reduction, a recovery model was developed to simulate the recovery of N_2O consumption activity after O_2 depletion ($V_{N2O\ recovery}$) as in Eq. (8):

$$V_{N2O\ recovery} = \frac{V_{max,\ N2O} \times S_{N2O}}{K_{m,\ N2O} + S_{N2O}} \times v_{N2O} \qquad (8)$$

The relative activity of N_2O consumption rates (v_{N2O}) was defined by dividing an N_2O consumption rate by that under a completely anaerobic condition (*i.e.*, $v_{N2O} = V_{N2O}/V_{max,\ N2O}$) (Suenaga et al., 2018a). v_{N2O} can be broken down as Eq. (9):

$$v_{N2O} = k' \times t + m \qquad (9)$$

where k' represents the recovery rate constant (h^{-1}), and m represents the initial v_{N2O} when O_2 was depleted.

5.2.5 Data analysis

O_2 and N_2O concentration data were smoothed to reduce electrical noises by the SigmaPlot 14.0 software (Systat, CA) as in a previous report (Martens-Habbena et al., 2009). The K_I and k' values were estimated by fitting the N_2O profiles to Eqs. (6) and (9) based on the least-squares method using the solver function of Microsoft Excel (Microsoft, Redmond, WA, USA). All statistical analyses were conducted using the SPSS 19.0 software (IBM Corp., Armonk, NY, USA). The Spearman's rank correlation analysis was conducted to assess the relationship between $V_{max,\ N2O}$ and recovery rate constants (k'). The level of significance was $p < 0.05$ for all tests. The statistical significance of those results was determined by a Duncan test at the 5% level.

5.3 Results

5.3.1 Biokinetic parameters of N_2ORB on O_2 respiration

O_2 and N_2O concentrations of N_2ORB harboring clade I type *nosZ* (*Ps. stutzeri* JCM5965 and *Pa. denitrificans* NBRC102528) and clade II type *nosZ* (*Azospira* sp. strains I09 and I13) were monitored with a microrespiration system. The presence of N_2O did not alter the biokinetics associated with oxygen (Fig. S5). The variation in O_2 and N_2O biokinetic parameters at different temperatures is shown in Fig. 1. The maximum O_2 consumption rates ($V_{max, O2}$) increased with an increase in temperature (Fig. 1a). The $V_{max, O2}$ of *Pa. denitrificans* NBRC102528 [$2.23 \pm 0.16 \times 10^{-9}$ μmol (cell h)$^{-1}$] harboring *nosZ* clade I was lower than that of the other tested isolates at 35 C ($p < 0.05$), which were statistically comparable. At 15°C, the $V_{max, O2}$ values of *Azospira* sp. strain I09 [$7.87 \pm 0.73 \times 10^{-10}$ μmol (cell h)$^{-1}$] and *Azospira* sp. strain I13 [$2.60 \pm 0.69 \times 10^{-10}$ μmol (cell h)$^{-1}$] were lower than that of *Ps. stutzeri* JCM5965 [$1.64 \pm 0.29 \times 10^{-9}$ μmol (cell h)$^{-1}$] ($p < 0.05$). The highest $V_{max, O2}$ values of *Azospira* sp. strain I09, *Azospira* sp. strain I13, *Ps. stutzeri* JCM5965, and *Pa. denitrificans* NBRC102528 were 5.26, 19.59, 2.64, and 2.04 times higher, respectively, than the lowest values, indicating that *Azospira* sp. strain I13 had the largest $V_{max, O2}$ variation with temperature. The $K_{m, O2}$ values of the tested N_2ORB consistently exhibited a marginal change with temperature ($p > 0.05$) (Fig. 1b). In light of the classification by *nosZ* clade types, the $K_{m, O2}$ values of *Azospira* sp. strain I13 (0.51 ± 0.03 to 0.75 ± 0.25 μmol L^{-1} at 15–35°C) were significantly lower than those of clade I type *nosZ*, *i.e.*, *Ps. stutzeri* JCM5965 (1.22 ± 0.54 to 1.99 ± 0.61 μmol L^{-1}) and *Pa. denitrificans* NBRC102528 (0.86 ± 0.29 to 1.50 ± 0.37 μmol L^{-1}) at each temperature ($p < 0.05$). The $K_{m, O2}$ values of *Azospira* sp. strain I09 were also lower than those of *Ps. stutzeri* JCM5965 and *Pa. denitrificans* NBRC102528 except for the ones at 25°C and 35°C. The highest $a_{0, O2}$ values were usually observed at 35°C for the tested bacteria, while the value for *Azospira* sp. strain I13 was significantly higher than those of the other tested bacteria ($p < 0.05$; Fig. 2a). Given the insignificant change in $K_{m, O2}$ with temperature (Fig. 1b), the $V_{max, O2}$

determined the $a_{0,\,O2}$ values. Except for *Azospira* sp. strain I13, the $a_{0,\,O2}$ values of these tested bacteria displayed no significant difference with temperature (Fig. 2a).

5.3.2 Biokinetic parameters of N_2ORB on N_2O respiration

The decremental trends of N_2O and O_2 concentrations were consistent irrespective of the tested bacterial species (an example in Fig. S3). The $V_{max,\,N2O}$ of *Pa. denitrificans* NBRC102528 was one or two orders of magnitude lower than the other tested N_2ORB at each temperature (Fig. 1c). Temperature increase concomitantly increased $V_{max,\,N2O}$ in the tested N_2ORB. The highest value for $V_{max,\,N2O}$, $7.12 \pm 1.26 \times 10^{-9}$ μmol (cell h)$^{-1}$, was attainted at 35°C for *Azospira* sp. strain I13, 2.82- to 47.47-fold higher than the other species at 35°C ($p < 0.05$). Over the tested temperature range, the highest $V_{max,\,N2O}$ values for *Azospira* sp. strain I09, *Azospira* sp. strain I13, *Ps. stutzeri* JCM5965, and *Pa. denitrificans* NBRC102528 were approximately 4.85, 24.52, 2.42, and 3.60 times higher, respectively, than those of the lowest values. Irrespective of the tested temperature, the $K_{m,\,N2O}$ values for *Ps. stutzeri* JCM5965 and *Pa. denitrificans* NBRC102528 were higher than those for *Azospira* sp. strains I09 and I13 ($p < 0.05$; Fig. 1d). For all tested N_2ORB except *Azospira* sp. strain I13, the $K_{m,\,N2O}$ values did not statistically differ over the tested temperature range ($p > 0.05$). Contrarily, the $K_{m,\,N2O}$ values for *Azospira* sp. strain I13 had a temperature dependence: the highest value (0.89 ± 0.09 μmol L^{-1}) at 35°C was 1.56 times higher than the lowest value (0.57 ± 0.09 μmol L^{-1}) at 15°C. As shown in Figs. 1d and 2b, the lower $K_{m,\,N2O}$ values for *Azospira* sp. strains I09 and I13 than for *Ps. stutzeri* JCM5965 and *Pa. denitrificans* NBRC102528 result in a higher $a_{0,\,N2O}$, especially at 30°C and 35°C ($p < 0.05$). In contrast, $a_{0,\,N2O}$ of *Ps. stutzeri* JCM5965 was comparable to the $a_{0,\,N2O}$ of *Azospira* sp. strain I13 at 25°C ($p = 0.22$). The $a_{0,\,N2O}$ values of *Pa. denitrificans* NBRC102528 were two to three orders of magnitude lower than the other tested N_2ORB. The low activity with an unknown reason was similar to previous reports (Suenaga et al., 2018a).

Regardless of the temperature range and tested bacterial species, the positive linear correlations between $V_{max,\,O2}$ and $V_{max,\,N2O}$ ($R^2 > 0.8$; $p < 0.05$) were obtained (Fig. S6).

Among the tested N_2ORB, the slope of the correlation for *Azospira* sp. strain I13 (slope, 1.41) was significantly higher than for the other N_2ORB, while the slopes for *Azospira* sp. strain I09 (slope, 0.59) and *Ps. stutzeri* JCM5965 (slope, 0.51) were comparable (Fig. S6). These slopes were lower than 2, that is the theoretical value assuming the same electron donor consumption rate coupled with N_2O ($N_2O + 2H^+ + 2e^- \rightarrow N_2 + H_2O$) and O_2 ($O_2 + 4H^+ + 4e^- \rightarrow 2H_2O$). A slope lower than 2 indicates that oxygen is a more favorable electron acceptor than N_2O for the electron donor consumption.

5.3.3 Activation energy and sensitivity to temperature

The activation energies of O_2 and N_2O for the N_2ORB were estimated (Fig. 3). From the linear correlations of $\ln V_{max}$ and $1/T$ in Fig. 3 ($R^2 > 0.8$), the highest $E_{a,\,O2}$ and $E_{a,\,N2O}$ of 122.2 ± 21.6 and 114.0 ± 22.6 kJ mol^{-1} were obtained for *Azospira* sp. strain I13 (Table S2), which had the largest temperature dependence. The ranges of $E_{a,\,O2}$ and $E_{a,\,N2O}$ for the other tested N_2ORB were from 36.0 ± 12.6 to 97.6 ± 20.2 kJ mol^{-1} and 38.3 ± 5.9 to 60.1 ± 13.0 kJ mol^{-1}, respectively. In addition, the Q_{10} value at 25–35°C for *Azospira* sp. strain I13 (9.04) was significantly higher than for the other N_2ORB (Table S2). Except for *Pa. denitrificans* NBRC102528, the relative activation energies ($E_{a,\,O2}/E_{a,\,N2O}$) were close to 1. *Ps. stutzeri* JCM5965 and *Pa. denitrificans* NBRC102528, harboring clade I type *nosZ*, possessed lower $E_{a,\,N2O}$ than *Azospira* sp. strains I09 and I13 (Table S2). The $E_{a,\,O2}$ and $E_{a,\,N2O}$ of *Ps. stutzeri* JCM5965 were the lowest.

5.3.4 Assessment of the O_2 inhibition constants

According to the V_{N2O} profile in the presence of O_2 and the fitting to Eq. (6), K_I values at different temperatures were estimated (Fig. 4). Because of the marginal N_2O consumption activity of *Pa. denitrificans* NBRC102528, the K_I value could not be numerically attained [Eq. (6)]; therefore, the data for *Pa. denitrificans* NBRC102528 were excluded hereafter. The highest K_I of *Azospira* sp. strain I09 (0.92 ± 0.24 μmol L^{-1}), *Azospira* sp. strain I13 (0.19 ± 0.04 μmol L^{-1}), and *Ps. stutzeri* JCM5965 (0.84 ±

0.31 μmol L^{-1}) were consistently attained at 35°C. The K_I values of the three bacteria were statistically comparable at 15°C ($p = 0.243$), while the K_I value for *Azospira* sp. strain I09 was significantly higher than for *Azospira* sp. strain I13 at the other tested temperatures ($p < 0.05$). For *Azospira* sp. strain I09 and *Ps. stutzeri* JCM5965, the K_I values increased with temperature, suggesting a lower O_2 susceptibility of N_2O reduction activity. In contrast, K_I was independent of temperature from 15°C to 35°C for *Azospira* sp. strain I13 ($p = 0.106$).

5.3.5 Recovery of N_2O consumption activity after O_2 depletion

The N_2O consumption by N_2ORB after O_2 depletion was evaluated using the relative activity of N_2O consumption rates ($v_{N2O} = V_{N2O}/V_{max, N2O}$). As shown in Fig. S7, v_{N2O} at 30°C linearly increased ($p < 0.01$) with time, but the degree of v_{N2O} recovery was distinct among the tested bacteria. The N_2O consumption rate after O_2 exposure ($V_{N2O\ recovery}$) at 30°C was fitted to the developed model in Eq. (8) (Fig. 5). By fitting Eq. (8) to the experimental results (Figs. 5, S8 and S9), the recovery rate constants (k') at different temperatures were acquired (Fig. 6). The highest k' was attained at different temperatures: *Azospira* sp. strain I09, *Azospira* sp. strain I13, and *Ps. stutzeri* JCM5965 displayed the highest recovery at 35°C (0.75 ± 0.08 h^{-1}), 30°C (1.36 ± 0.21 h^{-1}), and 35°C (0.37 ± 0.11 h^{-1}), respectively. For *Azospira* sp. strain I09 and *Ps. stutzeri* JCM5965, these temperatures coincide with those resulting in the highest N_2O consumption rates (Fig. 1). Among the tested temperature conditions, *Azospira* sp. strain I13 had a faster recovery after O_2 exposure compared with *Azospira* sp. strain I09 and *Ps. stutzeri* JCM5965 ($p < 0.05$). The Spearman's rank correlation analysis indicated medium-strong positive correlations between k' and $V_{max, N2O}$ in *Azospira* sp. strains I09 and I13, and *Ps. stutzeri* JCM5965 ($p < 0.05$) (Table S3).

5.4 Discussion

4.4.1 Temperature effect on O_2 and N_2O respiration biokinetics of N_2ORB

Harnessing N_2ORB in engineered systems for reducing N_2O emissions entails

more knowledge of their ecophysiologies (Hallin et al., 2018; Suenaga et al., 2019). In addition to typical *nosZ* clade I type canonical denitrifying bacteria serving as a N_2O sink (Table S1), the applicability of newly isolated *nosZ* clade II type denitrifying bacteria has demanded further investigation (Suenaga et al., 2019). This study was undertaken to comprehensively evaluate the temperature effect on the whole-cell biokinetics of N_2ORB in the two distinct *nosZ* clade types, including the *nosZ* clade II type *Azospira* spp., which has been considered promising as an efficient N_2O consumer in WWTPs (Suenaga et al., 2019; Kim et al., 2020). The four tested N_2ORB from the two different *nosZ* types have distinct biokinetic traits at different temperatures (Fig. 1), indicating that temperature is one of the potential factors governing the abundance and composition of the N_2ORB communities. Seasonal temperature variations are often observed in WWTPs, where N_2O emissions are correspondingly changed (Chen et al., 2019). Similarly, the temperature dependence of bioreactor performances is also reported (Watanabe et al., 2017), with lower observed N_2O consumption activity at a low temperature (Wang et al., 2018). Although the temperature effect on N_2O emissions has been investigated at the bioreactor level (Adouani et al., 2015; Chen et al., 2016), an in-depth analysis of N_2O consumption activity in pure cultures has not been reported. Our results demonstrate that the effect of temperature on N_2O consumption activity is N_2ORB species-dependent (Fig. 3 and Table S2), supporting the significance of enriching and leveraging efficient N_2ORB as an N_2O sink.

This study also highlights the positive correlation between inherent O_2 and N_2O respiration rates irrespective of temperature (Fig. S6). The relationship is somewhat expected as both N_2O and O_2 are preferable electron acceptors for facultative denitrifying bacteria possessing the N_2OR operon (Chen and Strous, 2013). More importantly, the relative $V_{max, N2O}$ over $V_{max, O2}$ (*i.e.*, the slopes in Fig. S6) differs among the four tested N_2ORB, with *Azospira* sp. strain I13 having the most preferential use of N_2O as an electron acceptor. The high relative $V_{max, N2O}$ over $V_{max, O2}$ by *Azospira* sp. strain I13 correlates with the behavior of N_2ORB-enriched biomass in a chemostat

(Conthe et al., 2018b). The higher slope indicates that *Azospira* sp. strain I13 is effective as a potential N_2O sink; however, *Azospira* sp. strain I09 does not show this potential as an N_2O sink, even though they are within the same species of clade II type *nosZ* N_2ORB (Fig. 1). Because N_2ORB with high N_2O affinities are affiliated with both *nosZ* clade I and clade II (Yoon et al., 2016; Conthe et al., 2018a; Suenaga et al., 2019), the classification of a physiological trait by *nosZ* clade types may be too simple (Kim et al., 2020), and the taxonomic classification may be explainable (Conthe et al., 2018c). Further holistic analysis on N_2ORB physiologies is therefore required.

The specific affinities (a_0) describes the bacterial abilities to acquire substrate from liquid (Button, 1991). Our respirometric analysis demonstrated that the values of $a_{0,\,O2}$ and $a_{0,\,N2O}$ and their temperature dependencies were different in the four N_2ORB, affiliated with either *nosZ* clade type (Fig. 2). Meanwhile, the K_m values did not significantly change with increasing temperature, except for *Azospira* sp. strain I13 at 35°C, indicating a drastic increase in $V_{max,\,O2}$ and $V_{max,\,N2O}$. *Azospira* sp. strains I09 and I13 had a higher $a_{0,\,N2O}$ than *Ps. stutzeri* JCM5965 and *Pa. denitrificans* NBRC102528 at 30°C and 35°C (Fig. 2b). This physiological trait rationally explains the predominance of the genus *Azospira* at 30°C in a bioreactor that is dedicated to the enrichment of N_2ORB (Suenaga et al., 2019). In contrast, the two *Azospira* sp. strains did not demonstrate an advantage over the other N_2ORB to consume N_2O at 15°C (Fig. 2b). This suggests that the specific affinity ($a_{0,\,N2O}$), dependent on a temperature in WWTPs, determines the predominant N_2ORB. According to the available N_2O biokinetics summarized in Table S4, the genera *Dechloromonas* and *Azospira* possess higher specific affinities for N_2O than other N_2ORB. Recent reports have indicated the presence of the family *Rhodocyclaceae* including the genera *Dechloromonas* and *Azospira* as N_2ORB in WWTPs (Kim et al., 2020), implying that *Azospira* spp. in this study may exert a N_2O reduction potential.

Analysis of the Arrhenius plot and E_a helps understand the reaction rates and temperature dependency of targeted bacteria. The differences in E_a values by different

bacteria in the same guilds, for example, aerobic and anaerobic ammonia-oxidizing bacteria, likely result in different reaction rates (Jiang and Bakken, 1999; Oshiki et al., 2011). To the best of our knowledge, this study is the first to showcase the E_a comparisons among pure culture N_2ORB. The calculation of the apparent E_a (Fig. 3) indicated a higher E_a for N_2O by *Azospira* sp. strain I13 (114.0 ± 22.6 kJ mol^{-1}) compared with the other N_2ORB (38.3–60.1 kJ mol^{-1}) as summarized in Table S2. The value is also higher than results from previous work in an arable field (28–76 kJ mol^{-1}) and denitrifying activated sludge (44.1 kJ mol^{-1}) (Holtan-Hartwig et al., 2002; Wang et al., 2014b). This trait has a stark contrast with the $E_{a,\ N2O}$ values of *Ps. stutzeri* JCM5965 and *Pa. denitrificans* NBRC102528, analogous to those for denitrification obtained in previous studies (Table S2). The Q_{10} values for N_2O consumption, except for *Azospira* sp. strain I13 [Q_{10} (25–35): 9.04], were comparable to those in the previous studies for denitrification, ranging from 2 to 3 (Heinen, 2006; Saleh-Lakha et al., 2009; Wang et al., 2018). The higher $E_{a,\ N2O}$ and Q_{10} for N_2O by *Azospira* sp. strain I13 indicate that this species functions as a better N_2O sink under mesophilic conditions than at the lower temperatures, such as 15°C, often found in WWTPs. Therefore, our results highlight the significance of biokinetics and temperature dependence in determining the predominant N_2ORB in a nitrogen removal system. The trend can indicate the intrinsic capacity for N_2O reduction to N_2 in microbial ecosystems, which is supported by a previous study (Holtan-Hartwig et al., 2002). To harness the N_2O consumption potential of *Azospira* sp. strain I13 at a relatively lower temperature, immobilization in a biofilm or entrapped gel would allow a high density of the N_2ORB (Suenaga et al., 2018b). In parallel with an immobilization strategy, exploring N_2ORB that display a high activity of N_2O consumption at a lower temperature warrants additional investigation.

4.4.2 Change in N_2O consumption dynamics from aerobic to anoxic conditions at various temperatures

This study displays that the change in N_2O consumption activity during the transition from aerobic to anoxic conditions is both temperature- and species-

dependent. The use of a microrespiration system allowed the direct observation of N_2O consumption dynamics at different temperatures, while the O_2 concentration was consumed (Fig. 5). N_2O reduction, the final step of denitrification mediated by the N_2OR, is reportedly inactivated in the presence of O_2 (Pomowski et al., 2011). Although *nosZ* gene transcription dynamics has been monitored under suboxic or fluctuating oxygen conditions (Qu et al., 2016; Marchant et al., 2017), monitoring the gene transcripts does not directly provide the context of N_2O consumption activities. We investigated the combined effect of O_2 concentration and temperature on N_2ORB activity in the transition of redox changes. Our results demonstrated that *Azospira* sp. strain I09 and *Ps. stutzeri* JCM5965 had increased oxygen resistance as a response to increased temperature, as indicated by higher K_I values with an increase in temperature (Fig. 4). This property corroborates the hypothesis that the N_2OR activity is affected by both O_2 and temperature. In contrast to the dependence on temperature in the other tested N_2ORB, the oxygen resistance potential of *Azospira* sp. strain I13 (K_I) did not change with temperature (Fig. 4). These distinct features of O_2 resistance correspond with the previous finding of the different O_2 sensitivities of various N_2OR (Cavigelli and Robertson, 2001). Interestingly, different O_2 tolerance was observed within N_2ORB belonging to the same species (Fig. 4). The O_2 tolerance mechanism of N_2OR is unclear; therefore, holistic evaluations are needed into the N_2OR activity of different N_2ORB species and the clarification of the underlying mechanism.

The parameterization of the N_2O activity recovery by N_2ORB after O_2 exposure is important for the use of N_2ORB in WWTPs for N_2O mitigation. Contrary to the previous study, which models the N_2O consumption activity in the presence of O_2 (Zheng and Doskey, 2015), our study highlighted the recovery process of N_2O consumption activity after O_2 depletion (Fig. 5). The N_2O reduction activity of N_2ORB linearly increased over time ($p < 0.001$; Fig. S7), supported by a previous study (Suenaga et al., 2018a). On the basis of the results, the recovery model incorporating the recovery of N_2O reduction activity (v_{N2O}) of N_2ORB into the whole-cell Michaelis-

Menten kinetics was successfully employed (Figs. 5, S8, and S9). The simple retrofitted model including v_{N2O} allowed the parametrization of the N_2OR response time against O_2 spikes. This parameter, capable of tracking a decrease in N_2O reduction activity after O_2 exposure, could predict N_2O emissions from WWTPs where aerobic and anoxic conditions spatiotemporally change.

The recovery rates (k') of N_2O reduction activity, estimated by the model, indicated a considerable N_2OR recovery variation by the tested N_2ORB at different temperatures (Fig. 6), indicating that temperature affected the recovery rates of N_2O consumption activity. Interestingly, the highest recovery rate was always in keeping with the higher N_2O consumption rate by these N_2ORB (Table S3), suggesting an interdependence of the maximum N_2OR turnover and recovery of N_2O consumption activity. Our results also demonstrated that the two *Azospira* spp., harboring *nosZ* clade II type enzymes, quickly recover N_2O consumption activities after O_2 exposure in the tested temperature range (Fig. 6). It is worth noting that the rapid recovery of N_2O consumption ability is conducive to mitigation of N_2O emission. Although more study is needed, *nosZ* clade II type N_2ORB may function as better N_2O sinks than *nosZ* clade I type N_2ORB in environments where the redox condition is spatiotemporally altered. Such condition provides another advantage for *nosZ* clade II type N_2ORB, in addition to those found in previous studies indicating that *nosZ* clade II type N_2ORB are better N_2O sinks than clade I type (Yoon et al., 2016; Suenaga et al., 2019). However, this trend may not be consistent with all N_2ORB belonging to either *nosZ* clade type, and more data are required to support the reduction of N_2O emissions in natural and engineered systems (Conthe et al., 2018b, 2018c; Hallin et al., 2018).

In conclusion, the N_2ORB with this high recovery ability are beneficial to rapidly reduce N_2O emissions after O_2 exposure events, which is required to develop an efficient N_2O sink in the WWTPs. This application of N_2ORB can be expanded to wetlands, woodchip bioreactors, and agricultural soil, where redox conditions dynamically change (Moorman, et al., 2010; Morse and Bernhardt, 2013; Song et al.,

2019). Therefore, exploring N_2ORB with high resilience after O_2 exposure and high N_2O consumption activity allows the development of N_2O mitigation technology, and our biokinetic study indicates that *Azospira* sp. strain I13 is a promising potential N_2O consumer that exhibits a high rate of N_2O consumption (high $V_{max, N2O}$) and rapid N_2OR recovery after O_2 exposure (high k'), especially at a mesophilic temperature.

5.5 Conclusions

This study presents the temperature effect on O_2 and N_2O consumption biokinetics of pure culture N_2ORB, which is deemed promising a N_2O consumer. The results of this study are summarized below:

- The effect of temperature on O_2 and N_2O consumption rates and the specific affinities are distinct among the tested N_2ORB species, which are not merely categorized by *nosZ* clade types.
- N_2O-reducing activities of *Azospira* sp. strain I09 and *Ps. stutzeri* JCM5965 are sensitive to temperatures in the presence of O_2, suggesting that the N_2ORB in response to oxygen tolerance is altered by temperature.
- The model incorporating the N_2O activity recovery after oxygen exposure can describe N_2ORB physiologies in the transient anoxia.
- The Arrhenius plot indicates that *Azospira* sp. strain I13 is a specialist as an N_2O sink at a temperature above 30°C, suggesting that dominant N_2OBR species dynamically change with different temperatures.

Taken together, our microrespiration analysis illuminates drastic changes in N_2O consumption capacities of N_2ORB at different temperatures and oxygen-level conditions.

5.6 References

Abdalla, M., Jones, M., Smith, P., Williams, M., 2009. Nitrous oxide fluxes and denitrification sensitivity to temperature in Irish pasture soils. Soil Use and Management 25, 376-388.

Adouani, N., Limousy, L., Lendormi, T., Sire, O., 2015. N_2O and NO emissions during wastewater denitrification step: Influence of temperature on the biological process. Comptes Rendus Chimie 15-22.

Button, D.K., 1991. Biochemical basis for whole-cell uptake kinetics: specific affinity, oligotrophic capacity, and the meaning of the michaelis constant. Applied and Environmental Microbiology 57,2033-2038.

Cavigelli, M.A., Robertson, G.P., 2001. Role of denitrifier diversity in rates of nitrous oxide consumption in a terrestrial ecosystem. Soil Biology and Biochemistry 33, 297-310.

Chen, J., Strous, M., 2013. Denitrification and aerobic respiration, hybrid electron transport chains and co-evolution. BBA-Bioenergetics 1827, 136-144.

Chen, L.L., Wen, Z.D., Wang, W.H., Liang, H., Gao, D.W., 2016. Effects of temperature on N_2O production in the process of nitrogen removal by micro-expansion aerobic granular sludge. Desalin. Water Treatment 57, 28743-28748.

Chen, X., Mielczarek, A.T., Habicht, K., Andersen, M.H., Thornberg, D., Sin, G., 2019. Assessment of full-scale N_2O emission characteristics and testing of control concepts in an activated sludge wastewater treatment plant with alternating aerobic and anoxic phases. Environmental Science & Technology 53, 12485-12494.

Conthe, M., Wittorf, L., Kuenen, J.G., Kleerebezem, R., van Loosdrecht, M.C.M., Hallin, S., 2018a. Life on N_2O: deciphering the ecophysiology of N_2O respiring bacterial communities in a continuous culture. ISME. Journal 12, 1142-1153.

Conthe, M., Parchen, C., Stouten, G., Kleerebezem, R., van Loosdrecht, M.C.M., 2018b. O_2 versus N_2O respiration in a continuous microbial enrichment. Applied and Environmental Microbiology 102, 8943-8950.

Conthe, M., Wittorf, L., Kuenen, J. G., Kleerebezem, R., Hallin, S., van Loosdrecht, M. C. M., 2018c. Growth yield and selection of *nosZ* clade II types in a continuous enrichment culture of N_2O respiring bacteria. Environmental Microbiology Reports 10(3), 239-244.

Hallin, S., Philippot, L., Löffler, F.E., Sanford, R.A., Jones, C.M., 2018. Genomics and ecology of novel N_2O-reducing microorganisms. Trends Microbiology 26, 43-55.

Han, Z., Lv, P., Gao, T., Luo, J., Liu, X., Song, M., Li, Z., Zhang, Y., Bai, Z., 2020. Diversity of culturable aerobic denitrifying bacteria in a rotating biological contactor combined with anaerobic-anoxic-oxic-oxic wastewater treatment system. Desalination and Water Treatment 188, 356-374.

Heinen M., 2006. Simplified denitrification models: Overview and properties. Geoderma 133: 444-463.

Holtan-Hartwig, L., Dörsch, P., Bakken, L.R., 2002. Low temperature control of soil denitrifying communities: kinetics of N_2O production and reduction. Soil Biology and Biochemistry 34, 1797-1806.

Huang, Z., Kong, F., Li, Y., Xu, G., Yuan, R., Wang, S., 2020. Advanced treatment of effluent from municipal wastewater treatment plant by strengthened ecological floating bed. Bioresource Technology 309, 123358.

IPCC, Climate change 2014: Mitigation of climate change, in: O. Edenhofer R. PichsMadruga Y. Sokona E. Farahani S. Kadner K. Seyboth A. Adler I. Baum S. Brunner P. Eickemeier B. Kriemann J. Savolainen S. Schlömer C. von Stechow T. Zwickel J.C. Minx (eds.) Contribution of Working Group III to the Fifth Assessment. Report of the Intergovernmental Panel on Climate Change, Cambridge University Press, Cambridge, United Kingdom and New York, NY USA, 2014.

Jiang, M., Zheng, X., Chen, Y., 2020. Enhancement of denitrification performance with reduction of nitrite accumulation and N_2O emission by *Shewanella oneidensis* MR-1 in microbial denitrifying process. Water Research 169, 115242.

Jiang, Q.Q., Bakken, L.R., 1999. Comparison of nitrosospira strains isolated from terrestrial environments. FEMS Microbiology Ecology 30,171-186.

Jones, C.M., Graf, D.R., Bru, D., Philippot, L., Hallin, S., 2013. The unaccounted yet abundant nitrous oxide-reducing microbial community: a potential nitrous oxide

sink. ISME. Journal 7, 417-426.

Kim, D.D., Park, D., Yoon, H., Yun, T., Song, M.J., Yoon, S., 2020. Quantification of *nosZ* genes and transcripts in activated sludge microbiomes with novel group-specific qPCR methods validated with metagenomic analyses. Water Research 185, 116261.

Kinh, C.T., Suenaga, T., Hori, T., Riya, S., Hosomi, M., Smets, B.F., Terada, A., 2017. Counter-diffusion biofilms have lower N_2O emissions than co-diffusion biofilms during simultaneous nitrification and denitrification: Insights from depth-profile analysis. Water Research 124, 363-371.

Kits, K.D., Sedlacek ,C.J., Lebedeva, E.V., Han, P., Bulaev, A., Pjevac, P., Daebeler, A., Romano, S., Albertsen, M., Stein, L.Y., Daims, H., Wagner, M., 2017. Kinetic analysis of a complete nitrifier reveals an oligotrophic lifestyle. Nature 549, 269-272.

Li, L., Qian, G., Ye, L., Hu, X., Yu, X., Lyu, W., 2018. Research on the enhancement of biological nitrogen removal at low temperatures from ammonium-rich wastewater by the bio-electrocoagulation technology in lab-scale systems, pilot-scale systems and a full-scale industrial wastewater treatment plant. Water Research 140, 77-89.

Lunau, M., Lemke, A., Walther, K., Martens-Habbena, W., Simon, M., 2005. An improved method for counting bacteria from sediments and turbid environments by epifluorescence microscopy. Environmental Microbiology 7, 961-968.

Marchant, H.K., Ahmerkamp, S., Lavik, G., Tegetmeyer, H.E., Graf, J., Klatt, J.M., Holtappels, M., Walpersdorf, E., Kuypers, M.M.M., 2017. Denitrifying community in coastal sediments performs aerobic and anaerobic respiration simultaneously. ISME. Journal 11, 1799-1812.

Martens-Habbena, W., Berube, P.M., Urakawa, H., de la Torre, J.R., Stahl, D.A., 2009. Ammonia oxidation kinetics determine niche separation of nitrifying Archaea and Bacteria. Nature 461, 976-979.

Massara, T.M., Malamis, S., Guisasola, A., Baeza, J.A., Noutsopoulos, C., Katsou, E.,

2017. A review on nitrous oxide (N_2O) emissions during biological nutrient removal from municipal wastewater and sludge reject water. Science of the Total Environment 596-597, 106-123.

Morse, J.L., Bernhardt, E.S., 2013. Using ^{15}N tracers to estimate N_2O and N_2 emissions from nitrification and denitrification in coastal plain wetlands under contrasting land-uses. Soil Biology and Biochemistry 57, 635-643.

Moorman, T.B., Parkin, T.B., Kaspar, T.C., Jaynes, D.B., 2010. Denitrification activity, wood loss, and N_2O emissions over 9 years from a wood chip bioreactor. Ecological Engineering 36(11), 1567-1574.

Miyahara, M., Kim, S.W., Fushinobu, S., Takaki, K., Yamada, T., Watanabe, A., Miyauchi, K., Endo, G., Wakagi, T., Shoun, H., 2010. Potential of aerobic denitrification by *Pseudomonas stutzeri* TR2 to reduce nitrous oxide emissions from wastewater treatment plants. Applied and Environmental Microbiology 76, 4619-4625.

Ni, B.J., Ruscalleda, M., Pellicer-Nàcher, C., Smets, B.F., 2011. Modeling nitrous oxide production during biological nitrogen removal via nitrification and denitrification: Extensions to the general ASM models. Environmental Science & Technology 45, 7768-7776.

Oshiki, M., Shimokawa, M., Fujii, N., Satohl, H., Okabe, S., 2011. Physiological characteristics of the anaerobic ammonium-oxidizing bacterium '*Candidatus* Brocadia sinica'. Microbiology-Sgm 157,1706-1713.

Peng, L., Ni, B.J., Erler, D., Ye, L., Yuan, Z., 2014. The effect of dissolved oxygen on N_2O production by ammonia-oxidizing bacteria in an enriched nitrifying sludge. Water Research 66, 12-21.

Poh, L.S., Jiang, X., Zhang, Z., Liu, Y., Ng, W.J., Zhou, Y., 2015. N_2O accumulation from denitrification under different temperatures. Applied and Environmental Microbiology 99, 9215-9226.

Pomowski, A., Zumft, W.G., Kroneck, P.M.H., Einsle, O., 2011. N_2O binding at a

[4Cu:2S] copper–sulphur cluster in nitrous oxide reductase. Nature 477, 234-237.

Qu, Z., Bakken, L.R., Molstad, L., Frostegård, Å., Bergaust, L.L., 2016. Transcriptional and metabolic regulation of denitrification in *Paracoccus denitrificans* allows low but significant activity of nitrous oxide reductase under oxic conditions. Environmental Microbiology 18, 2951-2963.

Rahman, M., Grace, M.R., Roberts, K.L., Kessler, A.J., Cook, P.L.M., 2019. Effect of temperature and drying-rewetting of sediments on the partitioning between denitrification and DNRA in constructed urban stormwater wetlands. Ecological Engineering 140, 105586.

Read-Daily, B.L., Sabba, F., Pavissich, J.P., Nerenberg, R., 2016. Kinetics of nitrous oxide (N_2O) formation and reduction by *Paracoccus pantotrophus*. AMB Express 6, 85.

Saleh-Lakha, S., Shannon, K.E., Henderson, S.L., Goyer, C., Trevors, J.T., Zebarth, B.J., Burton, D.L., 2009. Effect of pH and temperature on denitrification gene expression and activity in *Pseudomonas mandelii*. Applied and Environmental Microbiology 75, 3903.

Sanford, R.A., Wagner, D.D., Wu, Q., Chee-Sanford, J.C., Thomas, S.H., Cruz-Garcia, C., Rodriguez, G., Massol-Deyá, A., Krishnani, K.K., Ritalahti, K.M., Nissen, S., Konstantinidis, K.T., Löffler, F.E., 2012. Unexpected nondenitrifier nitrous oxide reductase gene diversity and abundance in soils. Proceedings of the National Academy of Sciences of the United States of America 109(48), 19709-19714.

Song, X., Ju, X., Topp, C.F.E., Rees, R.M., 2019. Oxygen regulates nitrous oxide production directly in agricultural soils. Environmental Science & Technology 53(21),1239-12547.

Suenaga, T., Hori, T., Riya, S., Hosomi, M., Smets, B.F., Terada, A., 2019. Enrichment, isolation, and characterization of high-affinity N_2O-reducing bacteria in a gas-permeable membrane reactor. Environmental Science & Technology 53, 12101-12112.

Suenaga, T., Riya, S., Hosomi, M., Terada, A., 2018a. Biokinetic characterization and activities of N_2O-reducing bacteria in response to various oxygen levels. Frontiers in Microbiology 9, 697.

Suenaga, T., Aoyagi, R., Sakamoto, N., Riya, S., Ohashi, H., Hosomi, M., Tokuyama, H., Terada, A., 2018b. Immobilization of *Azospira* sp strain I13 by gel entrapment for mitigation of N_2O from biological wastewater treatment plants: Biokinetic characterization and modeling. Journal of Bioscience and Bioengineering 126, (2), 213-219.

Terada, A., Sugawara, S., Hoio, K., Takeuchi, Y., Riya, S., Harper, W. F., Jr.,Yamamoto, T., Kuroiwa, M., Isobe, K., Katsuyama, C., Suwa, Y., Koba, K., Hosomi, M., 2017. Hybrid nitrous oxide production from a partial nitrifying bioreactor: hydroxylamine interactions with nitrite. Environmental Science & Technology 51(5), 2748-2756.

Tian, H., Xu, R., Canadell, J.G. et al., 2020. A comprehensive quantification of global nitrous oxide sources and sinks. Nature 586, 248-256.

US EPA, O., 2016. U.S. Greenhouse gas inventory report: 1990-2014 [WWW Document] accessed 1.25.17.

Vasilaki, V., Massara, T.M., Stanchev, P., Fatone, F., Katsou, E., 2019. A decade of nitrous oxide (N_2O) monitoring in full-scale wastewater treatment processes: A critical review. Water Research 161, 392-412.

von Schulthess, R., Wild, D., Gujer, W., 1994. Nitric and nitrous oxides from denitrifying activated sludge at low oxygen concentration. Water Science & Technology 30 (6), 123-132.

Wang, Z., Zhang, X., Lu, X., Liu, B., Li, Y., Long, C., Li, A., 2014a. Abundance and diversity of bacterial nitrifiers and denitrifiers and their functional genes in tannery wastewater treatment plants revealed by high-throughput sequencing. PLoS ONE 9(11): e113603.

Wang, X., Yang, X., Zhang, Z., Ye, X., Kao, C.M., Chen, S., 2014b. Long-term effect

of temperature on N_2O emission from the denitrifying activated sludge. Journal of Bioscience and Bioengineering 117, 298-304.

Wang, X., Ye, C., Zhang, Z., Guo, Y., Yang, R., Chen, S., 2018. Effects of temperature shock on N_2O emissions from denitrifying activated sludge and associated active bacteria. Bioresource Technology 249, 605-611.

Watanabe, R., Nie, Y., Wakahara, S., Komori, D., Li, Y.Y., 2017. Investigation on the response of anaerobic membrane bioreactor to temperature decrease from 25°C to 10°C in sewage treatment. Bioresource Technology 243, 747-754.

Wunderlin, P., Mohn, J., Joss, A., Emmenegger, L., Siegrist, H., 2012. Mechanisms of N_2O production in biological wastewater treatment under nitrifying and denitrifying conditions. Water Research 46(4), 1027-1037.

Yoon, S., Nissen, S., Park, D., Sanford, R.A., Loffler, F.E., 2016. Nitrous oxide reduction kinetics distinguish bacteria harboring clade I *nos*Z from those harboring clade II *nos*Z. Applied and Environmental Microbiology 82, 3793-3800.

Yoon, H., Song, M.J., Kim, D., Sabba, F., Yoon, S., 2019. A serial biofiltration system for effective removal of low-concentration nitrous oxide in oxic gas streams: Mathematical modeling of reactor performance and expermental validation. Environmental Science & Technology 53, 2063-2074.

Zheng, J., Doskey, P.V., 2015. Modeling nitrous oxide production and reduction in soil through explicit representation of denitrification enzyme kinetics. Environmental Science & Technology 49, 2132-2139.

Zumft, W.G., Kroneck, P.M.H., 2006. Respiratory transformation of nitrous oxide (N_2O) to dinitrogen by Bacteria and Archaea. Advances in Microbial Physiology 52, 107-227.

Figures

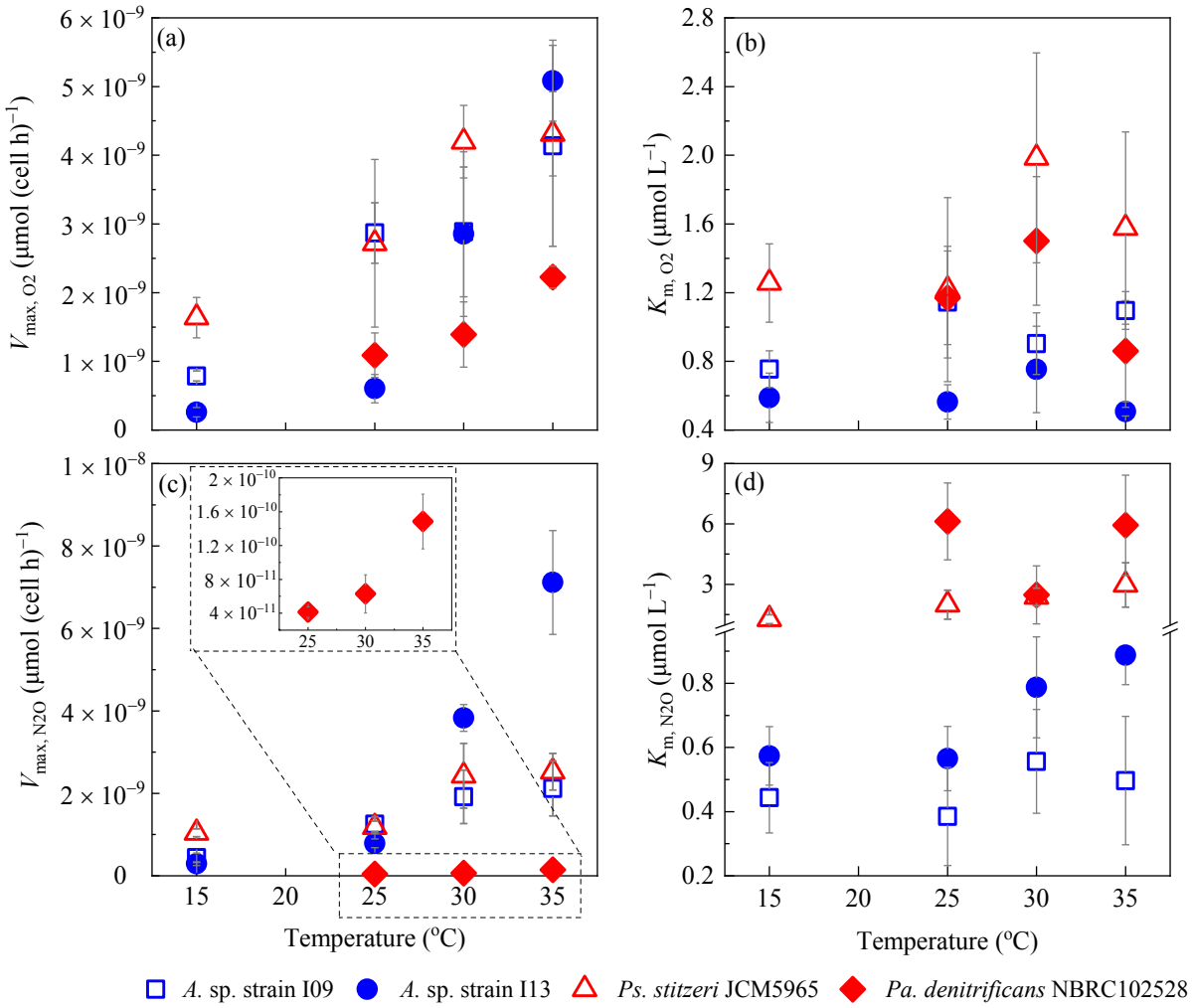

Fig. 1 The temperature dependence of biokinetic parameters (a: maximum O_2 consumption rate; b: O_2 half-saturation constant; c: maximum N_2O consumption rate; d: N_2O half-saturation constant). Bars denote standard deviations (n = 3). The clade I and II type of N_2ORB are represented in red and blue plots, respectively. The statistical analyses were performed by the Duncan test at the 5% level.

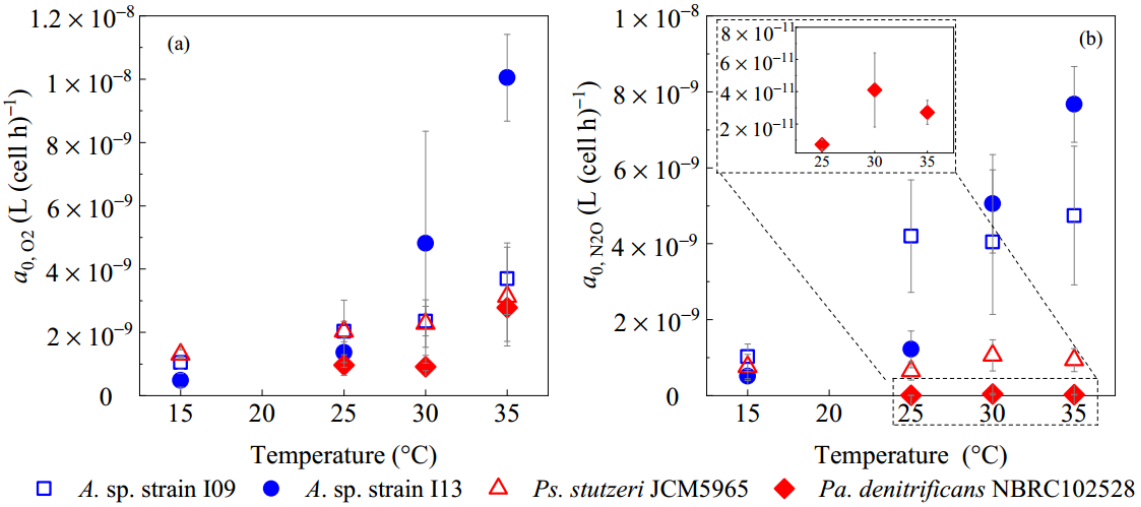

Fig. 2 The effect of temperature on the specific affinity constants for O_2 (a) and N_2O (b). Bars denote standard deviations (n = 3). The clade I and II type of N_2ORB are represented in red and blue plots, respectively. The statistical analyses were performed by the Duncan test at the 5% level.

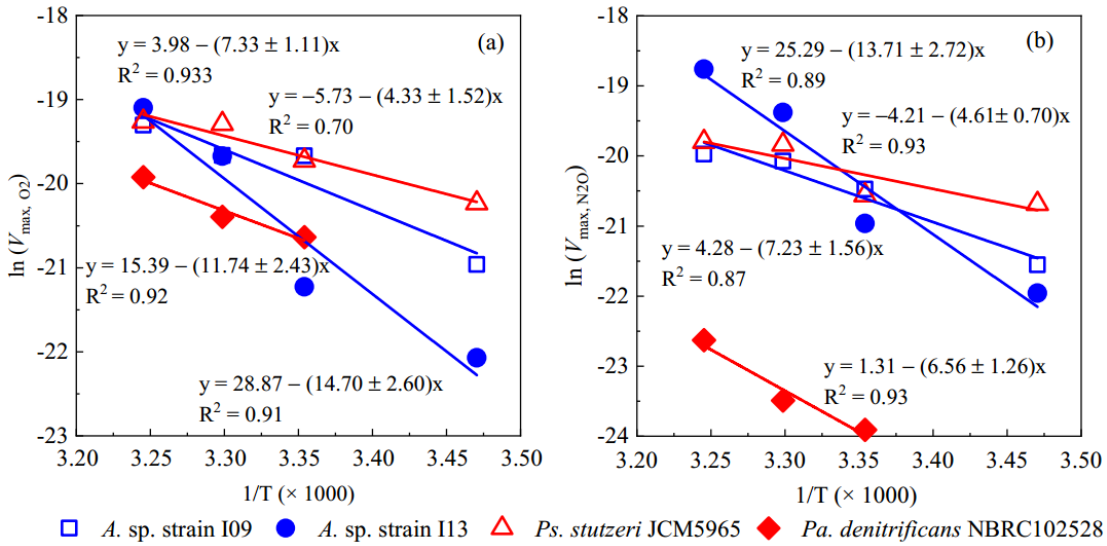

Fig. 3 Arrhenius plot for the calculation of activation energy for O_2 (a) and N_2O (b) showing the correlation between the maximum O_2 and N_2O respiration rates and the inverse temperature. Each point represents the average value from triplicate measurements. The clade I and II type of N_2ORB are represented by the red and blue, respectively.

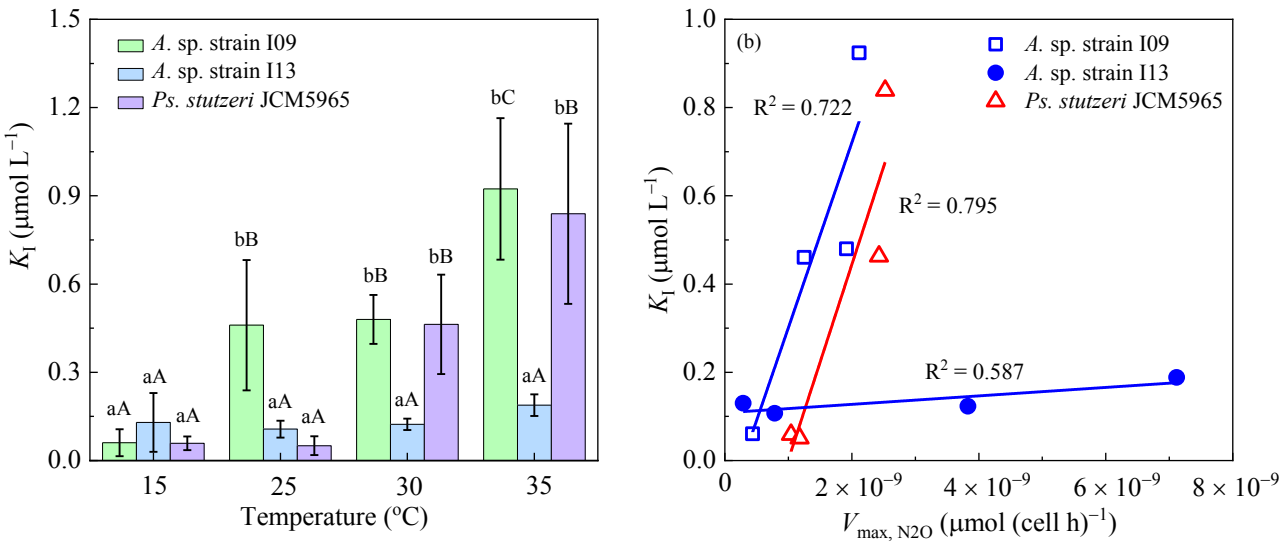

Fig. 4 Effects of temperature on the oxygen inhibition constants of *Azospira.* sp. strain I09, *Azospira.* sp. strain I13, and *Ps. stutzeri* JCM5965. Bars denote standard deviations (n = 3). The lowercase and uppercase letters indicate the significant differences among the bacteria at each temperature and those among the temperatures within each bacterium, respectively. The statistical analyses were performed by the Duncan test at the 5% level.

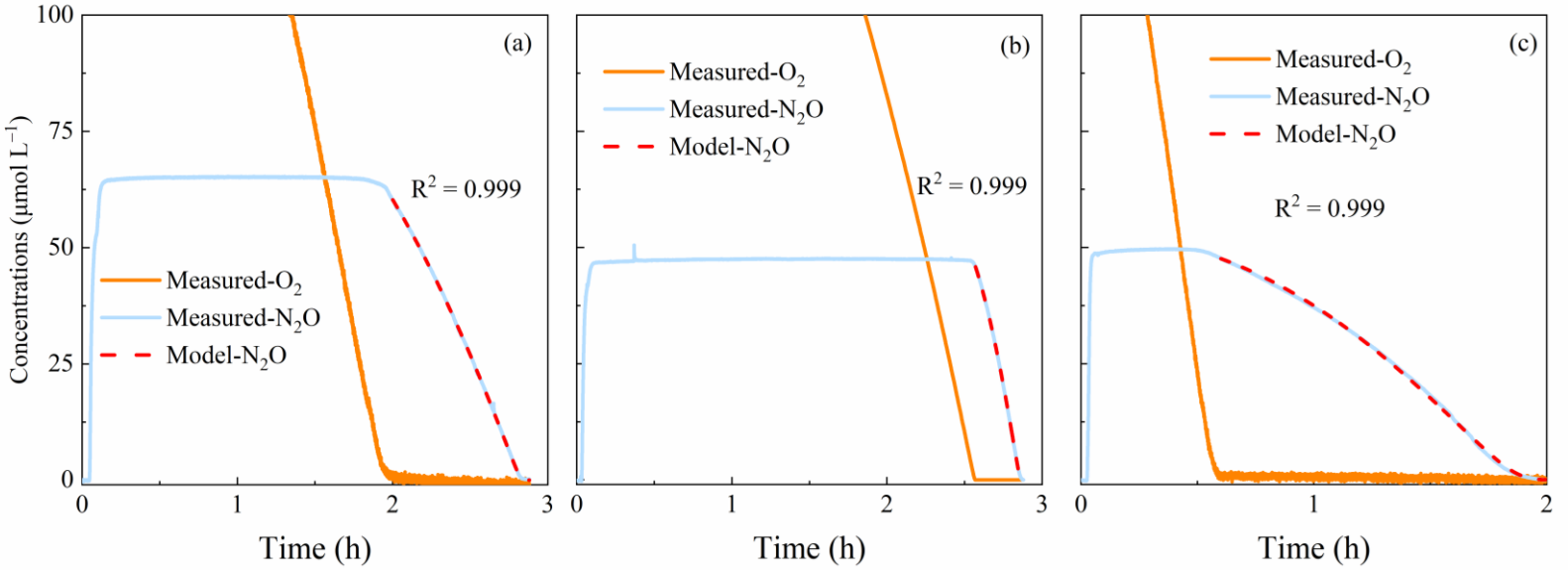

Fig. 5 Fitting the dynamics of N_2O consumption of *Azospira* sp. strain I09 (a), *Azospira* sp. strain I13 (b), and *Ps. stutzeri* JCM5965 (c), respectively, by the recovery model (Eq. 8) at 30℃. The least square method was used to estimate the recovery rates. The replicates are shown in Fig. S6.

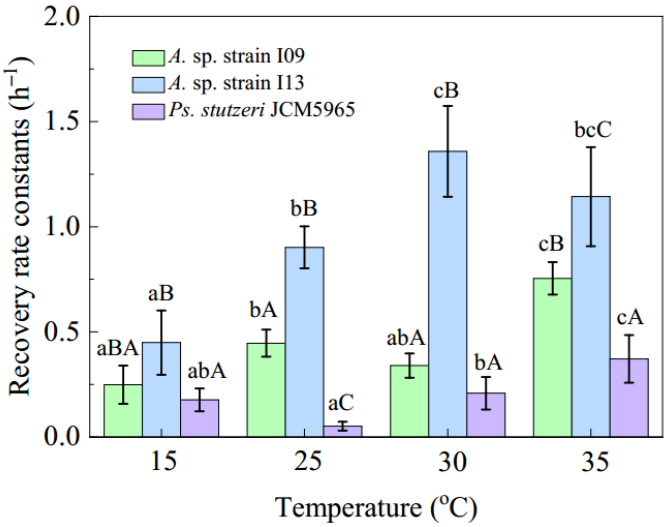

Fig. 6 The recovery rate constants of N_2O consumption activity by *Azospira* sp. strain I09, *Azospira* sp. strain I13, and *Ps. stutzeri* JCM5965. Bars denote standard errors (n = 3). The lowercase and uppercase letters indicate the significant differences among the temperatures for each bacterium and those among the bacteria at each temperature, respectively. The statistical analyses were performed by the Duncan test at the 5% level.

Supporting materials

Table S1 Targeted bacteria harboring *nosZ* used in this study

Organisms	Strain name	Type culture collection accession No.	*nosZ* clade	Genomic information (NCBI accession No.)	Source
Azospira sp. strain	I09	-	II	NZ_AP021844-NZ_AP021845	Bioreactor[1,2]
Azospira sp. strain	I13	-	II	BFBP01000001-BFBP01000026	Bioreactor[1,2]
Pseudomonas stutzeri	JCM5965	ATCC17588	I	CP002881	RIKEN BRC, Japan
Paracoccus denitrificans	NBRC102528	ATCC17741	I	BJUR01000001-BJUR01000161	NBRC, Japan

Table S2 Activation energy (E_a) and temperature coefficient (Q_{10}) for all tested bacteria compared to literature values. Values of Q_{10} were calculated between 15°C and 25°C; and between 25°C and 35°C.

Types	O_2-respriation			N_2O-respirattion			$E_{a,O2}/E_{a,N2O}$	Temperature range (°C)	References
	$E_{a,O2}$	Q_{10}		$E_{a,N2O}$	Q_{10}				
		Q_{10} (15–25°C)	Q_{10} (25–35°C)		Q_{10} (15–25°C)	Q_{10} (25–35°C)			
Azospira sp. strain I09	60.9 ± 9.2	3.65	1.44	60.1 ± 13.0	2.87	1.69	1.01	15-35	This study
Azospira sp. strain I13	122.2 ± 21.6	2.32	8.43	114.0 ± 22.6	2.71	9.04	1.07	15-35	This study
Pseudomonas. stutzeri JCM5965	36.0 ± 12.6	1.66	1.58	38.3 ± 5.9	1.13	2.14	0.94	15-35	This study
Paracoccus denitrificans NBRC102528	97.6 ± 20.2	Null	2.04	54.5 ± 10.5	Null	3.60	1.79	15-35	This study
Denitrifying soil (N_2O reduction)	-	-	-	28-76	-		-	5-20	3
Denitrifying activity sludge	-	-	-	48[a]	2.0		-	15-35	4
Pseudomonas aeruginosa	-	-	-	-	1.35		-	15-30	5
Denitrifying activity sludge (N_2O reduction)	-	-	-	44.1	-		-	4-34	6
River biofilm (denitrification)	-	-	-	136.9[a]	7.0		-	1-31	7
Constructed urban stormwater wetlands (denitrification)	-	-	-	41-64[a]	1.3-2.4		-	7.5-35	8
Lab-scale SBR (denitrification)	-	-	-	39.6[a]	-		-	15-30	9
Mixed bacterial culture (denitrification)	-	-	-	50.1[a]	2.3		-	15-35	10

[a] The data indicate the activation energy of denitrification.

Table S3 The Spearman's rank correlation between the recovery rate constants (k') and $V_{max,N2O}$ at different temperatures

	A. sp. strain I09	*A.* sp. strain I13	*Ps. stutzeri* JCM5965
Spearman correlation constants	0.556*	0.716**	0.596*

Significant correlation at the *$p < 0.05$ and **$p < 0.01$ levels.

Table S4 Summary of the biokinetics of N_2O-reducing bacteria.

Types	Type of *nos*Z	$V_{max, N2O}$ (10^{-9} μmol (cell h)$^{-1}$)	$K_{m, N2O}$ (μmol L^{-1})	a_0 ($V_{max,N2O}/K_{m, N2O}$) (10^{-9} L (cell h)$^{-1}$)	Culture conditions			References
					Temperature (°C)	pH	Carbon source	
Dechloromonas aromatica RCB	Clade II	7.75 ± 0.57[a]	0.32	24.22	30	Null	acetate	11
Dechloromonas denitrificans ED-1	Clade II	12.87 ± 1.08[a]	1.01	12.74	30	Null	acetate	11
Anaeromyxobacter dehalogenans 2CP-C	Clade II	0.29 ± 0.04[a]	1.34	0.21	30	Null	acetate	11
Dechloromona I20	Clade II	18.0 ± 4.6	2.04	8.82	30	7.5	acetate	12
Gemmatimonas aurantiaca T-27	Clade II	0.07 ± 0.01	Null	Null	30	7.0	glucose	13
Azospira sp. strain I09	Clade II	2.12 ± 0.67	0.50	4.74	35	7.5	acetate	This study
Azospira sp. strain I13	Clade II	7.12 ± 1.26	0.89	7.67	35	7.5	acetate	This study
Shewanella loihica PV-4	Clade I	7.49 ± 0.40[a]	7.07	1.06	30	Null	acetate	11
Pseudomonas stutzeri DCP-Ps1	Clade I	69.9 ± 7.4[a]	35.5	1.97	30	Null	acetate	11
Alycycliphilus denitrificans I51	Clade I	3.78 ± 2.29	8.98	0.42	30	7.5	acetate	12
Bradyrhizobium japonicum	Clade I	0.085	Null	Null	30	Null	yeast extract	14
Ps. stutzeri JCM5965	Clade I	2.52 ± 0.42	2.97	0.94	35	7.5	acetate	This study
Pa. denitrificans NBRC 102528	Clade I	0.15 ± 0.03	5.94	0.03	35	7.5	acetate	This study
Microbial enrichment bioreactor (mixed culture)	Null	Null	6.98	Null	20	7.0	acetate	15

[a] Converted using the 0.28 pg dry-weight per bacterial cell[1]. Null represents that the data are not reported

[References]

[1] Suenaga, T., Hori, T., Riya, S., Hosomi, M., Smets, B.F., Terada, A., 2019. Enrichment, isolation, and characterization of high-affinity N_2O-reducing bacteria in a gas-permeable membrane reactor. Environ. Sci. Technol. 53, 12101-12112. https://doi.org/10.1021/acs.est.9b02237

[2] Suenaga, T., Aoyagi, T., Hosomi, M., Hori, T., Terada, A., 2018. Draft genome sequence of *Azospira* sp. Strain I13, a nitrous oxide-reducing bacterium harboring clade II type nosZ. Genome. Announc. 6(20), e00414-18. https://doi: 10.1128/genomeA.00414-18

[3] Holtan-Hartwig, L., Dörsch, P., Bakken, L.R., 2002. Low temperature control of soil denitrifying communities: kinetics of N_2O production and reduction. Soil Biol. Biochem. 34, 1797-1806. https://doi.org/10.1016/S0038-0717(02)00169-4

[4] Foglar, L., Babić. A.M., Šiljeg, M.,2009. Nitrate removal from the Celtina surface water by using bacteria attached to Lewatit M600. Rec Adv Biol Biophys Bioengin. Comput. Chem. Proc. 39-44.

[5] Cavari, B.Z., Phelps, G., 1977. Denitrification in Lake Kinneret in the presence of oxygen. Freshwater Biology. 7(4), 385-391. https://doi.org/10.1111/j.1365-2427.1977.tb01686.x

[6] Wang, X., Yang, X., Zhang, Z., Ye, X., Kao, C.M., Chen, S., 2014. Long-term effect of temperature on N_2O emission from the denitrifying activated sludge. J. Biosci. Bioeng. 117, 298-304. https://doi.org/10.1016/j.jbiosc.2013.08.009

[7] Boulêtreau, S., Salvo, E., Lyautey, E., Mastrorillo, S., Garabetian, F., 2012. Temperature dependence of denitrification in phototrophic river biofilms. Sci. Total Environ. 416, 323-328. https://doi.org/10.1016/j.scitotenv.2011.11.066

[8] Rahman, M., Grace, M.R., Roberts, K. L., Kessler, A.J., Cook, P.L.M., 2019. Effect of temperature and drying-rewetting of sediments on the partitioning between denitrification and DNRA in constructed urban stormwater wetlands. Ecol. Eng. 140, 105586. https://doi.org/10.1016/j.ecoleng.2019.105586

[9] Noutsopoulos, C., Mamais, D., Statiris, E., Lerias, E., Malamis, S., Andreadakis, A., 2018. Reject water characterization and treatment through short-cut nitrification/denitrification: assessing the effect of temperature and type of substrate. J. Chem. Technol. Biotechnol. 93, 3638-3647. https://doi:10.1002/jctb.5745

[10] Foglar, L., Briški, F., Sipos, L., Vuković, M., 2005. High nitrate removal from synthetic wastewater with the mixed bacterial culture. Bioresource Technol. 96(8):879-888. https://doi.org/10.1016/j.biortech.2004.09.001

[11] Yoon, S., Nissen, S., Park, D., Sanford, R.A., Loffler, F.E., 2016. Nitrous oxide reduction kinetics distinguish bacteria harboring clade I *nos*Z from those harboring clade II *nos*Z. Appl. Environ. Microbiol. 82, 3793-3800. https://doi: 10.1128/AEM.00409-16

[12] Suenaga, T., Riya, S., Hosomi, M., Terada, A., 2018. Biokinetic characterization and activities of N_2O-reducing bacteria in response to various oxygen levels. Front. Microbiol. 9, 697. https://doi: org/10.3389/fmicb.2018.00697

[13] Park, D., Kim, H., Yoon, S., 2017. Nitrous oxide reduction by an obligate aerobic bacterium, *Gemmatimonas aurantiaca* strain T-27. Appl. Environ. Microbiol. 83:e00502-17. https://doi: org/10.1128/AEM.00502-17

[14] Itakura, M.; Tabata, K.; Eda, S.; Mitsui, H.; Murakami, K.; Yasuda, J.; Minamisawa, K. 2008. Generation of bradyrhizobium japonicum mutants with increased N_2O reductase activity by selection after introduction of a mutated dnaQ gene. Appl. Environ. Microbiol. 74, 7258−7264. https://doi: 10.1128/AEM.01850-08

[15] Conthe, M., Parchen, C., Stouten, G., Kieerebezem R., van Loosdrecht M., 2018. O_2 versus N_2O respiration in a continuous microbial enrichment. Appl. Microbiol. Biotechnol. 102, 8943–8950. https://doi.org/10.1007/s00253-018-9247-3

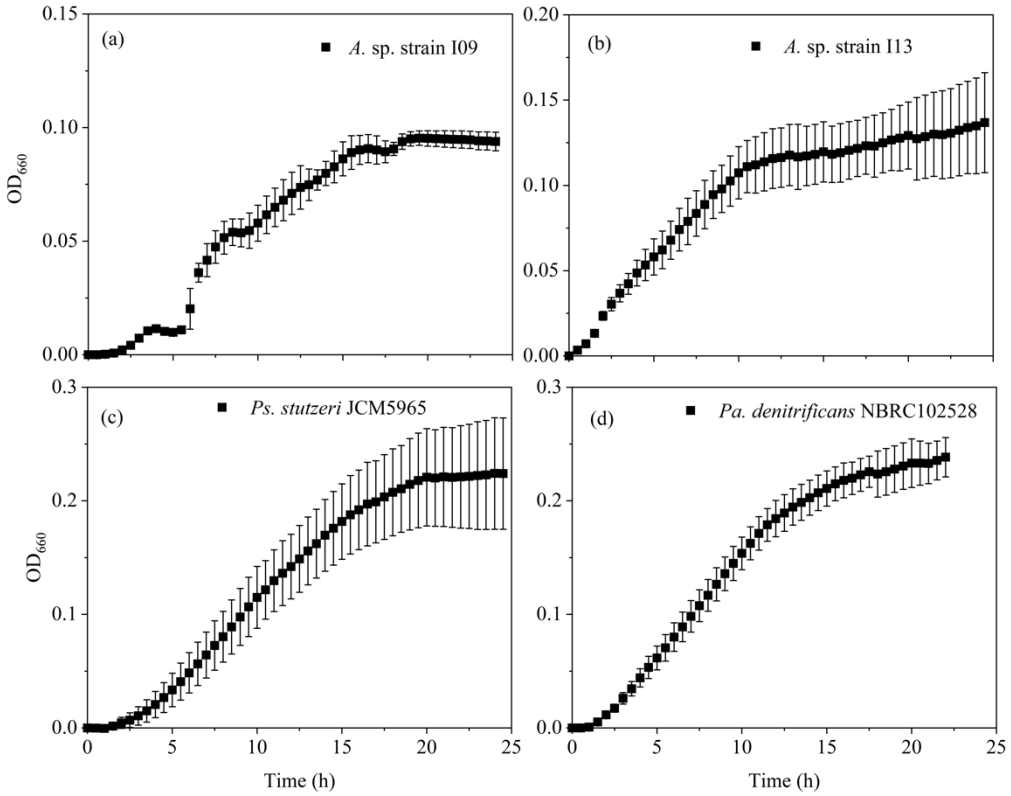

Fig. S1 The growth curves of (a) *Azospira* sp. strain I09, (b) *Azospira* sp. strain I13, (c) *Ps. stutzeri* JCM5965, and (d) *Pa. denitrificans* NBRC102528, respectively, at 30°C.

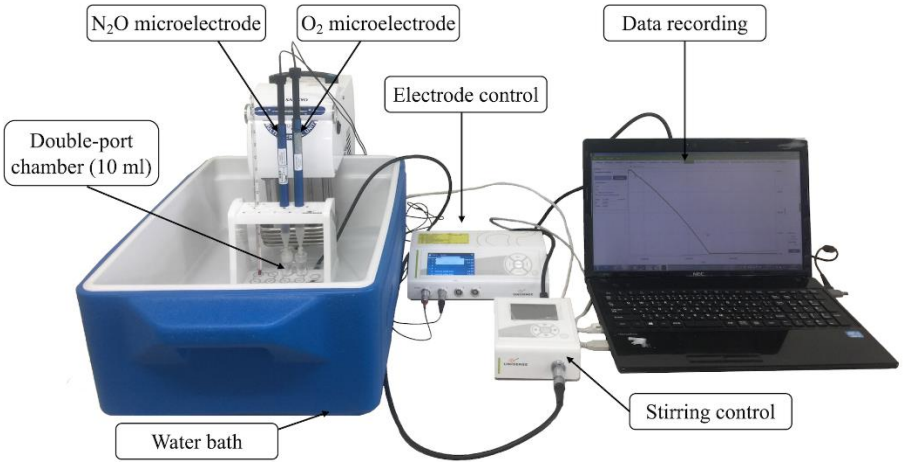

Fig. S2 Schematic diagram of a micro-respiration system using O_2 and N_2O sensors.

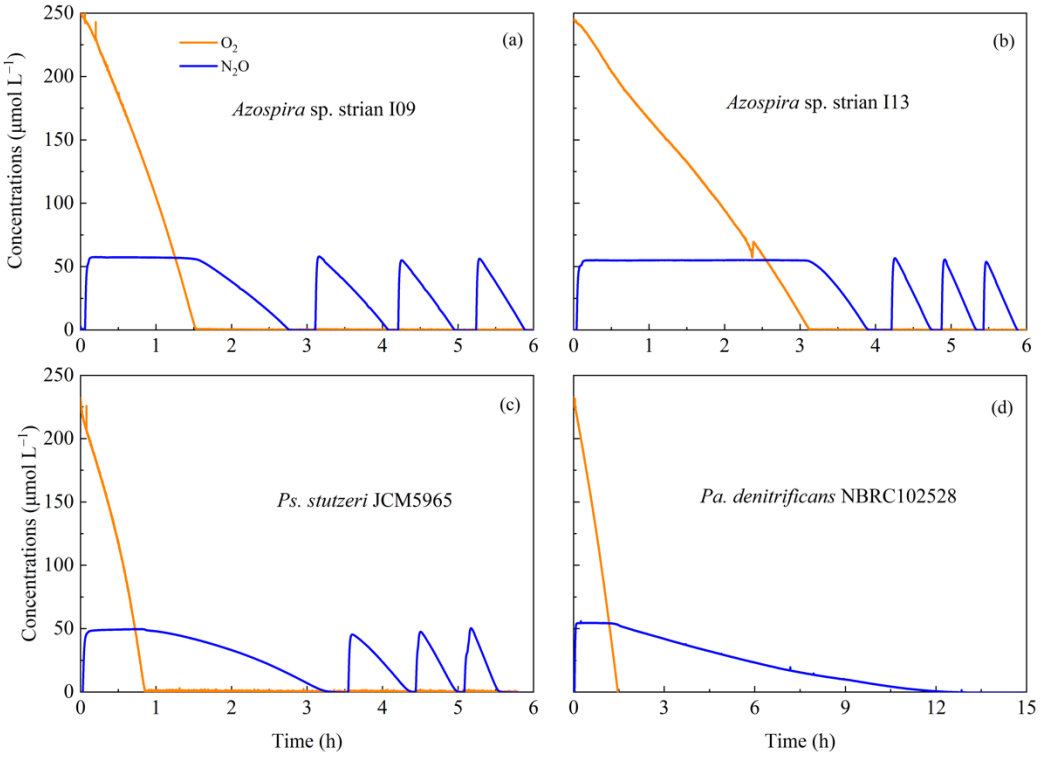

Fig. S3 Time courses of O_2 and N_2O concentrations consumed by (a) *Azospira* sp. strains I09, (b) *Azospira* sp. strain I13, (c) *Ps. stutzeri* JCM5965, and (d) *Pa. denitrificans* NBRC102528 at 25°C. The orange and green lines represent O_2 and N_2O, respectively.

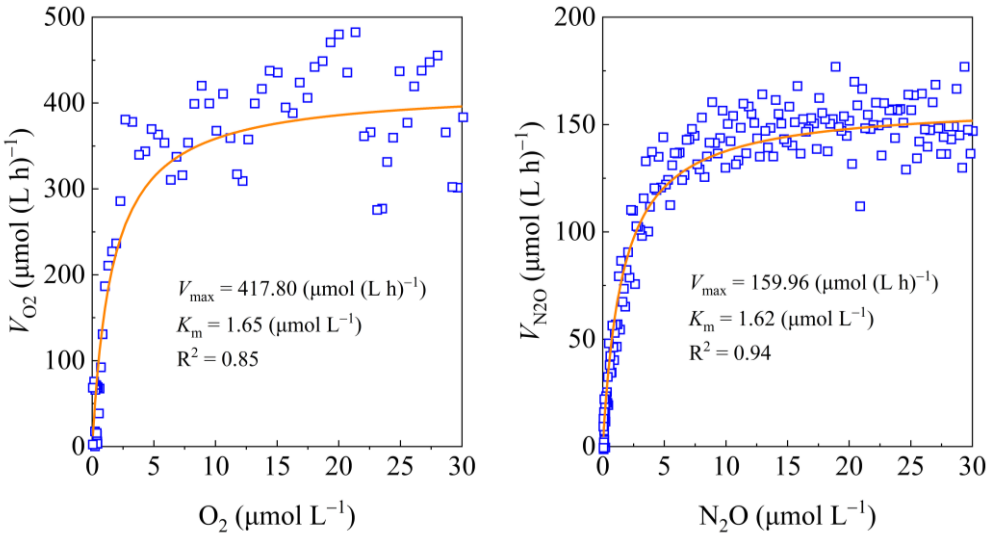

Fig. S4 Experimental and modeled V_{O2} and V_{N2O} as a function of (a) O_2 and (b) N_2O concentrations by *Ps. stutzeri* JCM5965 at 25°C.

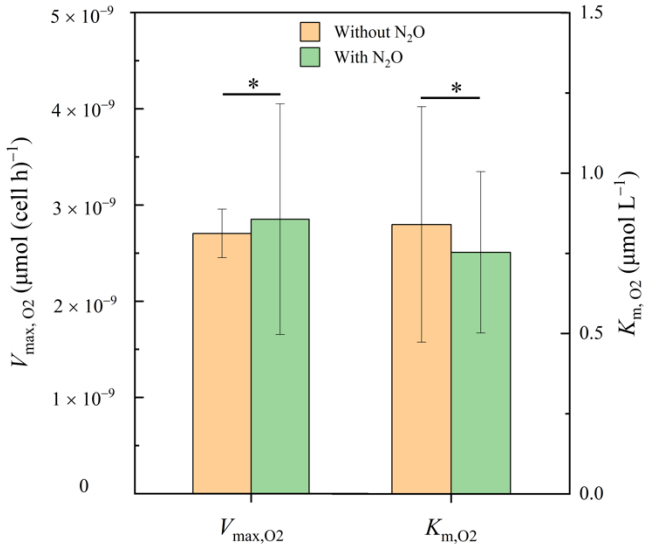

Fig. S5 The effect of N_2O on oxygen respiration kinetics of *Azospira* sp. strain I13 at 30°C. The result indicates that the presence of N_2O did not affect $V_{max,\ O2}$ and $K_{m,\ O2}$ (*$p > 0.05$).

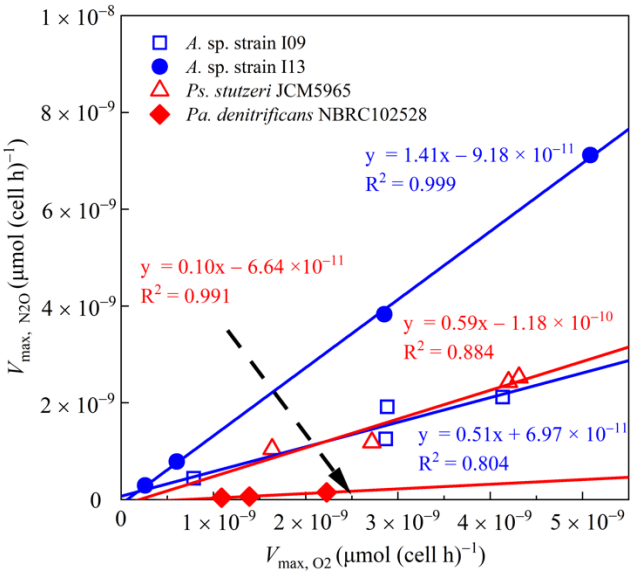

Fig. S6 The relationship between maximum O_2 consumption rates and maximum N_2O consumption rates among tested N_2ORB at different temperatures. The clade I and II type N_2ORB are plotted in red and blue, respectively. Note that the plots are derived from the tests at different temperatures.

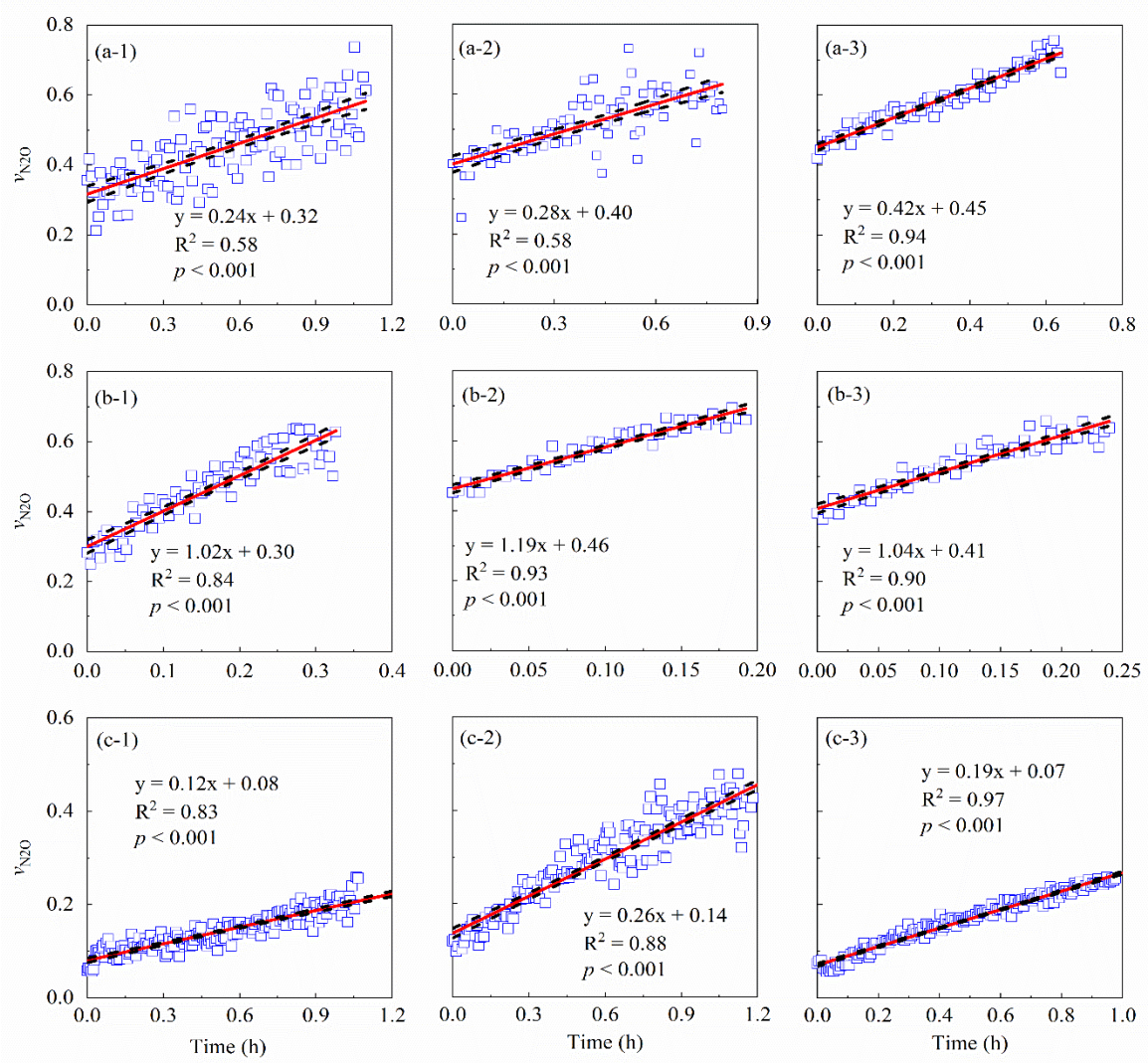

Fig. S7 The variations in relative N_2O consumption rates (v_{N2O}) of (a) *Azospira* sp. strain I09, (b) *Azospira* sp. strain I13, and (c) *Ps. stutzeri* JCM5965, respectively, at 30°C. Experiments were performed in triplicate. Solid and broken lines represent fitting v_{N2O} and the 95% confidence interval of each approximated line, respectively.

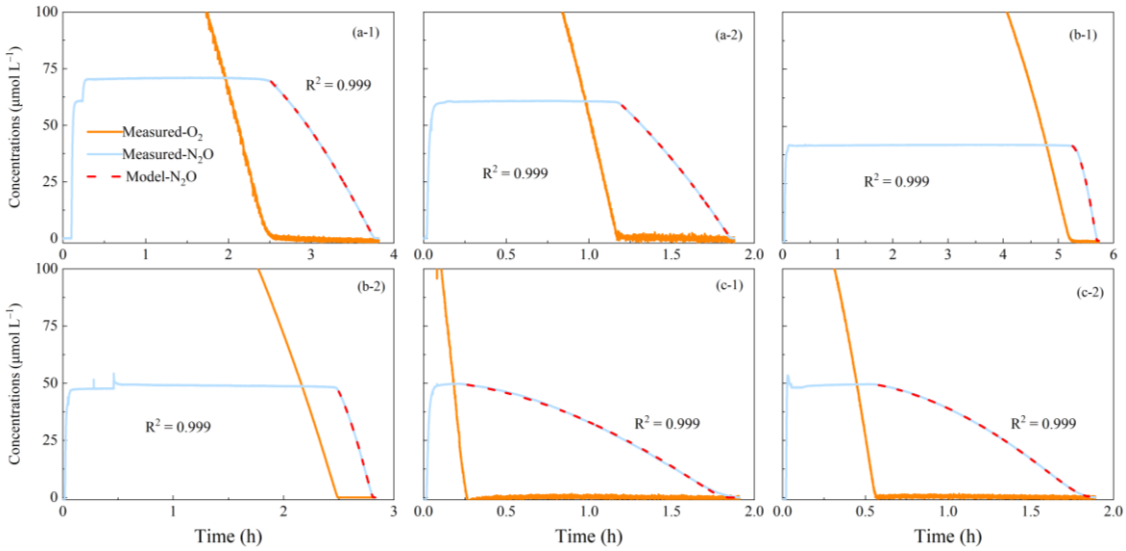

Fig. S8 Simulating N_2O concentration dynamics of (a) *Azospira* sp. strain I09, (b) *Azospira* sp. strain I13, and (c) *Ps. stutzeri* JCM5965 by the recovery model at 30°C.

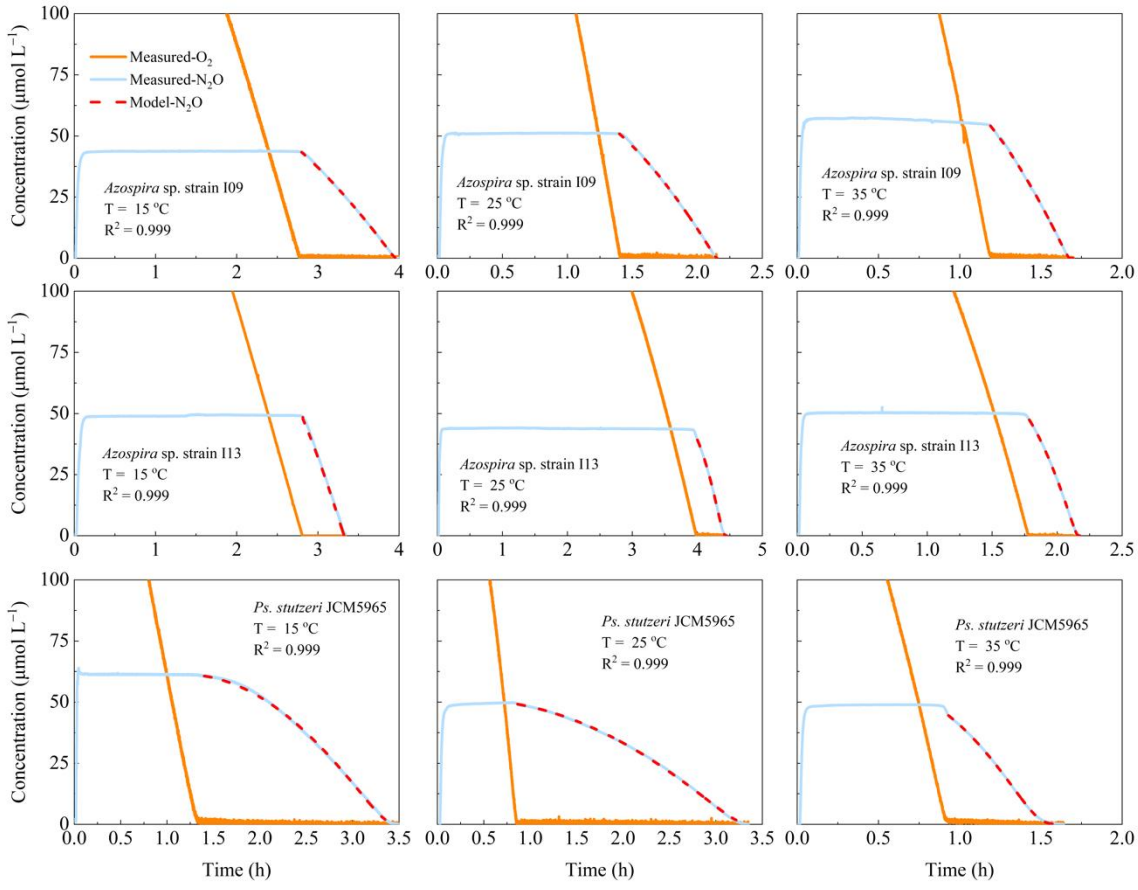

Fig. S9 Simulating N_2O concentration dynamics of *Azospira* sp. strain I09, *Azospira* sp. strain I13, and *Ps. stutzeri* JCM5965 by the recovery model at 15, 25, and 35°C, respectively.

Chapter 6: Summary

6.1 Main conclusions

Lake plays an important role in global carbon and nitrogen cycles, and there is still great uncertainty about the CH_4 and N_2O emissions in the increasing requirements of nutrients. In this study, 17 shallow lakes across the different trophic states in the Yangtze River basin, China, were selected to understand the characterizations and microbial driving mechanisms of CH_4 and N_2O emission in shallow lakes across different trophic states. Meanwhile, the biokinetic characterizations of N_2O consumption were elucidated for understanding the effects of temperature and oxygen on N_2O consumption. The conclusions of this study are summarized below:

(1) We performed a series of field measurements and characterized the CH_4 emissions in shallow lakes of different trophic state in the Yangtze River basin. This is the first study to elucidate the nonlinear response of the release of CH_4 from shallow lakes along a gradient of increasing eutrophication. An increase in the *TLI* of a lake by one level (*e.g.*, from mesotrophic to eutrophic) would correspond to a 10-fold increase in CH_4 emissions. This phenomenon is related to the fact that the accumulated nutrients and subsequent production of algae organic matter are the crucial drivers for the microbial community responsible for the CH_4 emissions from lakes. In addition, the decomposition of algae makes a significant contribution to the CH_4 emissions from eutrophic lakes, especially hyper-eutrophic lakes. Correspondingly, the NH_4^+ concentration in the water column can be used to predict the CH_4 emissions from lakes. Thus, our results strongly suggest that the eutrophication of lakes not only causes a deterioration in water quality, but also has a positive feedback effect on the global greenhouse effect.

(2) In addition, the N_2O emission fluxes of shallow lakes were most strongly affected by lake trophic state, suggesting that estimation of N_2O emission fluxes should consider lake trophic state; The nonlinear model incorporating trophic state levels can

describe the N_2O emissions from a shallow lake; The predicted N_2O emission fluxes based on the IPCC EF_{5r} overestimated the observed fluxes, particularly those in hyper-eutrophic lakes; Nutrient-rich conditions and algal accumulation were key factors determining N_2O emission fluxes in shallow lakes, and algal accumulation played a dual role in stimulating and impeding N_2O emissions, especially in hyper-eutrophic lakes; Changes in season accompanied the appearance and disappearance of algae and altered N_2O emission fluxes, especially in hyper-eutrophic lakes.

(3) Further elucidated the two key parameters *i.e.,* temperature and oxygen, to regulate N_2O consumption process of N_2ORB by biokinetic analyzation. The effect of temperature on O_2 and N_2O consumption rates and the specific affinities are distinct among the tested N_2ORB species, which are not merely categorized by *nosZ* clade types; N_2O-reducing activities of *Azospira* sp. strain I09 and *Ps. stutzeri* JCM5965 are sensitive to temperatures in the presence of O_2, suggesting that the N_2ORB in response to oxygen tolerance is altered by temperature; The model incorporating the N_2O activity recovery after oxygen exposure can describe N_2ORB physiologies in the transient anoxia; The Arrhenius plot indicates that *Azospira* sp. strain I13 is a specialist as an N_2O sink at a temperature above 30°C, suggesting that dominant N_2OBR species dynamically change with different temperatures; Taken together, our microrespiration analysis illuminates drastic changes in N_2O consumption capacities of N_2ORB at different temperatures and oxygen-level conditions.

6.2 Innovations and outlooks

This study major concerned that the eutrophication and GHGs emission in shallow lakes. Interestingly, the non-linear model is firstly proposed for quantifying the differences of CH_4 and N_2O emission fluxes in the shallow lakes across the different trophic states. This finding will deeply our knowledges regarding the eutrophication progress impacts on the CH_4 and N_2O emissions. It is implicated that the estimation of CH_4 and N_2O emission fluxes should be considered the trophic state of lakes.

Although we have clear that the eutrophication of lakes can significantly stimulate

the GHGs emission from lakes, the relationship between the eutrophication processes and global warming is still unclear. Further research should pay attention to the relationship between global climate changes, lake eutrophication, and GHGs emissions.

In addition, this study also evaluates the characterizations of N_2ORB to consume N_2O in different temperature and oxygen conditions, mitigations of N_2O by the N_2ORB in the shallow lakes are still unclear. In particular, how the N_2ORB regulates the reduction of N_2O in the heavy algae-accumulated zones needs further research.

List of Publications

1. **Zhou, Y.**, Xu, X., Han, R., Li, L., Feng, Y., Yeerken, S., Song, K. and Wang, Q., **2019**. Suspended particles potentially enhance nitrous oxide (N_2O) emissions in the oxic estuarine waters of eutrophic lakes: Field and experimental evidence. ***Environmental Pollution***, 252, 1225-1234. (Published) (Chapter 3 and 4)

2. **Zhou, Y.**, Song, K., Han, R., Riya, S., Xu, X., Yeerken, S., Geng, S., Ma, Y., Terada, A., **2020**. Nonlinear response of methane release to increased trophic state levels coupled with microbial processes in shallow lakes. ***Environmental Pollution***, 265, 114919. (Published) (Chapter 2)

3. **Zhou, Y.**, Suenaga, T., Qi, C., Riya, S., Hosomi, M., Terada, A., **2021**. Temperature and oxygen level determine N_2O respiration activities of heterotrophic N_2O-reducing bacteria: Biokinetic study. ***Biotechnology and Bioengineering***, 118, 1330-1341. (Published) (Chapter 5)

4. **Zhou, Y.**, Xu, X., Song, K., Yeerken, S., Deng, M., Li, Lu., Riya, S., Wang, Q., Terada, A., **2021**. Nonlinear pattern and algal dual-impact in N_2O emission with increasing trophic levels in shallow lakes. ***Water Research***. Doi.org/10.1016/j.watres.2021.117489 (Published) (Chapter 4)

Acknowledgments

Time flies, the three-years doctoral program is coming to an end. I am very fortunate to be able to come to Tokyo University of Agriculture and Technology (TUAT), Japan, and join Terada-Riya laboratory (Hosomi-Terada laboratory) to study and live. In this period, I have gained a lot of knowledge and also encountered many challenges.

I would like to appreciate my supervisor, Prof. Akihiko Terada for his kind support and continuity encouragement in my study. He's very serious and rigorous working attitude has benefited me a lot.

I would like to express my deeply respect for Prof. Masaaki Hosomi. His attitude towards life, work, and students are worthy of our lifelong learning.

Many thanks to my colleagues at the Terada-Riya laboratory (Hosomi-Terada laboratory), Department of Applied Chemistry, TUAT for their friendship help and kindly supports in my study and life. It is because of their friendly help and support in my experiment that I was able to carry out my experimental work smoothly. Especially, I would like to express my thanks to Riya-sensei, Suenaga-sensei, and all other laboratory members for giving me many meaningful suggestions in my study.

Grateful acknowledgment is for the China Scholarship Council (grant number CSC201808420224) to support my study in Japan.

Finally, I would like to express my many thanks to my friends and family members for all their love and encouragement. Too much gratitude is indescribable and will always be in my heart.